

Bulgarian Academy of Sciences, Space Research Institute  
Aerospace Research in Bulgaria. 16. 2001. Sofia

**AEROSPACE RESEARCH IN BULGARIA**

Volume 16 • Sofia • 2001

Space Research Institute  
Bulgarian Academy of Sciences

**Editorial Board**

Nikola Georgiev (*Editor-in-Chief*)

Garo Mardirossian (*Secretary*)

Petar Getzov, Plamen Angelov, Petar Velinov, Tanya Ivanova, Petko Nenovsky,  
Nencho Nechev, Pavel Penev, Hernani Spiridonov, Stavri Stavrev, Nikola  
Stoychev, Lachezar Filipov, Stefan Chapkunov

**Address**

AEROSPACE RESEARCH IN BULGARIA

Space Research Institute  
6, Moskovska St., Sofia 1000  
Bulgaria  
E-mail:

*Editor*

Elissaveta Mihaylova

*Technical Editor*

Valeri Vassev

*Translation*

Lubomira Krалеva

*Pre-Publishing Design*

Reni-Georgiya Sirkova



© Bulgarian Academy of Sciences  
Space Research Institute, 2001

# AEROSPACE RESEARCH IN BULGARIA

16

Sofia, 2001

## Contents

1. *Petar Getzov* - Bulgarian space studies - past, present, and future / 5
2. *Tanya Ivanova, Svetlana Sapunova, Plamen Kostov, Ivan Dandolov* - First Successful Space Seed-to-Seed Plant Growth Experiment in the SVET-2 Space Greenhouse in 1997 / 12
3. *Pavlin Gramaticov, Tanya Ivanova* - SVET-2 Space Greenhouse Light Unit / 24
4. *Genadiy Gdalevich, Ctefan Chapkanov, Tania Ivanova, Maria Petrunova, Bentzislav Markov* - Results Obtained Onboard the INTERCOSMOS-19 Satellite Using the P4 Device / 35
5. *Maria Petrunova, Boncho Peev* - Direct determination of ionospheric plasma structural parameters in the experiment with a spherical ion trap / 41
6. *Dimitar Teodossiev, Medy Astrukova, Rumen Shkevov, Georgi Galev* - Lowfrequency electric field measurement probes on board Intercosmos - 24 - Aktiven satellite / 46
7. *Medy Astrukova* - On the contact potential difference and the methods for its measurement for the purposes of space tribology / 54
8. *Kalinka Bakalova, Vitcho Tsanev* - Evaluation of the atmospheric optical characteristics impact on the solar corona observation / 61
9. *Nikola Georgiev, Rumen Nedkov, Dora Nedelcheva* - Using an orbital method and GPS measurements of the ground control points in georeference of space images / 70

10. *Nikolai Bankov, Liudmila Todorieva* - Data Processing of Microwave System R-400 on Board of the MIR Space Station / 82
11. *Garo Mardirossian, Dimitar Danov* - Preliminary analysis of the ballistic parameters of a penetrator for ecological studies / 89
12. *Georgi Jeleв, Eugenia Rumенина* - Monitoring the Studen Kladenets reservoir using air and space images / 97
13. *Venzislav Markov* - Systems for prelaunch test and inflight calibration of the device "Podsolnuh" - project "Granat" / 107
14. *Ventsislav Markov, Arkadii Melioranski, Lachezar Filipov* - Podsolnuh-d X-RAY telescope from the granat projec: Research program and some specifics in its harware implementationc / 112
15. *Hristo Hristov, Victor Baranov* - Isoperimetrical task for optimization of the cumulative charge for pseudometeorite particles / 119
16. *Vladimir Damgov, Petar Georgiev* - Non-linear oscilator under external synchronizing influence: Comparison of perturbation and canonical methods of analysis / 124

#### Scientific announcement

17. *Maria Dimitrova* - On the expected observational behaviour of the accretion flow in a close binary / 144
18. *Maria Dimitrova* - The influence of inflow gas temperature on the efficiency of accretion energy production / 148

## Съдържание

1. *Петър Гецов* - Космически изследвания в България - минало, настояще и бъдеще / 11
2. *Таня Иванова, Светлана Сапунова, Пламен Костов, Иван Дандолов* - Първи успешни опити за отглеждане на растения "От семе до семе" в космическата оранжерия СВЕТ-2 през 1997 година / 23
3. *Павлин Граматиков, Таня Иванова* - Блок осветление на космическата оранжерия СВЕТ-2 / 34
4. *Генадий Гдалевич, Стефан Чапкынов, Таня Иванова, Мария Петрунова, Венцислав Марков* - Обзор результатов, полученных при помощи спутника "ИНТЕРКОСМОС-19" с использованием прибора П4 / 40
5. *Мария Петрунова, Бончо Пеев* - Непосредствено определяне на йоносферните плазмено - структурни параметри в експеримент със сферичен йонен уловител / 45

6. *Димитър Теодосиев, Меди Аструкова, Румен Шкевов, Георги Галев* - Сонди за измерване на нискочестотни електрични полета на борда на спътника "Интеркосмос-24 - Активен" / 53

7. *Меди Аструкова* - Върху контактната потенциална разлика и методите за измерването и за целите на космическата трибология / 60

8. *Калинка Бакалова, Вичко Цанев* - Оценка на въздействието на атмосферните оптични характеристики върху наблюденията на слънчевата корона / 69

9. *Никола Георгиев, Румен Недков, Дора Неделчева* - Използване на орбитален метод и GPS измервания на опорните точки от терена при координатното привързване на космически фотографски изображения / 81

10. *Николай Банков, Людмила Тодориева* - Обработка на данни от микровълновата система Р-400 на борда на орбиталната станция "МИР" / 88

11. *Гаро Мардиросян, Димитър Данов* - Предварителен анализ на балистични параметри на пенетратор за екологични изследвания / 96

12. *Георги Желев, Евгиния Руменина* - Мониторинг на яз. "Студен кладенец" с използване на аеро и космически изображения / 102

13. *Венцислав Марков* - Системи за предпускови изпитания и калибровка по време на полета на устройството "Подсолнух" по проекта "Гранат" / 111

14. *Венцислав Марков, Аркадий Мелиорански, Лъчезар Филипов* - Ренгенов телескоп в апарата "Подсолнух-Д" по проекта "Гранат": Научна програма и някои особености в хардуерната му реализация / 118

15. *Христо Христов, Виктор Баранов* - Изопериметрична задача за оптимизация на кумулативен заряд за псевдометеоритни частици / 123

16. *Владимир Дамгов, Петър Георгиев* - Нелинеен осцилатор под външно синхронизиращо въздействие: Сравнение на пертурбационните и канонични методи на анализ / 143

#### Съобщения

17. *Мария Димитрова* - Очаквани наблюдателни проявления на акреционно течение в тясна двойна, предвиждани от двумерен числен експеримент / 147

18. *Мария Димитрова* - Влияние на температурата на фличащата се газова струя върху ефективността на енергоотделянето при акреция / 150

## **BULGARIAN SPACE STUDIES – PAST, PRESENT, AND FUTURE**

Assoc.Prof. P.Getsov,  
Director of the Space Research Institute  
of the Bulgarian Academy of Sciences

Bulgarian participation in space conquer is impressive, systematic, and effective. It started in 1969 when, at the Presidium of the Bulgarian Academy of Sciences (BAS), a research group in Space Physics was established. With the course of time this group grew into the Central Laboratory for Space Research (CLSR), and later, into the Space Research Institute (SRI). Meanwhile, more than 100 units, equipment, and systems were designed and launched in space.

In 1972, Bulgaria launched its first space equipment, P-1, onboard the *Intercosmos-8* satellite. Later, this equipment operated on the *Intercosmos-12 and 14* satellites, on the *Vertical-3, 4, 6, and 7* heavy geophysical rockets, and on a number of other meteorological rockets. At this time, a series of space units were designed at the CLSR, mainly in the field of Space Physics and Remote Sensing of the Earth from Space where some unrivalled achievements and unique equipment were made.

Under the *Intercosmos* Program were developed 19 joint satellites and automatic stations, 7 heavy geophysical rockets, and about 60 meteorological rockets. Bulgarian equipment and systems were flown on 4 *Intercosmos* satellites, 4 *Vertical* heavy geophysical rockets, and 5 *M-100* rockets. Bulgaria became the 18<sup>th</sup> country to launch space equipment and conduct space experiments. The plasma research units P-2, P-3, and X-4 flown later as a part of different satellite equipment were also very successive.

Bulgaria was specialized in the development of space electrophotometers for weak light emissions in Earth-surrounding space and planet atmosphere. These stations were used to measure the light emission of nightly skies in Cuba, India, and Guinea.

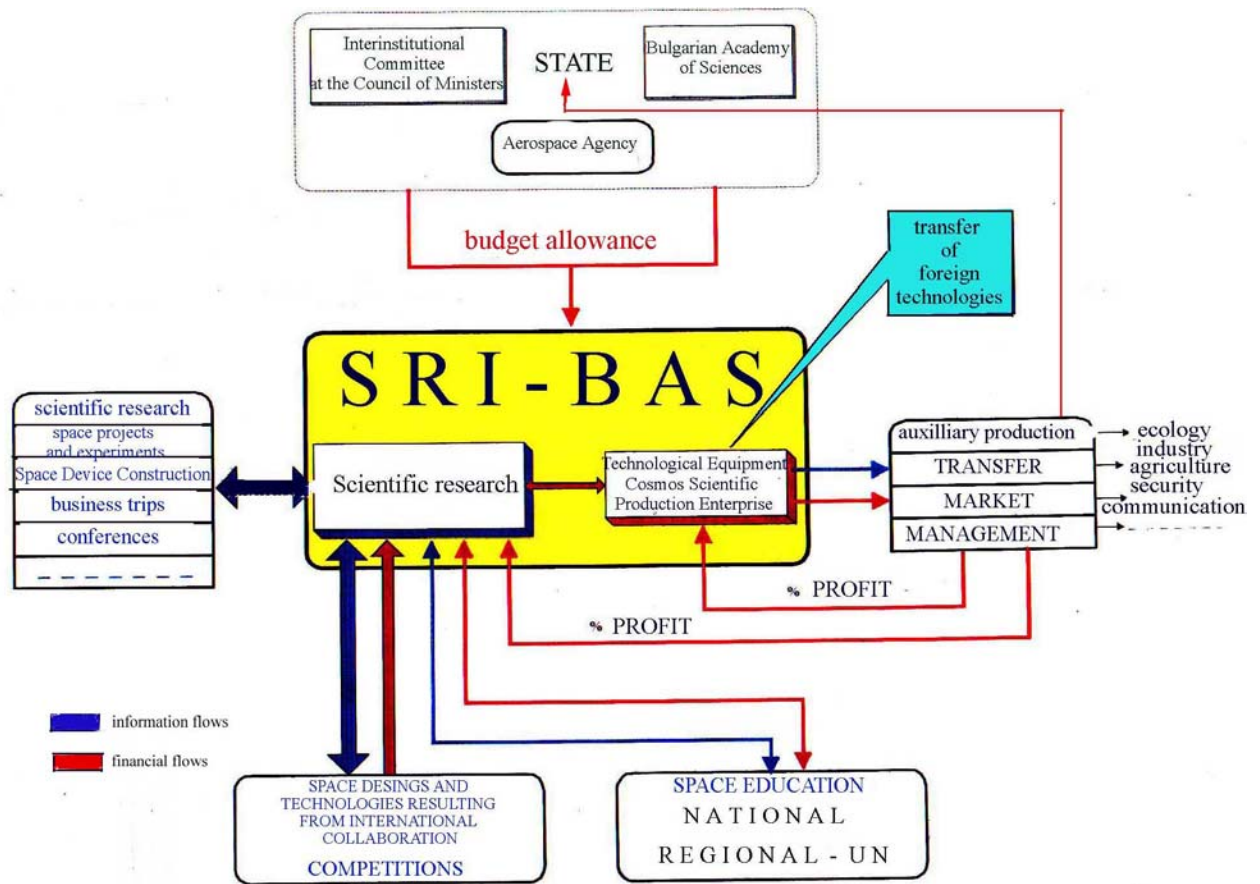
The Bulgarian units *ISOH-20* measuring the spectral reflection characteristics of soils, agricultural crops, rocks, and water have operated in Russia, Cuba, and Poland.

The apogee of Bulgarian space research achievements was the development of the research programs of the two Bulgarian astronauts including 11 units and systems by which more than 60 space experiments were conducted.

The activity of the SRI might be provisionally divided into several periods. First was the so-called *child* period related with mankind's first steps in space. Next came the *romantic* period part of which was described above. Its aim was to provide an answer to scientific curiosity but, quite often, it was as well an arena of political and technological rivalry between the two systems. Now we are in the so-called *pragmatic* period where space studies face mostly the problems of the Earth, aiming to solve the topical tasks of mankind related with ecology, communication, navigation, meteorology etc.

The restricted financial potentials of the country called for the need of concentrating researchers efforts on a nation-wide scale to prevent different institutions from performing more or less similar activities. To this end, the Council of Ministers founded an Interinstitutional Committee on Space Issues that adopted a National Program for Space Studies.

This program's implementation is to be based on market approach, competitiveness, targeted funding, and program teams which actually means the mode of operation of space studies in Bulgaria is going to be changed (Fig.1).



Accounting for the Committee's resolutions, the SRI which is the base BAS institution in the field of space studies undertook some serious actions to the implementation of these new commitments, specifying precisely the sources to fund its activity.

**First, we believe that the budget funds provided by BAS to support the Institute must be spent on purpose** through the organization of program teams to work on contract tasks with specified assignors, terms, and funding. This mode of operation calls for active science management where all the elements of scientific studies in the developed countries will be available.

**As a second source of funding we regard participation in the international allocation in the field of space studies.**

Since, so far, the developed western countries are the solvent ones, we try to establish international cooperation with them participating in various competitions, projects, or activities. The Institute has great experience in this field. Some of the successful projects in this field are **Corine Land Cover** and **PHARE-MERA** funded by Western Europe, the **SVET Space Greenhouse**, and the system for complex study of the astronauts psycho-physiological status, **Neurolab-B**. The last two projects, funded respectively by American and German institutions, were launched onboard the **MIR** Orbital Station (OS). In 1998, Bulgaria signed with Italy an Intergovernmental Agreement for Scientific-Technical Collaboration. A detailed Concept for the implementation of **7 projects** was elaborated that provoked the keen interest of a number of Italian universities, research centers, and space companies. Italy is expected to provide options

for mounting of scientific equipment onboard of the International Space Station (ISS) to be launched in September 2003 (within the module of the European Space Agency, ESA). In 2000, activities were started for Bulgaria's acquisition in the ESA which will greatly expand the opportunities for international participation.

The continuation of Bulgaria's collaboration with Russia is of great importance to the development of space studies. Since 1997 the Institute participates in the *Priroda* International Project which was realized on board of the *MIR* OS, based on the module bearing the same name.

A contract was concluded with our traditional partner, the State Research Center of the Russian Federation, the Institute of Medico-Biological Problems (IMBP), for scientific-technical collaboration to the development of a life-support system (LSS) for the long-term missions of the future space crews, based mostly on higher plants. Yet in 1997, a suggestion was forwarded to the Russian Space Agency for the inclusion of a new modification of the *SVET-3* Space Greenhouse in the biological research program of one of the Russian modules onboard of the ISS. Unfortunately, so far the project has been postponed for financial reasons.

Since 2000, teams from the Institute participate in **3 projects under the Fifth Frame Program of the European Community: Use of Space Images in Thematic and Cadastre Mapping for the Purpose of Agricultural Restructuring and Privatization with a View to Sustainable Development of the Environment**, and two projects in the field of Space Material Science.

Following the nearly ten-year long drop of the international research community's interest towards the study of Earth-surrounding plasma, recently, a growing interest has been witnessed in the field. Two global programs were initiated, namely: **Monitoring of Earth Catastrophes from Space** and **Space Time**. It is worth emphasizing that Bulgarian and Russian experts were the first in *Intercosmos* to address the problem of using space data for studying the reaction of ionospheric-magnetospheric plasma to forthcoming earthquakes. An essential part of the future studies in the SRI and its participation in satellite experiments will be related to the study of ionospheric-seismic effects and the options for using them as a precursor. The immediate future will witness the accomplishment of the **Predvestnik (Precursor) Projects**. The **Space Time Program** is aimed at studying both the direct and indirect (through anthropogenic systems and equipment) impact of Earth-surrounding space on man. Another topic of interest to Space Physics is the study of geomagnetic storms, development of models related with the reaction of ionospheric-magnetospheric plasma, dynamics of solar wind, operation of space units and equipment at the time of geomagnetic storms.

A team of the Institute is working on an international contract jointly with researchers and experts from the Institute for Problems of Material Science (IPMS) at the Ukrainian National Academy of Sciences and on the **BALKANBEARINGS United Project** under the EUREKA Program of the European Union in the field of new technological materials and covers to operate under extreme conditions.

We are resolved to find a way to participate in the projects of the ISS. The SRI has concluded a contract with the Brazilian company **BRAZSAT**, the only trade company in Latin America that coordinates their space programs onboard of American space shuttles. Through it we plan to design a space green house for the ISS.

Researchers of the SRI-BAS have been dealing for many years with the theoretical and technical problems of **space navigation**. This direction is of strategic importance since there is no airplane or ship already that does not use satellite navigation. The overall control of air and sea traffic, and recently also of land traffic is based on space navigation. It is also being introduced on a large scale in cars and this is going to result in a boom in the field of car construction and prevention of car theft that will have great economic and scientific-technical consequences.

Accounting for this fact we opened a **subsidiary in the town of Plovdiv** which will work only with navigation and communication.

In the next years, the construction of the *Galileo* Global European Navigation System will start which we are willing to join as well.

The active participation in international competitions and projects calls for a serious policy in staff selection and young researchers development. To this end we should:

- **incorporate young researchers** in the Institute by organizing competitions to the formation of program teams;
- **allow science leaders to emerge naturally** in the process of looking for and formulation of financially provided tasks of public significance. Gradually, the artificial structures and positions will fade away since they are funded only by the budget which gets more and more restricted;
- **replace the available assisting-technical staff by younger people.** This is going to take place gradually in the process of performing the activities related to the contract tasks these people will be involved in. In the recent years many of them lagged behind in their qualification, so, in looking for new tasks we should look as well for new people with new thinking, possessing the needed qualification;
- **make wide use of the need for lecturers and researchers of the universities and higher institutes.** This will not only preserve the competitiveness of our scientists and enable them to get some additional remuneration, but it will also provide an opportunity to detect the young people needed to solve the tasks in the field of space studies.

**The solution of our strategic tasks may be also funded through implementation of the obtained results,** minding the predominating applied-scientific or technological nature of the researches. We shall be greatly assisted in this respect by the forthcoming High-Tech Parks Act. We plan to create such a high-tech park based on the *Cosmos* Research-Production Enterprise located in the town of Stara Zagora and the technological sections and laboratories located in the city of Sofia and the town of Shoumen.

This technological center will assist us implement in practice both our, and foreign technological achievements. A bright example of this trend is the implementation of the **PLEVEN-87 equipment** flown with the second Bulgarian astronaut, Alexander Alexandrov, in the army, transport, industry, and the psycho-physiological studies of dispatchers, pilots, drivers, operators of complex systems etc.

The **NEUROLAB-B psycho-physiological complex** designed jointly with German scientist, currently operating in space, will be used, upon adequate adaptation, in hospitals and clinics, and will probably be competitive in price and potentials to similar medical equipment.

During the recent years, the small-sized multi-channel **HOLTER system** was designed in the SRI intended to record physiological parameters such as electrocardiogram, respiration, blood pressure, temperature etc. At the moment, the system is being tested in English clinics.

Contracts were also signed with the Japanese company **CORE** for the development of communication systems software products. Work is underway on a technical mission of the German company **Dedo Weigert Film**, Munich, for design of dedicated secondary power supply sources.

The **Laboratory for Study and Repair of Gyroscopic Units and Aggregates** founded at the SRI is licensed by the Ministry of Transport. It provides service to most Bulgarian aviation

companies. It will intensify its activity by participating in the updating and service of military avionics.

The introduction of an expert computer system for selection of soldiers-to-be for the Bulgarian army that has been developed for nearly 10 years by the institutes of BAS is forthcoming. It is foreseen to use this system in the transition to a professional army and in the recruitment of post-graduate students for the needs of the Ministry of Defense.

**We have concluded contracts with the Technological Institute for Supersolid and New Carbon Materials, Troitsk, Russia, Morgen Ceramics Company and Oryx Technology, CA, USA.** Now, diamond pads for assembly of microelectronic components are studied. Heat conductivity of 860 Watt/Kelvin.m has been achieved. The assembly of hot press is forthcoming for compacting of these pads that are awaited for on the USA market.

Bulgaria has an access to space images provided by both its western and Russian partners.

In the recent 10 years, research and applied activity in the field of remote sensing and geographic information systems is continuing. A digital map of the **Central Balkan National Park** is being created, a project for preservation of biological diversity funded by a Bulgarian-Swiss program.

The Institute is licensed to distribute images through the Russian state company **SOVINFORMSPUTNIK**. A contract has been signed with the Greek center for space images **Space Imaging Europe S.A.** about the space images taken from the American satellites **IKONOS**.

The Institute relies on its high-quality experts and equipment (Silicon Graphics and Numelec) for the processing of these images. It has the opportunity to work with the Ministry of Agriculture in relation with the identification of crop quality, the Ministry of Ecology in relation with soil, water, atmospheric, and transborder pollution, mapping of Bulgaria etc.

Systemizing, archiving, and storage of space data is an important element of the activity of the SRI. The interest of some western scientist to our data from **Intercosmos Bulgaria 1300** is notable. In 2001, an agreement was signed with the SRI, Moscow, for joint activity in this field.

Another source of funding shall be the reasonable use of our equipment. The best way to utilize this equipment is:

- to temporarily rent part of the equipment should its being used by ourselves be impossible;
- selling of part of the outdated and multiple equipment so as to accumulate the minimal operative funds needed for buying of new equipment providing for carrying out of modern research.

In conclusion, I would like to point out that pragmatic course of development the Space Research Institute assumed in the recent years will undoubtedly **provide a definite answer** to the question haunting our society in the present hard economic reality: **Does Bulgaria really need to conduct space research nowadays?**

#### **Summarru**

- In paper is shown chronology of creation and development on Space Research Institute and observed the most important periods.
- Conception for SRI activities in new condition in Bulgaria is shown.

1 – Interinstitutional Committee at the Council of Ministers

2 – STATE

3 – Bulgarian Academy of Sciences

4 – Aerospace Agency

5 – budget allowance

6 – transfer of foreign technologies

7 – SRI-BAS

8 – scientific research

9 – space projects and experiments

10 – Space Device Construction

11 – business trips

12 – conferences

13 – scientific research

14 – Technological Equipment

*Cosmos Scientific Production Enterprise*

15 – auxilliary production

16 – TRANSFER

17 – MARKET

18 – MANAGEMENT

19 – ecology

20 – industry

21 – agriculture

22 – security

23 – communication

24 - % PROFIT

25 – information flows

26 – financial flows

27 – SPACE DESINGS AND TECHNOLOGIES RESULTING FROM INTERNATIONAL COLLABORATION  
space designs and technologies resulting from international collaboration

28 – COMPETITIONS  
competitions

29 – SPACE EDUCATION  
education

30 – NATIONAL

31 – REGIONAL - UN

## Data Processing of Microwave System R-400 on Board of the MIR Space Station

N. G. Bankov, L. J. Todorieva

In the end of 1996, on board of the MIR Orbital Space Station was activated the microwave system R-400 [1] (launched in orbit in the spring of the same year) as a part of the complex of research instrumentation for remote sensing of the Earth. The system provides for implementation of the experiments from the Priroda Project [2]. R-400 is a scanning radiometer that observes the earth's surface under an angle of  $40^\circ$  relative to the vertical axis of the station while the scanning system provides 40 scans through 0.1 seconds with wideness of the scanning angle along the horizontal line  $72^\circ$ ; i.e. with respect to the movement's direction, scanning is performed in the interval  $[-36^\circ, +36^\circ]$ . To obtain a correct picture of the observed earth stripe it is necessary to find with maximal accuracy the coordinates of the borders and the center of the spot, from which the device registers data at each given moment. The coordinate systems used for data processing are:

**Oxyz** - geocentric equatorial system with origin in the mass center of the Earth O,

axis **x** - directed to the point of the vernal equinox,

axis **z** - coincides with the axis of earth's rotation directed to the north pole,

axis **y** - complements the system to a right-handed one;

**Sabc** — baro-centric orbital system (fig. 1a) with origin in the spacecraft mass center S,

axis **c** - collinear to the radius-vector along its increasing direction,

axis **b** - directed along the normal of the orbital plane,

axis **a** - complements the system to a right-handed one;

**S $\alpha\beta\gamma$**  - satellite system, stationary linked with the spacecraft construction axes, with origin in S;

$O r_o \varphi_g \lambda_g$  - geographic system,  $r_o$  - radius vector,  $\varphi_g$  - geographic latitude,  $\lambda_g$  - geographic longitude.

The problem of computing of the navigation data, needed for processing and visualization of the received information, can be divided in two separate processes:

a) estimation of the satellite coordinates **S(x<sub>s</sub>, y<sub>s</sub>, z<sub>s</sub>)** and the velocity vector **v(x<sub>v</sub>, y<sub>v</sub>, z<sub>v</sub>)** relative to **Oxyz** for a given value of the time **t**;

b) estimation of the spot center coordinates in **Oxyz** for the same moment **t**.

Since the first problem is a part of each research space experiment data processing task it is well-known. For this reason it will not be considered here. We will only assume that for any **t**, the values of **(x<sub>s</sub>, y<sub>s</sub>, z<sub>s</sub>)** and **(x<sub>v</sub>, y<sub>v</sub>, z<sub>v</sub>)**

needed to find the coefficients of the transition matrix to migrate from **Sabc** to **Oxyz**, can be obtained calling some procedure.

The position of the instrument and the motion parameters of the scanning device are known relative to the satellite coordinate system **Sαβγ**. In general, the current orientation of the station, respectively of the device, must be determined by the help of angles:  $\theta=\theta(t)$  - rotation about an axis **b** (pitch),  $\varphi=\varphi(t)$  - rotation about an axis **a** (roll),  $\psi=\psi(t)$  - rotation about an axis **c** (hunting) that account for the current state of the axes of the satellite system relative to the orbital one. These angle values are calculated by processing the orientation system sensors' data (solar, star, magnetic, etc.). A method for estimation of the current orientation using data from solar sensors, a magnetometer, and angle velocity sensors can be found in [3].

In the case discussed here, the values of these angles are not available, but it is known that, before the beginning of the measurement cycle, the station is rotated so that the axes of the satellite system coincide with those of the orbital one, i.e.  $\theta=\varphi=\psi=0$ .

To calculate the coefficients of the transition matrix to change from **Sabc** to **Oxyz**, we need the directivity cones of the angles between the corresponding axes. For the coordinates of the unit director vectors of the coordinate axes of **Sabc** relative to **Oxyz** we obtain:

$$e_c(c_1, c_2, c_3) = \frac{\overline{OS}}{|\overline{OS}|}, \text{ i.e. } c_1 = x_s/c, c_2 = y_s/c, c_3 = z_s/c, c = \sqrt{x_s^2 + y_s^2 + z_s^2};$$

$e_b(b_1, b_2, b_3)$  - normal to the orbital plane with an equation

$$m: \begin{vmatrix} x - x_s & y - y_s & z - z_s \\ x_v & y_v & z_v \\ x_s & y_s & z_s \end{vmatrix} = 0,$$

After appropriate calculations we obtain

$$b_1 = b_x/b, b_2 = b_y/b, b_3 = b_z/b, b = \sqrt{b_x^2 + b_y^2 + b_z^2},$$

where  $b_x = y_s z_v - z_s y_v$ ,  $b_y = z_s x_v - x_s z_v$ ,  $b_z = x_s y_v - y_s x_v$ ;

$e_a(a_1, a_2, a_3)$  complements the system to right-handed coordinate one, i.e.

$$a_1 = b_2 c_3 - b_3 c_2, a_2 = b_3 c_1 - b_1 c_3, a_3 = b_1 c_2 - b_2 c_1$$

Note that, as far the orbit of the station is quite near to circular,  $e_a$  almost coincides with the velocity vector.

Now point **M** with coordinates  $(a_m, b_m, c_m)$  in **Sabc**, relative to **Oxyz** will have coordinates:

$$\begin{aligned} x_m &= a_1 a_m + b_1 b_m + c_1 c_m + x_s \\ y_m &= a_2 a_m + b_2 b_m + c_2 c_m + y_s \\ z_m &= a_3 a_m + b_3 b_m + c_3 c_m + z_s \end{aligned} \quad (1)$$

Now, let us denote by  $t_n$  the start time of the n-th scan and let us assume (for definiteness) a left-right motion, i.e. at this moment the scanning head is initialized to the left end, ready to move right. Also, let us denote by  $\lambda_k = \lambda_0 - (k-1)\Delta\lambda$  the angle between the axis  $\mathbf{a}$  and the projection of the directivity device arrow on the plane  $\mathbf{Sab}$ , with  $\mu$  the angle between arrow and axis  $-\mathbf{c}$ , with  $t_k = t_u + (k-1)\Delta t$  the time of the momentary (k-th) measurement,  $\lambda_0 = 36^\circ$ ,  $\Delta\lambda = 72^\circ/39$ ,  $\mu = 40^\circ$ ,  $\Delta t = 0.1\text{sec}$ ,  $k = 1.40$ . When  $t = t_k$ , the vector  $l^k$  (fig.1b), collinear with the device directivity arrow, will have in  $\mathbf{S}^k\mathbf{abc}$  coordinates:

$$l_a = \sin(\mu)\cos(\lambda_k), l_b = \sin(\mu)\sin(\lambda_k), l_c = \cos(\mu).$$

Then the line, representing the directivity arrow, will have parametric equation

$$\mathbf{g}_k: [\rho\sin(\mu)\cos(\lambda_k), \rho\sin(\mu)\sin(\lambda_k), -\rho\cos(\mu)].$$

Replacing the coordinates of  $\mathbf{g}_k$  in the equation of the sphere

$$\mathbf{s}_k: (\mathbf{x}-\mathbf{o}_a)^2 + (\mathbf{y}-\mathbf{o}_b)^2 + (\mathbf{z}-\mathbf{o}_c)^2 = r^2$$

that approximates the earth ellipsoid (by Krasovsky), where  $\mathbf{o}_a, \mathbf{o}_b, \mathbf{o}_c$  and  $r$  are respectively the coordinates of the Earth mass center in  $\mathbf{S}^k\mathbf{abc}$  and the radius-vector of the projection point, we achieve a quadratic equation for  $\rho$ . Solving the equation and denoting the smaller root by  $\rho_1$ , we obtain the coordinates of the center of the spot  $\mathbf{P}$  in  $\mathbf{S}^k\mathbf{abc}$

$$a_p = \rho_1\sin(\mu)\cos(\lambda_k), b_p = \rho_1\sin(\mu)\sin(\lambda_k), c_p = -\rho_1\cos(\mu),$$

from where, using (1), we can go over into  $\mathbf{Oxyz}$ , and thus problem (b) is solved.

The boundary line of the spot on the earth surface for  $t = t^k$  can be determined by finding the coordinates of the cross-points of the sphere  $\mathbf{s}_k$  and the generating arrow of a circular cone with a central axis  $\mathbf{g}_k$ , vertex  $\mathbf{S}$  and cone angle  $\delta$ . Similarly to the determination of  $\mathbf{g}_k$ , we search for the coordinates of a vector through  $\mathbf{S}$ , collinear with the generating arrow. For this reason, let us look at the system  $\mathbf{S}l^k$  where the orientation of  $l$  and  $l^k$  is not important. It can easily be seen that vector  $\mathbf{h} = \mathbf{h}(\eta)$  with coordinates

$$[\sin(\delta)\cos(\eta), \sin(\delta)\sin(\eta), -\cos(\delta)], \eta \in [0, 2\pi]$$

is a generating line of a cone with central axis  $l^k$  and angle between them  $\delta$ . To determine its coordinates related to  $\mathbf{S}^k\mathbf{abc} \equiv \mathbf{S}^k\alpha\beta\gamma$ , we use the fact that the angle determines such a rotation of  $\mathbf{S}^k\mathbf{abc}$  that the axis  $\mathbf{c}$  coincides with  $\mathbf{g}^k$  and the unit vector of the negative semi-axis  $[0, 0, -1]$  coincides with  $l^k$ . Really, when one rotates  $\mathbf{S}^k\mathbf{abc}$  about the axis  $\mathbf{c}$  on an angle  $\lambda_k$ , after that, on an angle  $\mu$  about the axis  $\mathbf{b}$  for the transition matrix we obtain

$$\mathbf{W}(\mathbf{0}, -\mu, \lambda_k) = \begin{pmatrix} \cos(\lambda_k)\cos(\mu) & -\sin(\lambda_k) & -\cos(\lambda_k)\sin(\mu) \\ \sin(\lambda_k)\cos(\mu) & +\cos(\lambda_k) & -\sin(\lambda_k)\sin(\mu) \\ \sin(\mu) & \mathbf{0} & \cos(\mu) \end{pmatrix}$$

from where it is easy to verify that  $l = \mathbf{W}(\mathbf{0}, -\mu, \lambda_k) * [\mathbf{0}, \mathbf{0}, -1]$ . Then, for the coordinates of  $h$  we will obtain  $[h_a, h_b, h_c] = \mathbf{W} * [h_i, h_j, h_k]$ .

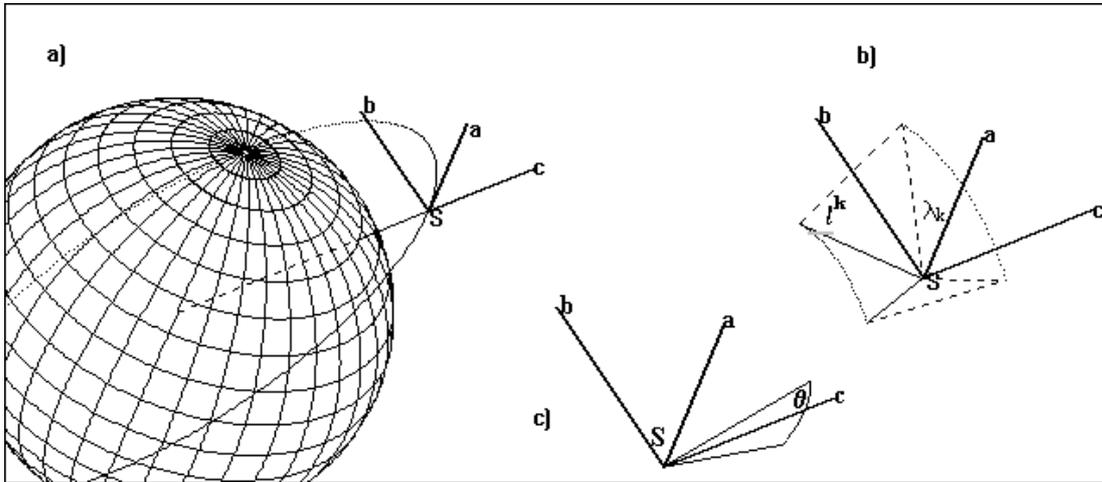


Fig.1

The formulae derived so far were obtained under the assumption  $\theta = \varphi = \psi = \mathbf{0}$ , i.e.  $\mathbf{S}^k \mathbf{abc} \equiv \mathbf{S}^k \mathbf{\alpha\beta\gamma}$ . Let us now discuss briefly the case when this is not true, i.e. the stabilization of the station is disturbed and it drifts about its mass center  $\mathbf{S}$ . Let us assume that one of the angles  $\theta\varphi\psi$ , e.g.  $\theta$ , oscillating around the axis  $\mathbf{b}$  (Fig. 1c), is not 0. The case  $\varphi \neq \mathbf{0} \wedge \theta \neq \mathbf{0} \wedge \psi \neq \mathbf{0}$  will differ only in the transition matrix coefficients of  $\mathbf{W}(\varphi, \theta, \psi)$ . The coordinates of the unit directivity vectors  $\mathbf{e}_\alpha, \mathbf{e}_\beta, \mathbf{e}_\gamma$  of the coordinate axes of  $\mathbf{S}^k \mathbf{\alpha\beta\gamma}$  are to be found from  $\mathbf{e}_\alpha, \mathbf{e}_\beta, \mathbf{e}_\gamma$  by multiplication from the left with  $\mathbf{W}(\mathbf{0}, \theta, \mathbf{0})$  and then formula (1) where  $\mathbf{a}_i, \mathbf{b}_i, \mathbf{c}_i$  have been substituted respectively by  $\alpha_i, \beta_i, \gamma_i, i=1..3$ , will perform the transformation from  $\mathbf{S}^k \mathbf{\alpha\beta\gamma}$  into  $\mathbf{Oxyz}$ . The equations for  $\mathbf{g}_k$  and  $\mathbf{s}_k$  remain the same, and the coordinates of the Earth center for  $\mathbf{s}_k$  should be recalculated for  $\mathbf{S}^k \mathbf{\alpha\beta\gamma}$ . As a result of the calculations following the algorithm described above we obtain a data set containing the measured values and their coordinates in  $\mathbf{Oxyz}$ , from which a transition into geographical coordinate system  $\mathbf{Or\phi\lambda}$  must be made where it is enough to remember only  $\varphi$  and  $\lambda$  ( $\mathbf{r}$  can be obtained as a function of  $\varphi$ ). However, the information increases considerably, because for each number of the incoming data we have added  $2M+2$  numbers. What amount of this information is to be stored in the data base (or another type of archiving) depends of the research problems to be solved as well as on the capacity of the PC. If the error resulting from the approximation of the outlines of the area by an ellipse is assumed tolerable and the points are selected properly, then  $M$  can be equal to 3.

In the discussed algorithm, it is indirectly assumed that the telemetry and read-write data systems behave normally. But in fact, maybe due to an error

in the system exchanging data with the buffer storage (memory) of the telemetric system, the data from the strobes whose numbers lies in the intervals [9-16] and [25-32] repeat the information of the preceding strobe group, i.e. [1-8] and [17-24], respectively. So, at the input of the data processing system, “authentic” is only the data from [1-8], [17-24] and [33-40]. (Let us note that exactly this situation was the reason to discuss the problem of coordinates estimation of the spot boundaries, thus obtaining the possibility to consider the instrument as a tracing one).

It is natural to try to recover missing data with the help of mathematical methods and the problem we want to solve can be described in two ways:

- to recover the indications of the n-th scan by using only data from the same scan,
- except for the indications of the n-th scan, scans from 2K neighbor scans are used,  $K \geq 1$ .

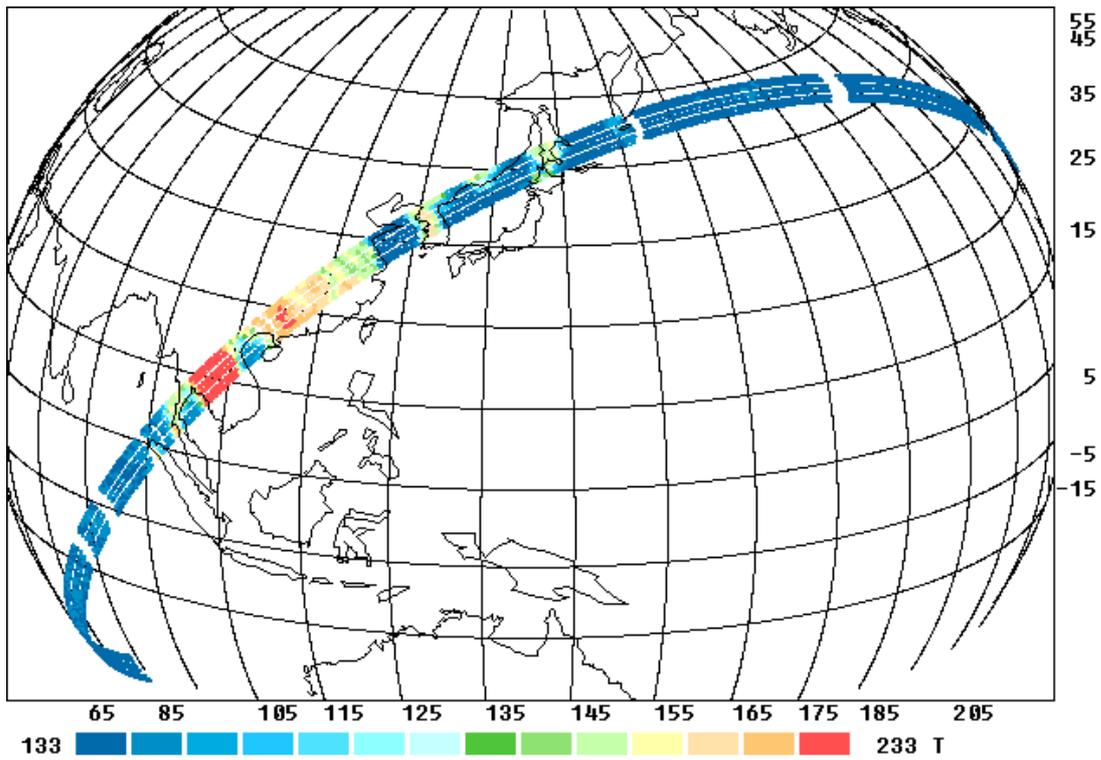
The plots shown below represent the results from solving the first problem by the spline approximation procedure.

In Fig. 2, orbit No292 from 26.01.97, or a “tracing” version is shown. The non-realistic behavior of the color range is due to the inadequate reproduction of RGB-set by BW-printing.

In fig. 3, a fragment of the same orbit is shown.

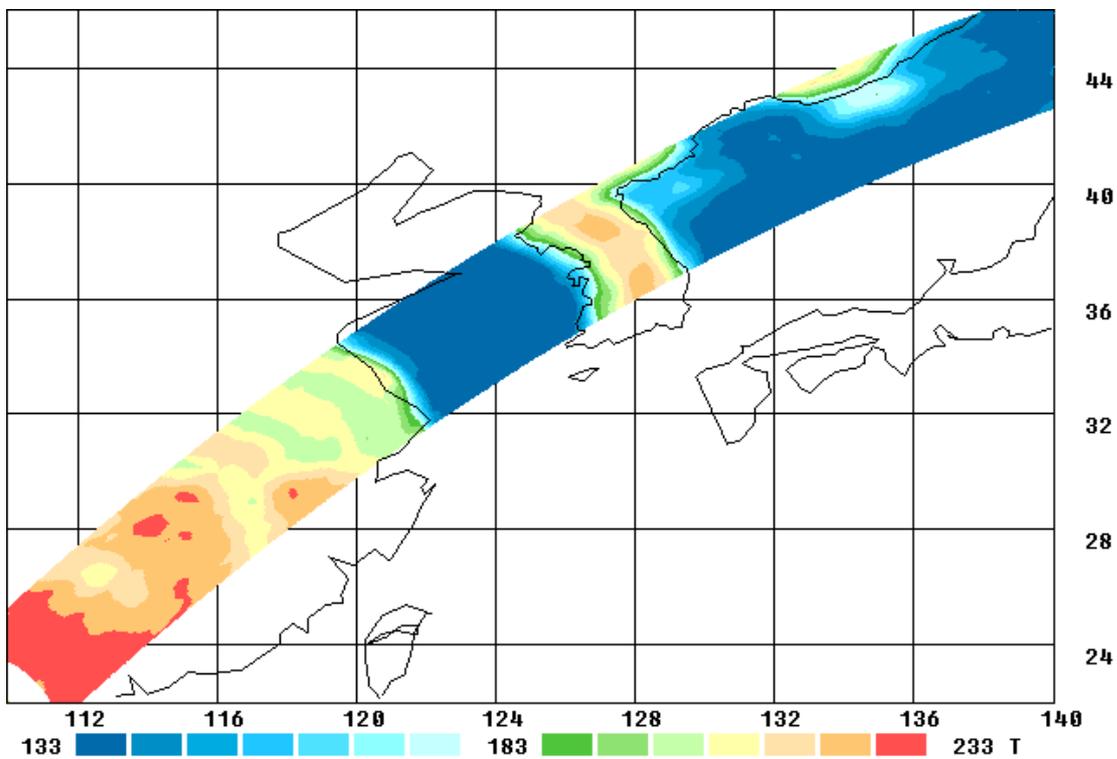
### Literature:

1. T. Nazarski, G. Dimitrov, Ch. Levchev, The Basic Principles Determining the Operation of the Microwave Scanning Radiometric System R-400, Turk. J. of Physics, 19(1995), pp. 1059-1062.
2. Scientific Program of the “PRIRODA” International Project, Moskow 1991.
3. Īĕāīāāđīā Ī.Ĕ., Ī.Ā.Ýĕüŷñāāđā, Īāđīāĕĕā ĩđāāāĕĕāīĕŷ ōāĕĕĕ÷āñĕĕĕ ĩđĕāīđāĕĕĕ ĔÑÇ “Ĕīđāđĕĕĩĩĩ-Āīĕĕāđĕŷ-1300”, ĔĔĔ ĀĪ ĨÑÑĐ, ĩđ - 785, 1983.



PRIRODA: R-400 / ORBIT: 2492 DMY 260197 GMT 17.24.17/18.14.19  
 Space Research Inst. of the Bulgarian Acad. of Science

fig2.



PRIRODA: R-400 / ORBIT: 2492 DMY 260197 GMT 17.46.26/17.56.06  
 Space Research Inst. of the Bulgarian Acad. of Science

fig 3

The paper describes an algorithm solving the task for calculation of the coordinates of some geometric sections on the Earth's surface resulting from some experiments for remote sensing of the Earth from space. The suggested algorithm is an essential part of the data processing software of the R-400 microwave system on board of the MIR Orbital Station.

# PRELIMINARY ANALYSIS OF THE BALISTIC PARAMETERS OF A PENETRATOR FOR ECOLOGICAL STUDIES

*Garo Mardirossian, Dimitar Danov\**

*Space Research Institute, Bulgarian Academy of Sciences, 1113 Sofia*

*\* Central Laboratory for Solar-Terrestrial Influences, Bulgarian Academy of Sciences, 1113 Sofia*

## **1. Necessity**

Quite often, the necessity of making some hardware geophysical and ecological studies in hardly accessible places of the Earth arises. Examples of such places are the active volcanic areas, the epicentres of calamitous earthquakes, the polar and desert areas, the radiation-hazardous areas (for instance, the areas of nuclear-power-plant failures), the flooded areas, the gas-penetrated areas, the areas with thick snow cover, etc. In all these cases, the instalment of the relevant equipment involves a lot of difficulties and risks for the engaged people, and very often it is even impossible.

To a certain extent, the problem can be solved by using a penetrator with geophysical and ecological equipment mounted in it. Usually, The penetrator consists of two parts. When launched by an aircraft, in most cases, its basic body penetrates the ground. Whereas the depth of penetration depends on a number of factors: the velocity at the moment of accessing the ground, the mechanical characteristics of the ground, the geometric characteristics of the fore part of the penetrator, its mass etc. The other part of the penetrator remains above the Earth's surface, mainly with purpose of providing reliable radio connection. Having in mind the fact that the goal here is to fix the device into the ground, rather than penetrate it (see item 4), the term "penetrator" is somewhat provisional.

## **2. Prerequisites**

One prerequisite for the development of a penetrator for ecological studies was the studies of the three-component penetrator accelerometer for studying the Mars planet under the "Mars'94" project [1,2]. Another important prerequisite was the tiny and minimal-power-consumption means of telemetric data transfer.

Naturally, the scientific tasks and the conditions for penetration of Mars's surface differ in many ways. They depend on both the technical and technological possibility for

launching the penetrator (height, initial velocity, trajectory, velocity of accessing the ground, mass and geometric characteristics of the penetrator, etc.), and the characteristics of the atmosphere and the ground at the site of penetration of Mars or the Earth, respectively.

### **3. Scientific program**

The concrete scientific program for ecological studies with a penetrator depends on the concrete object, goals, and tasks. Hardly any discussion is needed to substantiate the statement that ecological studies are, in their essence, geophysical studies, since they are aimed at studying the physical and geophysical parameters of the surrounding medium. The same fact refers to the ecological calamities of natural and anthropological origin which are, in fact, extreme changes of these same parameters [3]. For this reason, in most cases, the scientific problems, related to penetrator studies, are studies of some geophysical parameters: temperature, humidity, micro- and macro-seismic oscillations, radiation background, etc.

### **4. Differences between the penetrator studies of Mars and the Earth**

Several fundamental differences between a "marsian" and an "earth" penetrator can be pointed out.

The purpose of the marsian penetrator is to penetrate to relatively greater depth, so that it can operate within smaller temperature range, having in mind the marsian diurnal range, which is about 50°C. However, the penetration to greater depth  $H$  necessitates greater initial velocity of penetration  $V_0$ . But this greater velocity involves greater shock acceleration, the value of which is limited by the shock-resistance of the scientific-research and official equipment. On the other hand, the greater shock generates seismic waves with greater amplitude range, which provides a more effective amplitude and frequency registration of the reflected waves. Besides, the greater penetration time  $t$  provides greater resolution of registration during the penetration process [4].

With the earth penetrator, the change of temperature is not so important to the equipment's operation. The penetrator for geophysical and ecological studies must not penetrate to a great depth. It must be solidly fixed into the ground. As for the artificial generation of seismic waves, dropping from an aircraft of special weights with prescribed

mass, from prescribed height, and a prescribed distance away from the research penetrator, can generate them.

In the marsian experiment, the penetrator is launched from the board of an orbital station - an artificial satellite of Mars, which makes it rather more difficult to technologically provide the prescribed velocity with which the penetrator must access the marsian surface, i.e. the velocity  $V_0$ .

In the Earth version, this latter velocity can be provided for with great enough accuracy since the launch of the penetrator from an aircraft can be performed precisely from the prescribed height, guaranteeing the prescribed velocity in accessing the Earth's surface.

## 5. Movement of the penetrator through the atmosphere

### 5-a. Movement of the mass centre and velocity of accessing the Earth's surface

The position of a body in space is determined by six parameters: 3 co-ordinates of the mass centre (MC), and 3 rotation angles. The movement of the body is determined if the time function of these parameters is known. Often, rotation is assumed to be independent on the movement of MC. In the general case, however, this is not true.

The movement of the MC of a body, moving freely through the atmosphere, is described by the following differential equation:

$$(1) \quad m \frac{d\mathbf{V}}{dt} = -C \rho \mathbf{V} + \rho \mathbf{g}$$

where  $m$  and  $\mathbf{V}$  are respectively the mass and the velocity of MC,  $\mathbf{g}$  - the Earth's acceleration.

Besides on the parameters of the environment (density, viscosity etc.), the coefficient  $C$  depends as well on the orientation of the velocity vector as to the body. In the general case, this coefficient is a tensor (matrix), and obviously, the movement of MC depends on the body's rotation.

If the body has a symmetry axis, and the velocity of MC is parallel to this axis, then  $C$  is a scalar (a unit matrix multiplied by a scalar). In this case,  $C$  is a function of:

- 1) Mah's number ( $M=v/a$ ,  $a$  being the sound velocity);
- 2) air density  $\rho$ ;

- 3) the form of the body;
- 4) the velocity of the body.

The dependence on the other parameters (for instance, viscosity) can be neglected [5]. Then we can write:  $C=k.\rho.S.V.C_x(M)$ , where  $S=\pi.d^2/4$  - a cross-section, perpendicular to velocity (middle section);  $C_x(M)$  is a function, called resistance law, which depends on the general form of the body (but not on its size), and is usually provided in table form;  $k$  is a coefficient, depending on the concrete size (determined experimentally, and depending, in the general case, on the Mah's number, too, but in the calculations assumed to be constant).

If we replace  $C(M)=k.\pi.d^2.V.C_x(M)/8m$ , we can write (1) in the following way:

$$(2) \quad \frac{d\mathbf{V}}{dt} = -\mathbf{C}(M).\mathbf{V} + \mathbf{g}$$

If we choose a co-ordinate system with axis  $Oy$  directed vertically upwards, horizontal axis  $Ox$  such that the velocity be lying in the  $xOy$  plane, and axis  $Oz$  supplementing the coordinate system to a right-oriented one, then (2) can be written as follows:

$$(3) \quad \left\{ \begin{array}{l} \frac{dV}{dt} = -\mathbf{C}(M)\rho V^2 - \mathbf{g} \sin(\lambda) \\ \frac{d\lambda}{dt} = -\frac{\mathbf{g} \cos(\lambda)}{V} \\ \frac{dx}{dt} = V \cos(\lambda) \\ \frac{dy}{dt} = V \sin(\lambda) \end{array} \right.$$

where  $\lambda$  is the angle between the velocity vector  $V$  and the axis  $Ox$ . In the case of a body falling downwards,  $\lambda < 0$  and the earth gravitation force  $g \sin \lambda$  and resistance  $C(M).\rho.V^2$  are opposite whereas with a body rising upwards,  $\lambda > 0$  and the forces are parallel.

In the general case, the system of differential equations (3) can be solved only numerically at least because  $C_x(M)$  is provided in table form. Besides, the density  $\rho$  depends on height, in a complex way on temperature, season, and solar activity. The sound velocity (and from there,  $M$ ) depends on temperature and density  $\rho$ . Temperature

is a function of height etc. Tables and algorithms for the determination of  $C_x(M)$  and  $\rho$  are given in [5]. The coefficient  $k$  is determined experimentally.

Here, an analytical solution of system (3) for one simple case is suggested, namely for the case of launching the penetrator from an airplane. This has a number of advantages since it provides a better choice for the penetration site, launching from a smaller, and more precisely determined height, tracing the process of launch and penetration etc. The use of an airplane is better justified for a number of organizational, technological, and economic reasons, too, moreover when regions of ecological calamities are concerned.

In this case, the movement proceeds only along the vertical, i.e.  $\lambda = -\pi/2$ , the velocity  $\mathbf{V}$  changes a little and within limits where  $C_x(M)$  remains nearly constant (these are velocities up to 0,7 of the sound velocity:  $V < 0,7a$ ), the body passed a distance within which the change of the density of the medium  $\rho$  is insignificant. Then in (3),  $C(M) = c = \text{const}$ , and (3) is transformed into:

$$(4) \quad \left\{ \begin{array}{l} \frac{d\mathbf{V}}{dt} = -c\mathbf{V}^2 + \mathbf{g} \\ \frac{d\lambda}{dt} = 0 \\ \frac{d\mathbf{x}}{dt} = 0 \\ \frac{d\mathbf{y}}{dt} = -\mathbf{V} \end{array} \right.$$

The second and third equations in (4) show that the movement will remain directed along the vertical. If we assume the initial velocity  $V=0$ , the first equation of (4) will have the following analytical solution:

$$(5) \quad \mathbf{V}(t) = \sqrt{\frac{\mathbf{g}}{c}} \cdot \mathbf{tgh}(t\sqrt{\mathbf{g}c})$$

After substituting (5) in the last equation in (4) and assuming the initial shift to be zero, we obtain:

$$(6) \quad \mathbf{y}(t) = -c^{-1} \ln(\mathbf{ch}(t\sqrt{\mathbf{g}c}))$$

It can be shown that  $\mathbf{V}(t) \xrightarrow{c \rightarrow 0} \mathbf{gt}$ , and  $\mathbf{y}(t) \xrightarrow{c \rightarrow 0} \mathbf{gt}^2 / 2$ . Thus, with negligibly small aerodynamic coefficient, (5) and (6) are the solutions for a free-falling body.

The solution here obtained has at least two advantages over the numerical integration over (4): i. it can be found by calculator; ii. it is not sensitive to the chosen method or step of integration.

In this case, the most essential thing is that equations (5) and (6) allow for the time to be excluded, and the velocity to be determined as function of height. As shown in [3], under given physic-mechanical properties of the ground, and geometric characteristics of the penetrator, the penetration depth  $H$  depends directly on the velocity  $V_p$ , with which the earth's surface is accessed.

If  $t$  can be found from (6) and substituted in (5), we get:

$$(7) \quad \mathbf{V} = \mathbf{exp}(\mathbf{c} \cdot \mathbf{h}) \sqrt{\frac{\mathbf{g}}{\mathbf{c}}} \sqrt{\mathbf{exp}(-2 \cdot \mathbf{c} \cdot \mathbf{h}) - 1}$$

where  $h$  is the launch height.

With negligibly small aerodynamic coefficient, we have  $\mathbf{V} \xrightarrow{c \rightarrow 0} \sqrt{2\mathbf{gh}}$ , which is the well-known relationship for a free-falling body.

To approximately calculate the relationship  $V=V(h)$ , the following values are assumed: sound velocity  $a=340,294$  m/s, mean atmospheric density  $\rho=1,225$  kg/m<sup>2</sup>, resistance function  $C_x(M)=0,255$  (if  $0 < M < 0.7$ ). These are the average atmospheric parameters for heights up to 1000 m and temperature  $T=290$  K [5].

In Fig.1, the relationship  $V=V(h)$  according to (7) is shown, with aerodynamic coefficient ( $\mathbf{C}(\mathbf{M}) = \mathbf{k} \rho \pi \mathbf{d}^2 \mathbf{C}_X(\mathbf{M}) / 8\mathbf{m} = 3.10^{-4} \mathbf{k}$ ), penetrator diameter  $\mathbf{d}=25$  cm,  $\mathbf{m}=25$  kg). For comparison, the curves for  $k=1$  (curve 2),  $k=2,5$  (curve 3) and the case of a free-falling body (curve 1), are shown.

As might be expected, the atmospheric influence on velocity increases with increase of the launch height.

The error that would be made had the atmospheric resistance been not accounted for, is illustrated in Fig.2 for three different launch heights: 800 m (curve 1), 500 m (curve 2), and 300 m (curve 3). On the X-axis, the value of the form coefficient  $\mathbf{k}$  is

marked. As it was said already, it depends on the concrete size of the penetrator and should be determined experimentally. For most elongated bodies, its value is between 0,1 and 3.

### **5-b. Flugler stability of the penetrator**

An essential condition is that the penetrator must access the earth's surface with its fore part, the angle of ground attack being close to  $90^\circ$ . It is well-known that a body, moving through the atmosphere, as a result of the generated aerodynamic moments, displays the tendency to rotate itself around its axes. To diminish this rotation, the penetrator must rotate about its vertical axis. Thus, as a result of the law for conservation of the quantity of motion, it will try to preserve the direction of this axis. Besides, it is necessary that the centres of gravity and aerodynamic pressure be far from one another, the centre of gravity being lower than the centre of aerodynamic pressure.

These requirements naturally impose an elongated form for the penetrator, as well as the eventual provision of stabilizers.

## **6. Conclusion**

With other values of  $m$  and  $d$ , the values obtained for the coefficient of aerodynamic resistance  $c$  are different. For instance, with the standard aviation bomb, in which  $m$  is considerably greater than the value assumed in the present modelling, and the ratio between the length  $L$  and the diameter of the middle section  $d_m$  is:  $L/d_m \cong 5$ , the result shows that air resistance can be neglected. The modelling made here provides the option to decide where the above value can be neglected, depending on the penetrator's mass-size characteristics and launch conditions.

The present works lays the beginning of a pioneer (in the authors' estimation) development to the design of a technical mission for the construction of a penetrator for geophysical and ecological studies, as well as for the formulation of the scientific problems in these studies. We consider the performed preliminary analyses and obtained first results to be merely the basis for further continuation of the development.

R e f f e r e n c e s

1. M a r d i r o s s i a n, G., V. F r e m d. Some apparatus Problems concerning the seismological research of the Mars and the possibilities for their solution. 40th Congress of the IAF, Malaga, 1989, IAF - 89 -487.
2. M a r d i r o s s i a n, G., D. K o l a r o v, V. F r e m d et al. The Performance of a Penetrator Accelerometer for Mars Exploiration - Approach and Initial Results. COSPAR, The Hague, 1990.
3. Ì à ð ä è ð î ñ ý í, Ā., Ā. Í á ä ä ë ÷ á â à, Ò. Ç ä ð à â á â. Íìòèèçàòèííáí àíàèèç íà òáðíèèí-âèñíèíàðòòèííèðòá òàðàèðòáðèñòèèè íà íáíáððòáðíðáí àèñáèáðííáðúð çà ñàèçíèííè÷-íè èçñèáááàíèý íà íèàíáðàðà Ìàðñ. Āáðíèíí. èçñèáá. â Áúèáàðèý, N 9, 1993, ñðð. 31–36.
4. Ì à ð ä è ð î ñ ý í, Ā., Ā. Ó ð á ì ä. Òðáðèííííðíúé íáíáððòáðíðíúé àèñáèáðííáðð äèý èññèááíáàíèý Ìàðñ. Āáðíèíí. èçñèáá. â Áúèáàðèý, N 8, 1991, ñðð. 39-46.
5. Í î ñ ò í è ê î á, Ā., Ā. × ó é ê î. Āíáðíáý áàèèèñòèèà íáóíðàáèýáíúð ààèàòèííúð ðàèáð è ñíàðýáí. Ìàèèíðððíáíèà, Ìíèèà, 1985, 248 ñðð.

## Preliminary Analysis of some Ballistic Parameters of a Penetrator for Ecological Studies

*Garo Mardirossian, Dimitar Danov*

### ( S u m m a r y )

Quite often, it is necessary to perform some instrumentation geophysical or ecological studies at hardly accessible sites of the Earth: active volcanoes, epicentres of calamitous earthquakes, polar or desert areas, areas with radiation danger, flooded territories, gas-invaded areas, areas covered by deep snow cover, etc. In all these cases, instrumentation mounting is related with great difficulties and much risk for the people, and sometimes it is even impossible.

The paper is dedicated to an optional solution of the problem, namely the design of a penetrator for ecological and geophysical studies. Based on the expertise wiith the development of a penetrator accelerometer for studying of the Mars planet, analysis and preliminary calculations of some major technical-operational parameters of a penetrator with geophysical equipment mounted on it are made. The obtained results can be considered as the first step in this direction. They provide grounds for the development of a technical statement and a relevant research program.

$$\sqrt[3]{\frac{0.7}{8}} = 0.255$$

$$(C(M) = k \rho \pi d^2 C_x (0.7) / 8m = 3.10^4 k)$$

$$C(M) = k \rho \pi d^2 C_x (0.7) / 8m = 3.10^{-4} k$$

# MONITORING THE STUDEN KLADENETS RESERVOIR USING AIR AND SPACE IMAGES

*Georgi Jelev, Eugenia Rumenina*

*Space Research Institute, Bulgarian Academy of Sciences*

## **Introduction**

The observation and control of the state environment by air and space instrumentation is a subsystem of the monitoring system. The successful operation of the monitoring system depends on the precision of the standard and remote sensing measurements and observations, the GIS-data base and on the systems for prompt data transmission to the management authorities. In the developed countries in the last decade for the environment monitoring more and more local geographic information systems are built which use air and spatial images as the basic source of information [1]. For the territory of Bulgaria, and in particular for study of the dynamics of artificial humid zones, these methods are not much applied yet. As for the artificial humid zone Studen Kladenets reservoir such a local GIS is not yet instructed. This area changes periodically its state, different types of land cover (TLC) appearing on the drained lands. The objective of this study is to establish the changes of the land cover after the reservoir was built, as well as to trace out the water surface dynamics at different benches of water level. To the fulfillment of this goal, GIS data-base is created describing the structure and dynamics of the land cover in this region.

## **Studied area**

Reservoir Studen Kladenets is located in the Mid-Arda region of the East Rhodopian sub region of the Rila-Rhodope massif. In morphographic, respect the region around the reservoir is distinguished by the wide development of the hill type relief within the 200-600 m sea level zone. The reservoir shores are

bounded to the north by the rock Kayadjik talus hill. The slopes of the different hills are steep, deforest area and strongly eroded.

The great lithological variety, the multiple and fast alternation with different properties determine the great activity and clearly expressed selectivity of denudation in the examined region. A number of landslide events are related with it. They provide the initial material for the solid runoff of the rivers in the watershed of Studen Kladenets reservoir. The geological pattern of the region is formed by rocks of the polyphase Palaeogenic volcanism and the lava and pyroclastics connected with it [2]. The acid differentiates of this volcanism predominating in the region are a prerequisite for the formation of relatively high single structures situated along the reservoir shores. These are: Saint Ilia, Dambalak, Perperek, Hisar, Studen Kladenets. The reservoir itself is the northern border of a big volcano-tectonic depression – Nanovishka (**Appendix 1**).

Later, during the Miocene and Pliocene, the volcanogenic relief was greatly transformed without being completely changed and at that time, the foundations of the modern hydrographic network and its orientation were laid.

Studen Kladenets reservoir was built up in 1957. It is a hydrotechnical equipment including: gravity dam with height of 71.0 m, full volume of 489 million m<sup>3</sup> of which death storage of 150 million m<sup>3</sup> and lake area of 25.6 km<sup>2</sup>, overflow water level bench of 255 m and death storage bench of 208 m. On the reservoir left shore, in its tail, the “Kardjali” lead-zinc plant is located built, in 1955.

The precipitation fallen on the watershed does not wholly flow away. Part of it gets into the earth layers, the other part evaporates. For the watershed, area of the reservoir the runoff coefficient is highest in January, there after to attain its lowest values in September. Then, only about 14% of the precipitation amount flows into the reservoir. The mean yearly runoff coefficient is 0.47 while the runoff coefficient assumed when the reservoir was designed was 0.52.

The reservoir watershed is slightly wooded with completely bare regions at some places featuring fragile, easily erosive soils, which facilitate intensive erosion. On the other hand, the atmospheric and geomorphologic conditions favor greatly the formation of big quantities of solid runoff. This increases the quantity of bottom and floating sediments, which form the mechanic pollution of the reservoir. They determine the mechanical and chemical water composition. The floating sediments of mechanic origin are predominantly gravel, sand and traces of waste from the lead-zinc plant and the ore dressing factories along the valley of the Arda River.

On the reservoir right is the Valchi dol reserve (774.7 ha). Its territory is a representative biom for the Mediterranean zone with respect to ornithofauna. In it, on data of P.Yankov et al. [3] 7 bioms of little spread species are existing, typical for this zone from an altogether 9 for Bulgaria. The region around Studen Kladenets reservoir includes 205 species of birds, including 52 species introduced in the Red Book of Bulgaria and 117 species of European environmental protection importance [3].

### **Materials and methods**

The main information sources used are given on Table 1. The present work integrates two technologies – geographic information systems and remote sensing methods. The processing of the available information passed through several stages, the most important ones being:

1. Creating the foundations of GIS data base by using information from topographic and thematic maps. It the following characteristics: reservoir borders, geology, soil, relief and land cover before the reservoir was built.
2. Construction of a 3D spatial model of the reservoir lake and the adjacent area.
3. Performing a computer visual interpretation of air and space images surveyed during different years. Different types of land cover of the areas freed

of the water – sands, saturated area, humid grassland, wetland vegetation, brush and aborescent formation, arable land and water surface are decoded.

4. Drawing up of thematic maps.

5. Analysis of the area distribution and dynamics of the water surface of the established types of land cover.

### **Results and discussion**

In the region of the Kardjali valley expansion of the Arda, river by the construction of Studen Kladenets reservoir a local technogenic anomaly - an artificial humid zone - has been created. It arises and operates on the basis of a natural landscape which appears to be initial. The main processes running in the natural landscape continue to operate although modified in the anthropogenic one. The transformation of the natural landscape into the anthropogenic one has occurred thanks to the abrupt man's influence on several components of the environment. This has caused a change of the entire complex without the geological fundament.

After barraging the Arda River and the formation of the reservoir lake, the two flooded terraces beneath the town of Kardjali, in the reservoir tail, were eroded. A wide alluvial bed was formed. Depending on the reservoir hydrological regime, its height was either eroded or increased owing to the new silty sediments. The same is valid for the outflow sections of the Varbitsa, Perperek and Kjachukdere rivers.

Before the reservoir was built, there were 14 types of land cover on the area under investigation (Appendix 2), the sparse wood and shrubs occupying about 50% of it. After it was constructed in the zones of temporary draining, seven types of land cover were established. Their number depends on the duration of the period during which they were not flooded.

The reservoir is distinguished by large fluctuations of the water level, which are determined to a great extent by the agricultural needs and the region hydroclimatic characteristics. From the map of the water, surface change

presented in Appendix 3 it is seen that the areas of temporary flooding and draining reach up to 10.77 km<sup>2</sup>. On these lands, the hydrological regime changes abruptly and the underground water level raises in the immediate vicinity the reservoir. This causes vegetation change giving rise to water-loving plants. The unfavorable fact here is that flooding and increase underground water level of occur on some of the best agricultural lands in the region. A significant part of them, which after the reservoir was constructed were turned into shallow lands, grows over with wetland vegetation. After the interpretation of the images recording the reservoir state, at water level benches near to the death storage bench, the presence of great turbidity was established in its shallow part reaching the region of the Island. By means of the constructed 3D model, one can judge about the reservoir lake depth increase. This area appears to be a borderline with respect to the propagation of sediment material. The small water volume in this period also suggests greater concentration of sediment particles and increased water turbidity.

When decoding the air and space images surveyed in 1977, 1978 and 1992, two test areas, located in the regions of the Varbitsa river mouth and the village of Shiroko Pole have been picked out (Appendix 3, 4.). These areas are periodically drained and new types of land cover (TLC) appear on them. Let us comment in brief their change.

#### ***Shiroko Pole test area***

Before the construction of the reservoir, there were nine TLC (Appendix 4), sparse wood and shrub being spread most (more than 60%, Appendix 2). The water body including the Arda River covered only 9.2%. At the end of October 1977, the section was drained and only 5% of it is now covered by water. The greatest spread was of the saturated area (38%) and wetland vegetation (29%). 26% of the territory under investigation is of interest. It was used for growing tobacco and vegetables. In August 1978, the test area was water flooded (Appendix 4) and only 2.2% of its territory was covered with

wetland vegetation. 14 years later, in 1992, also in August, the water area was 81.8 % of its territory. A part of the drained lands (3.8%) is again used for agricultural purposes.

### ***Varbitza test area***

This area is situated in the reservoir tail and is very frequently drained (Appendix 3).

Before the reservoir was constructed the main TLC were sparse woods and shrubs occupying more than 50% of its territory (Appendix 4). Very characteristic for this area is the spread of sands, which occupy about 31.6%. In October 1977, sands (43.7%), wetland vegetation and humid grassland (Appendix 2) mainly occupied the reservoir-drained part. Here, too, 18.9% of the area territory was arable land. In August 1978, only 10% of the test area was drained and occupied by wetland vegetation and sands. In August 1992, the drained territory occupied 65%. Most widely, spread was humid grassland and arable land (Appendix 2). Brush and aborescent formation covers the southwest part of the reservoir (Appendix 4).

On data of the carried out investigations of the reservoir bottom sediments in these areas [4], increased concentrations of lead, zinc, copper, arsenic, cadmium, cobalt were sometimes surpassing 2 to 3 times the admissible norms, i.e. the lands freed from the reservoir are not fit for agricultural use.

### **Conclusions**

In the region of the Kardjali valley expansion of the Arda River with the construction of Studen Kladenets reservoir, a local technogenic anomaly, an artificial wet zone, is created.

The main processes, which have run in the natural landscape, continue to operate although modified in the anthropogenic one. After the reservoir construction the TLC in the zones of temporary draining have decreased from 14 (forests and shrubs predominating) to seven types of land cover, sands and humid grassland mainly spread.

The zone in the area next to the Island appears a borderline with respect to the sediment material spread.

In the case of draining part of the lands are used for growing tobacco and vegetables. The identified high concentrations of heavy metals give us a good reason to recommend not using these areas for agricultural practice.

The regime of the flooded terraces beneath the town of Kardjali, in the reservoir tail is abruptly changed. The flooded terraces are eroded, forming a wide alluvial bed.

The created GIS-data base will be kept expanded and supplemented with new information. This will assist the creation of a local geographic information system, which will be used for monitoring Studen Kladenets reservoir.

## **Summary**

The results of an experimental study of the Studen Kladenets reservoir using remote sensing methods and Geographic Information Systems (GIS) technologies are presented in the paper. The purpose of this study is to identify the changes on the earth land cover as a result of the reservoir construction as well as to trace out the dynamics of the water surface at different water level benches. Topographic and subject maps have been used as well as archive air photographs and images from Landsat TM. The foundations of a GIS data-base are land covering following layers: reservoir borders, geology, soil, relief and land cover before building the reservoir. A computer visual interpretation of the air and space images, taken during the different years is made. The following classes have been decoded: water surface, floating sediments of mechanical character and different types of and cover of the areas freed from water – sands, saturated areas, humid grassland, wetland vegetation, brush and aborescent formations, arable land. The data obtained are input in the GIS data-base. A 3D spatial model of the reservoir lake and its adjacent land is made as well as an analysis of the area distribution and the dynamics of the studied types of land cover.

The GIS-data base will allow the formation of a local geographic information system for monitoring of Studen Kladenets reservoir by air and space images.

## **References**

1. Rediscovering Geography, New Relevance for Science and Society - National Academy Press, Washington, DC. 1997.
2. Harkovska, A., Y. Yanev, P. Marchev. - General features of the Paleogene orogenic magmatism in Bulgaria. - Geol. Balc., 19, 1, Sofia, 1989, pp. 37-72.

3. Янков П., Х.Христов, Б.Бъров, Е.Стойнов. - Студен кладенец. В: Орнитологично важни места в България. - Природозащитна поредица БДЗП, кн. 1, Костадинова И. /съст./, С., 1997, стр. 87-88
4. Spiridnov H., E.Roumenina, L. Milenova. - Complex Investigation of a Sistem "Industrial Site-Environment" Using Remote Sensing and Landscape-Geochemical Methods. - pros. European ISY 92 Conf. Environment Observation and Climate Modelling through International Space Projects, Munich, 1992, pp. 81-88

## **МОНИТОРИНГ НА ЯЗ. "СТУДЕН КЛАДЕНЕЦ" С ИЗПОЛЗВАНЕ НА АЕРО И КОСМИЧЕСКИ ИЗОБРАЖЕНИЯ**

*Г. Н. Желев, Е. К. Руменина*

*Институт за космически изследвания - БАН*

### **(Резюме)**

В статията са представени резултатите от експериментално изследване на яз."Студен кладенец" с използване на дистанционни методи и ГИС технологии. Целта на това изследване е да се установят измененията на земното покритие, вследствие построяването на язовира, както и да се проследи динамиката на водното огледало при различни коти на водно ниво. Използвани са топографски и тематични карти, архивни аероснимки и изображение от Landsat TM. Създадената основа на ГИС-база данни включва следните слоеве: граници на язовира, геология, почва, релеф и земното покритие преди построяване на язовира. Извършена е компютърно подпомогната визуална интерпретация на аеро и космическите изображения, заснети през различни години. Дешифрирани са следните класове: водно огледало, плаващи наноси от механичен произход и различни типове земно покритие на освободените от водата площи - пясъци, преовлажнени участъци, хигрофитни тревни съобщества, блатна растителност, върби и тополи, ниви. Получените данни са въведени в ГИС-базата данни. Съставен е пространствен модел на язовирната чаша и прилежащата територия и е извършен анализ на площното разпределение и динамиката на изследваните типове земно покритие.

Създадената основа на ГИС-база данни ще позволи да се изгради локална географска информационна система за мониторинг на яз."Студен кладенец", чрез аеро и космически изображения.

Used materials

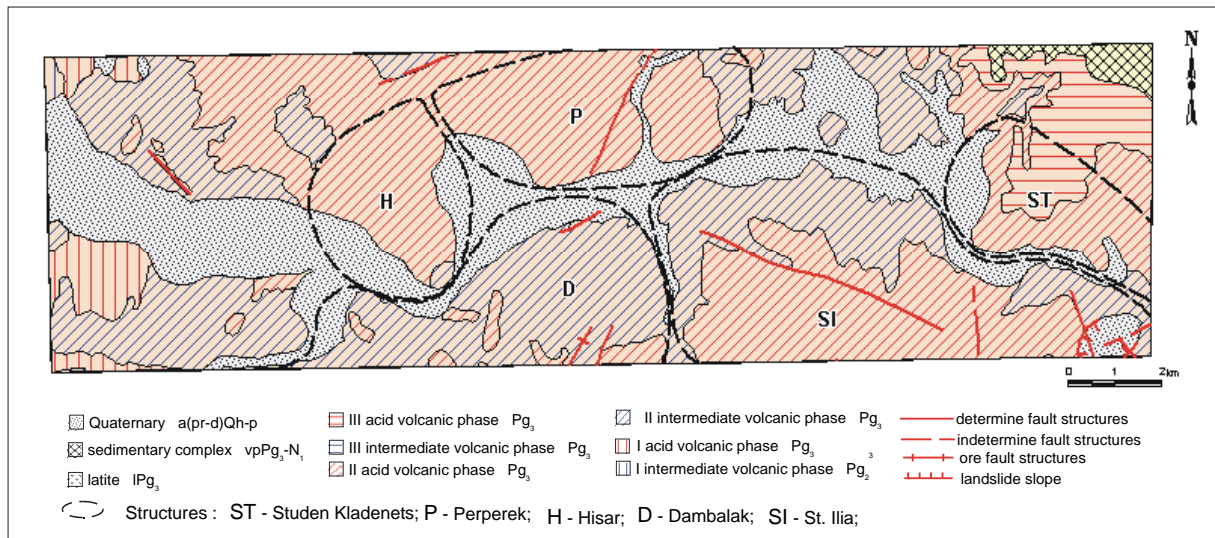
Table 1

Maps	Scale	Images	Scale
<b>Topographic</b>	1:200 000	<b>Air photographs:</b> MRB, 23.X.1977 г. MRB, 16.VIII. 1978 г. MKF, 23.X. 1977 г. MKF 16.VIII. 1978 г.	1:130 000
	1:100 000		1: 70 000
	1: 50 000		1: 40 000
	1: 25 000		1: 40 000
<b>Soil and Geology</b>	1:200 000	<b>Space:</b> LANDSAT TM 1992	1:100 000
	1:400 000		
	1:100 000		
	1: 50 000		1:100 000

Appendix 1

The geological map of the study region

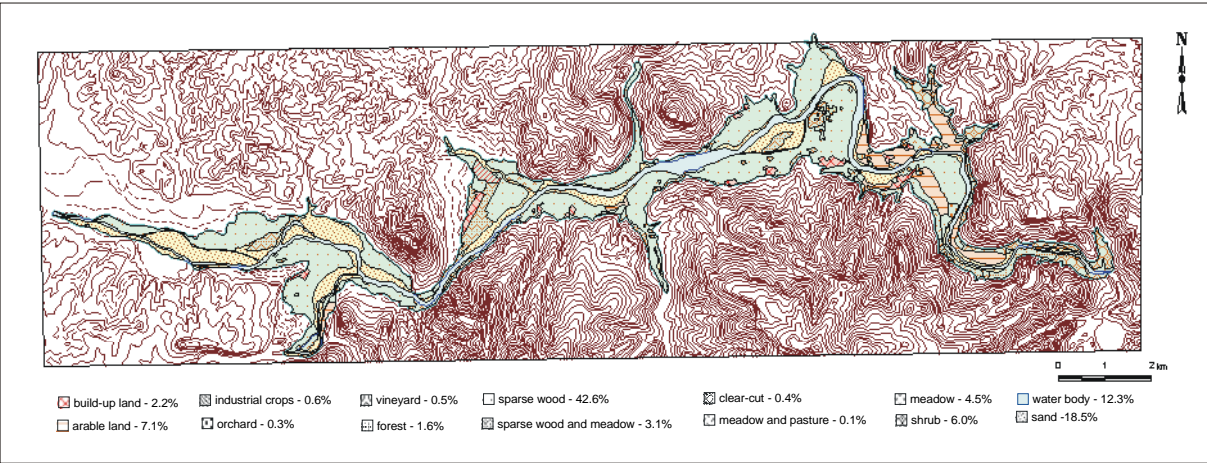
Appendix 1



# Appendix 2

## Map of the land cover types on the study area before the reservoir was built

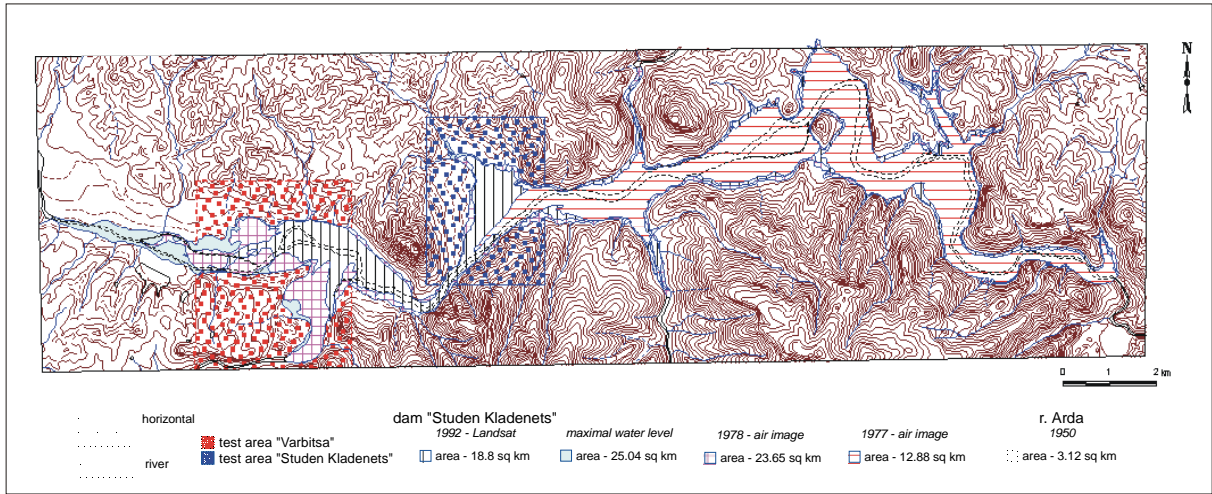
Appendix 2



### Appendix 3

### Map of the water surface change

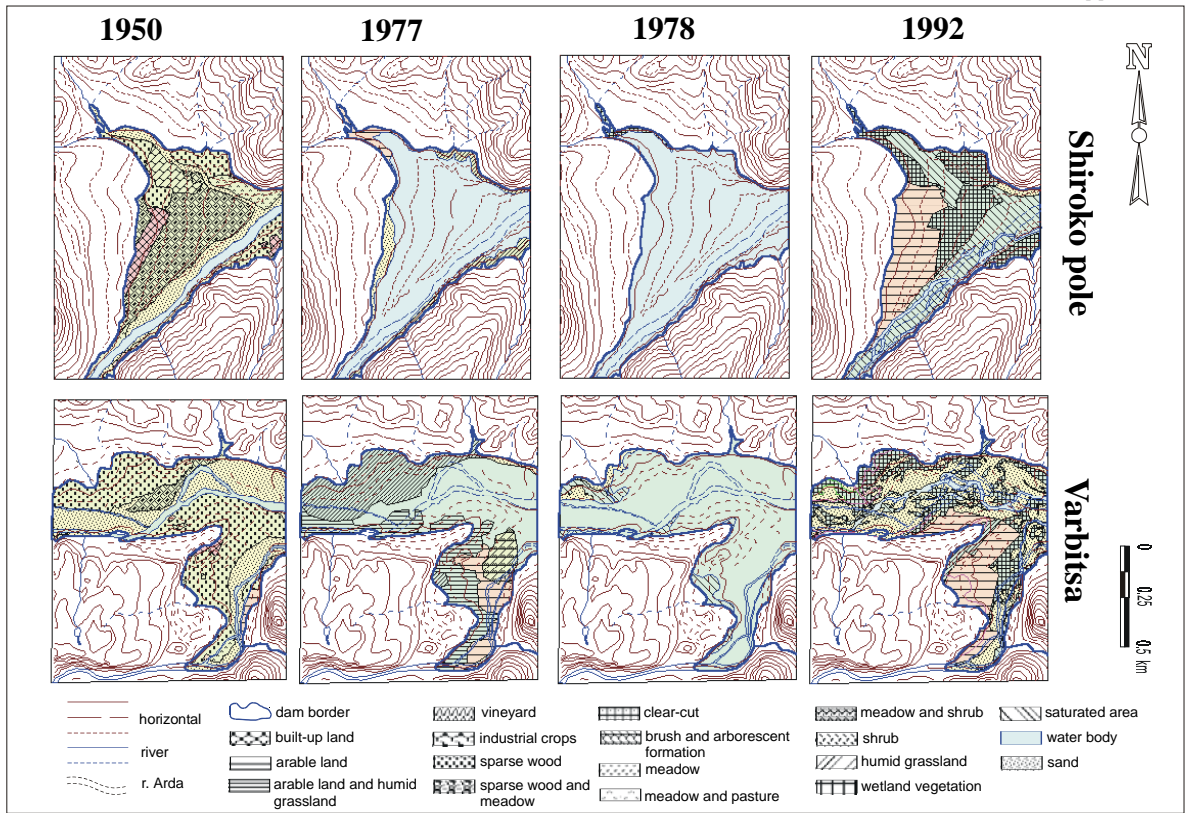
Appendix 3



# Appendix 4

## Map of the land cover types on the test area Shiroko Pole and Varbitsa

Appendix 4



# SYSTEMS FOR PRELAUNCH TEST AND INFLIGHT CALIBRATION OF THE PODSOLNUH DEVICE OF THE GRANAT PROJECT

Venzislav Markov  
Space Research Institute-Bulgarian Academy of Sciences

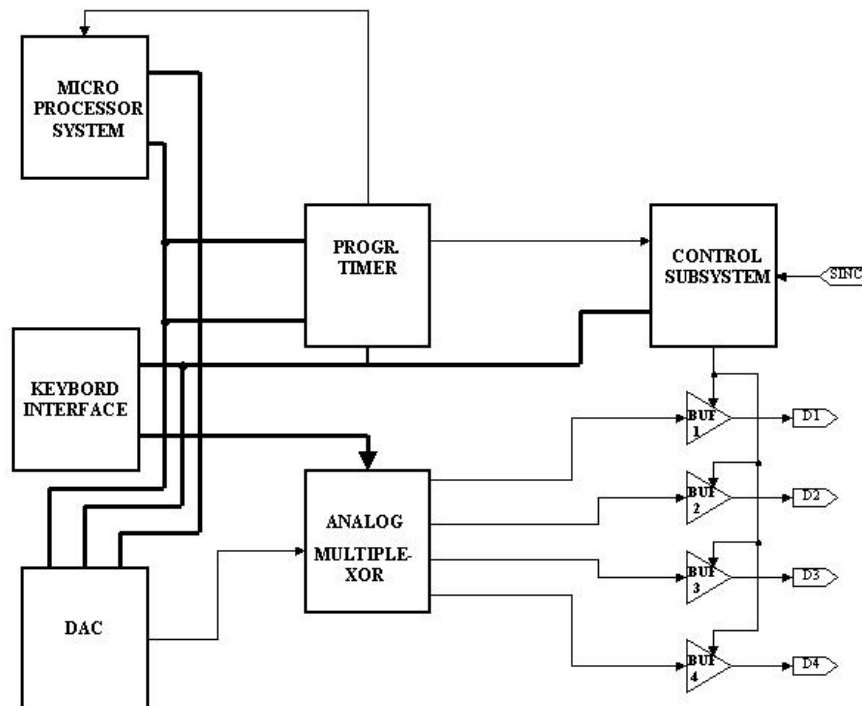
## Introduction

The Podsolnuh device is intended mainly to perform amplitude and intensity analysis of the input signals from the detector system which are previously processed by the input subsystem of the system for analog-to-digital conversion (ADC) and estimation of their parameters and also to perform real-time analysis of the input pulse intensity in correlation with the diffuse X-ray background, thus providing high-fidelity identification of X-ray bursts [1, 2]. This system requires ground-based adjustment and testing as well as periodic verification of its accuracy and performance in flight.

## Structure and operation base of the systems

### 1. System for ground-based calibration and testing

The system for ground-based calibration and testing (GBCT) contains the following main blocks (Fig.1): microprocessor subsystem, programmable timer, control subsystem, ADC, analog multiplexor, keyboard with interface, output buffers and communication block for external test equipment.



This system works in two main operation modes. The first one is used for calibration and testing of: 1- input device system for separation of the pulses caused by X-ray and charged particles; 2 - subsystems for analog-to-digital conversion and amplitude and intensity analysis.

The keyboard is used to set up the code of the required operation mode after which the system is set up either in autonomous mode or in testing mode using an external test equipment in order to be synchronized with the onboard control systems.

Upon decoding of the mode code, the programmable timer is started, providing the frequency of the signals entering outputs D1, D2, D3, and D4. In sequence with the same frequency the ADC provides 32 analog amplitudes corresponding to the operation levels of the amplitude analyzer. Via the analog multiplexor these signals are successively fed to the buffer amplifiers. The circuitry of these amplifiers allows them to provide analog output signals with maximum parametric likeliness to those of the gas-filled counters.

After a given time interval the parameters of the output buffer amplifiers are changed to simulate pulses obtained in charged particle detection. At the end of this time interval the system is automatically stopped and the light indicator announces the end of the test.

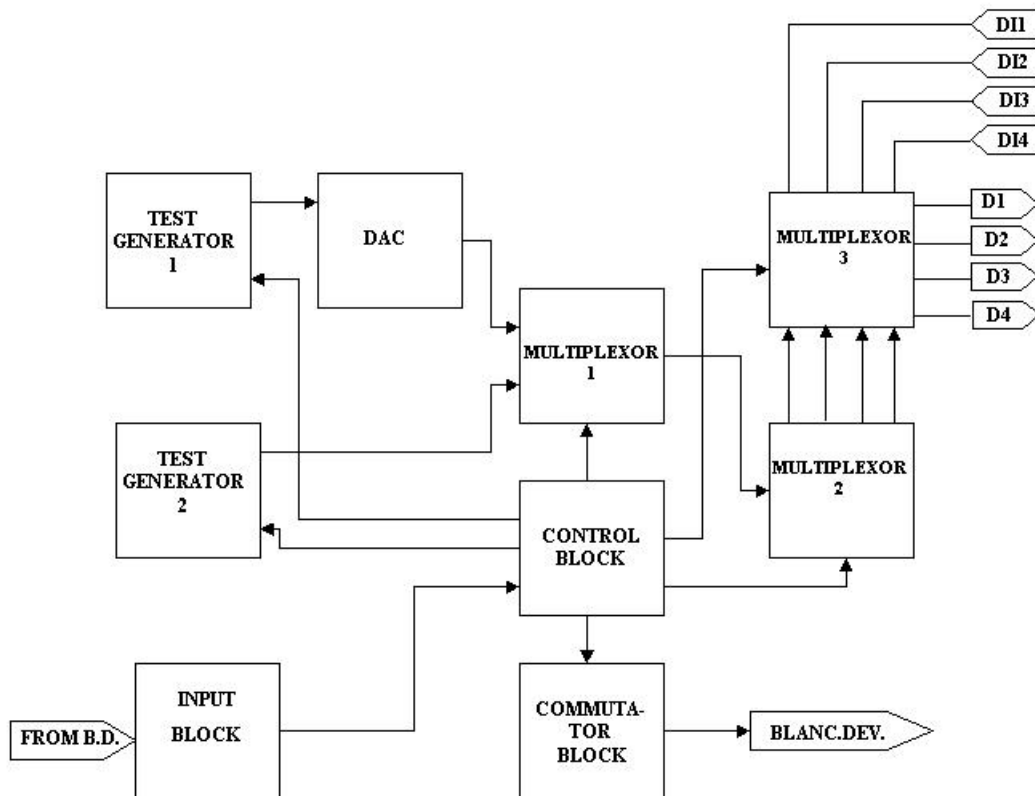
By this test the differential and integral non-linearity of the ADC and the amplitude analyzer can be evaluated. There is a possibility of varying the main frequency to test the amplitude and intensity analyzer at different accumulation times.

The second main operation mode is used for testing and calibration of the block for adaptive determination of the accumulation times of both analyzers and the system for high-fidelity identification of X-ray bursts. In this mode DAC operates with constant amplitude of the output signals.

On starting the system, during fixed time intervals, the constant frequency of the output signals simulates the diffuse X-ray background. Then, the frequency is varied by an algorithm defined by a code set from the keyboard. Thus we may simulate X-ray bursts with different characteristics. This mode provides for the verifications of the accuracy with which the accumulation times of the amplitude and intensity analyzer are determined in function of the input pulses and the fidelity of X-ray burst identification.

## **2. System for inflight calibration and testing**

The Podsolnuh device is supplied with an electronic system for inflight verification of the performance and accuracy of the above-described system. It is set in operation by a command from the onboard system. The testing proceeds in three main stages.



During the first stage the blinking devices of the four detectors are switched on via the communication block and Fe 55 isotope is introduced in the view field. After storing of one amplitude spectrum the amplitude analyzer (AA) provides a signal to reswitch the system to the next operation mode.

The blinking devices are switched off and multiplexor 3 switches off the outputs of the detector amplifiers, thus switching the signals entering from test generator 1 to the pulse of the system for ADC and input signal parameter calibration. The test generator provides 8 amplitudes corresponding to predefined channels of the amplitude analyzer. By multiplexor 2 the signals are fed to multiplexor 3 at equal time intervals, thus simulating the successive performance of the four detectors. When one spectrum is stored, the amplitude analyzer reswitches the system into the next operation mode.

Here, test generator 1 is switched off and test generator 2 is switched on. This mode activates the intensity analyzer and the device for adaptive determination of the accumulation times of the two analyzers [3]. The signals are with constant amplitude. During a given time interval their frequency simulates the frequency of the X-ray background after which, during the next time intervals, it varies by a defined algorithm, thus simulating various thresholds of reswitching of the accumulation times of the adaptive system.

Upon completion of the test stage the device automatically feeds an "End of test" signal and is switched off electrically. The data stored during the test is transmitted to the onboard telemetric system. The obtained data provides to perform express evaluation of the test system. Based on the results from this analysis, adequate corrections can be introduced during the interpretation of the data obtained from the device.

The system for prelaunch test and inflight calibration of the PODSOLNUH X-ray telescope provides reliable ground tuning and stable inflight control of its measurement functions.

## **References**

1. Filipov, L. ,V. Markov, Ch, Bliznakov, V. Genov. 1986a. Anaysis of X-Ray Bursts, Adv. Space Res., vol. 6, №4, pp. 109-112.
2. Filipov, L. ,V. Markov, Ch, Bliznakov, V. Genov. 1986b. A Device for Energy and Intensity Analysis of Data from X-Ray Telescope, Acta Astronautica, vol. 17, № 1, pp.141-142
3. Марков, В. 1993. Устройство за определяне и регистрация изменението в интензивността на импулсни нестационарни потоци. - Авторско свидетелство N 47771/ 1993г

Текст към фигури:

Fig. 1. Flow-chart of the system for ground based calibration and testing of the Podsolnuh device

Fig. 2. Flow-chart of the system for inflight calibration and testing of the Podsolnuh device.

## ***Abstract***

# **SYSTEMS FOR PRELAUNCH TEST AND INFLIGHT CALIBRATION OF THE PODSOLNUH DEVICE OF THE GRANAT PROJECT**

*Venzislav Markov*

The main purpose of the Podsolnuh experiment is the study of X-ray bursts, X-ray pulsars, and the location of variable X-ray sources within the energy range of 2-25 KeV as well as the study of their temporal structure.

The operation principles and the technical characteristics of the electronic system for ground-based calibration and tuning of the input circuitry, analog-to-digital converter, amplitude analyzer, intensity analyzer and the independent system for registration and estimation of X-ray bursts are described.

The test system generates successive input signals to the four detectors and according to the operation mode their parameters are changed.

The calibration device is a part of the electronic system for ground-based calibration and tuning; it simulates the signals from the onboard command systems with high-fidelity.

In flight, this device gives the possibility for periodical testing and estimation of the operability and accuracy of the the Podsolnuh unit.

# **PODSOLNUH-D X-RAY TELESCOPE FROM THE GRANAT PROJECT: RESEARCH PROGRAM AND SOME SPECIFICS IN ITS HARWARE IMPLEMENTATION**

*Ventsislav Markov, Arkadii Melioranski, Lachezar Filipov  
Space Research Institute, BAS, 1000 Sofia, 6, Moskovska St.*

## **Abstract.**

*The paper describes the tasks of the scientific program of the Podsolnuh instrument for the Granat Project. The main purpose of the Podsolnuh experiment is the study of X-ray bursts and X-ray pulsars, and the location of variable X-ray sources within the energy range of 2-25 KeV and the study of their temporal structure. The detector structure based on proportional gas-tilled counters installed on a rotating platform is examined. Via commands from the ground the Podsolnuh platform is directed so that the instrument may be also used to obtain spectra and to determine the time periodicity of stationary X-ray sources.*

*Keywords: X-ray burst, X-ray pulsar, X-ray telescope.*

## **Introduction**

The studies of  $\gamma$ -ray bursts were differentiated as an individual field of study after they were discovered. Usually, their energy spectra were measured in the energy range above 20-30 KeV. Measurements in the X-ray range were made quite rarely (Apollo-16, Vela-5) because of the high background level of wide-angle X-ray detectors.

A controlled orientated platform (Podsolnuh-P) which automatically directed the spectrophotometer (Podsolnuh-D) to the source of  $\gamma$ -bursts was constructed. This allowed to measure energy spectra within 31 channels in the energy range of 2-24 KeV as well as to perform intensity analysis in the same energy range.

The two basic modes of operation of the spectrophotometer significantly improved the observation potentials of the device.

1. The "burst" mode is switched on by a signal from the X-ray bursts registration system from a command line of the other devices watching for  $\gamma$ -ray bursts in energy spectra higher than 30 KeV. In this case, the prehistory of the  $\gamma$ -ray bursts is not recorded. The energy spectra are measured with accumulated times  $t = 100$  ms, 500 ms, 5 s, and 10 s.

The intensity spectra are done within time  $t = 10$  ms, 100 ms, 500 ms, and 1 s. The measurement times can be set constant by a ground-based control station or changed by the accumulation time adaptive estimation system.

2. The "observe" mode allows to measure energy spectra and to perform intensity analysis of stationary sources, X-ray pulsars, and other types of sources. The accumulation times for one spectrum in this mode are  $t = 0.1, 0.5, 1.0, 5.0, 10,$  or 30 s. One point from the energy spectra can be recorded within some of the following times: 0.01, 0.1, 0.5, 1, 5, or 10 s. These times are set by a command from a ground-based control station.

## **Research tasks of the Podsolnuh-D device**

The Podsolnuh-D spectrometer is designed for:

1. Study of the energy and temporary variations of the intensity of  $\gamma$ -ray bursts registered in the hemisphere opposite to the Sun in the energy range 2-24 KeV.
2. Study of the energy and temporary variations of the intensity of bursters, quasiperiodical sources, and X-ray pulsars.
3. Joint studies of low-energy X-ray sources using the Sigma, ART-P, and Art-S devices mounted on the Granat satellite.

In the first case, when the device Conus-S registering  $\gamma$ -bursts in the "X-ray burst" mode with amplitude of the flow  $\sim 10$  erg, the data obtained from its detectors is fed to a platform control block where the  $\gamma$ -ray coordinates are calculated and the rotating platform orientates the Posolnuh device to this point. In bursts of the mentioned intensity the orientation accuracy is approximately  $1^\circ$  which provides for localization of the  $\gamma$ -bursts within a view angle of  $2^\circ \times 2^\circ$  of the Podsolnuh device. The Podsolnuh-D spectrometer starts measuring energy spectra and radiation intensity variations by the command "End of orientation" from the platform. It records 30 spectra, the accumulation times of which can be set by a command from a ground-based control station or by the accumulation time adaptive estimation system, assuming values from 0.1 to 5.0 s.

In the second case, the rotating platform orientates the Podsolnuh-D device to a given point from a chosen source to be studied as a priority mode. The mode of operation in which the platform periodically orientates to a point with diffuse background radiation can be used to separate the constant X-ray radiation. In case of observation of a burster and registration of an X-ray burst, the X-ray bursts registration system is switched on and 8 energy spectra preceding this moment are registered. Then, 30 subsequent energy spectra with accumulation time set adaptively or by a command from the ground are registered. The device measures intensity profiles with accumulation times estimated in a similar way. During the observation of semi-periodical sources and pulsars, the energy and temporal characteristics are measured with accumulation times accounting for the expected periodicity.

In the third case, the axis of the Podsolnuh-D spectrometer is orientated by the rotating platform in parallel to the axes of the Sigma, ART-P, and Art-S devices mounted on the Granat satellite. Energy spectra are measured and temporal analysis of the investigation source selected by the whole complex is made. The measurement times of the spectra are determined depending on the studied object and are set by a command from a ground-based station. In this mode, the X-ray bursts registration system can be switched on and thus the device is ready for registration of fast source intensity variations, for example, a transition from low to high condition of the Cyg X-1 source.

### **Description of the Podsolnuh-D device**

The Podsolnuh-D device consists of two detector blocks mounted on a rotating platform, an analysis block, and a power supply and control block.

In the detector block, two proportional counters, CPIIO-304 M, with working surface of 120 cm are used. The input window of the sensor is covered by a  $130 \mu\text{m}$  beryllium foil. The counters are filled up with composite gases: argon (63%) + helium

(27%) + methane (10%), with pressure of 0.8 atm. The sensors height is 6 cm. The detectors operate within the energy range of 2 to 24 KeV. The energy resolution is about 18% on the line of Fe<sup>55</sup>.

To provide for calibration of the detectors during the flight, in their view field, an isotope Fe<sup>55</sup> (10 μCu) is introduced by the “Calibration” command from the ground. A passive square-shaped collimator of 2° by 2° limits the view field of each detector. The detectors axes are displaced from the platform axes along the X and Y coordinates by ± 1°, thus creating in the center of the common view field a square of 2° by 2° in which the common area of the detectors is constant (176 cm<sup>2</sup>). In this zone, the accuracy of localization of the X- and γ-bursts with respect to intensity is lower or equal to 10 angle minutes with intensity of approximately one Crab in the maximum and duration of a couple of seconds. In the 4°x4° square, outside the 2°x2° zone, localization may be more inaccurate. To control and verify the device axes and detectors efficiency, scanning of the Crab source in two orthogonal directions in autonomous operation mode is provided.

The signal from the proportional counters is amplified and formatted by preamplifiers mounted near the detectors. The signal thus processed is then fed to the input circuitry of the analyzers block mounted within the hermetic section of the satellite. The signal thus processed is fed to the input circuitry of the analyzers block, mounted within the hermetic section of the satellite. The charged particles are separated from X-ray photons and the front slope of the pulses and their amplitude is estimated. The pulses thus processed are fed to the integral intensimeters for X-ray photons and charged particles.

The amplitude analyzer has 32 channels. In order to fill in smoothly its channels, the amplitude-to-code converter operates after a pseudo-logarithmic law. The code generated at its output is fed to the microprocessor system and, upon processing, the signal is recorded in the respective channel. The maximal conversion time of the 32<sup>nd</sup> channel is about 16 μs. The intensity analyzer has 480 channels whereas, depending on the operation mode. The accumulation time for one spectrum may be either constant set up by a command from the ground, or variable defined by an adaptive block.

The device for registration and estimation of X-ray bursts consists of four identical channels, one for each detector, and operates with four accumulation times: 0.5, 1.0, 2.0, and 4.0 s. The algorithm identifying whether the phenomenon is an X-ray burst is the following: for 30 s, the mean intensity of the diffuse X-ray background is measured, and then for 1 s, it is standardized. The reliability of the sensor measurements is verified by comparison with some previously given values. From the sheet previously stored in the RAM, the threshold values of the number of pulses for the above mentioned four times is determined. Should the value of the pulses thus determined for any of the four times or for any of the four detectors be greater than the corresponding value from the sheet, a signal for an X-ray burst is generated. The number of pulses within a time interval of 50 ms for all detectors is accumulated. Once in 4 s, the information for the intensity of the X-ray background is updated.

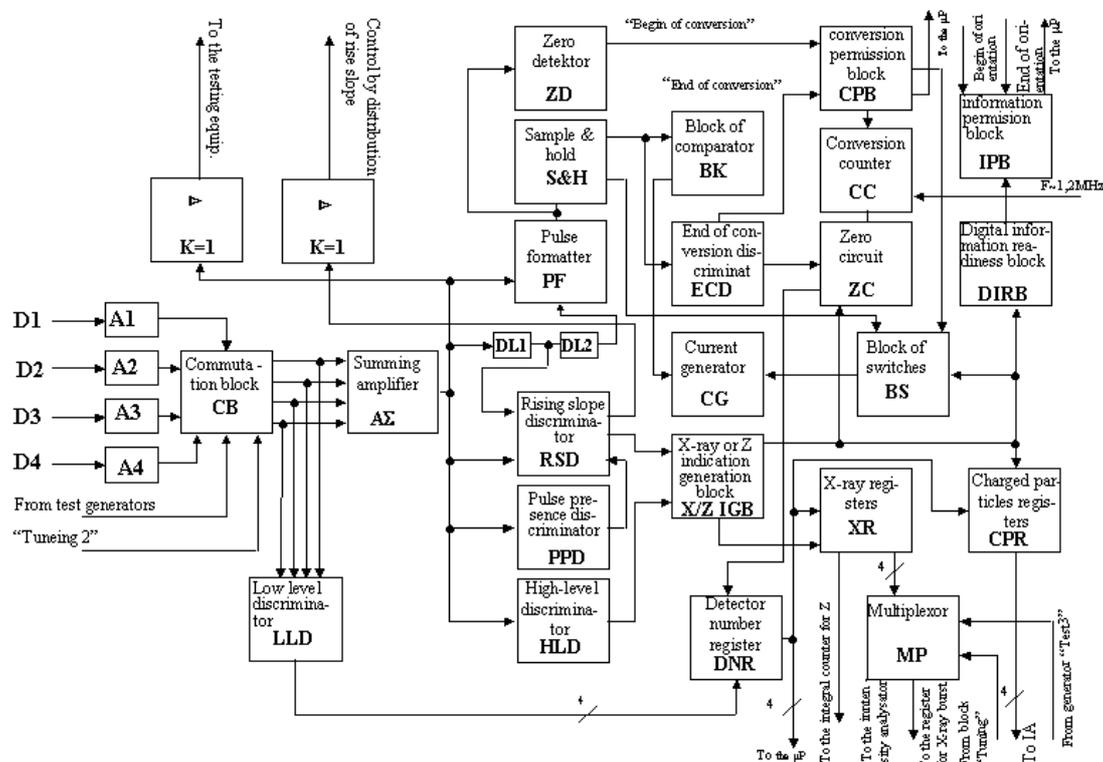
The device for adaptive estimation of the accumulation time accumulates periodically the number of the pulses for each detector within a time interval of 0.5 s. The maximal value is calculated and compared with three previously given threshold values. As a result of the comparison, the accumulation times of the two analyzers

mentioned in the introduction are estimated. The structure of the analyzers is described more precisely in [2,3].

In this paper, the operation principle of the system for estimation of the input signals and their digital conversion is considered in greater details (Fig.1). By the input amplifiers **A1**, **A2**, **A3**, and **A4** with amplifying coefficient of  $2 \pm 25\%$ , the signals from the preamplifiers are matched, and their amplitude for the given energy range is equalized. Then, through the commutation block **CB** which passes the signals from the detectors or from the test generators in the "Tuning-2" mode, the signals are fed to the summing amplifier **A $\Sigma$** . There, the signal from the detectors is amplified and then fed first to the low-level amplitude discrimination circuitry **LLD** where the signal indicating the presence of a pulse in the detectors is generated. From the output of LLD the signal goes to the detector number register **DNR**. From its output, along four channels, the information goes to the microprocessor and to the X-ray registers **XR** or to the charged particles registers **CPR** which are controlled by the X-ray or Z-ray indication generation block **X/Z IGB**. From the output of CPR, along four channels, the information goes to the intensity analyzer **IA**. From the output of XR, along four channels, the information is fed to multiplexor **MP** from whose output it is fed to the intensity analyzer, the device for registration of X-ray bursts, and to the platform if the signal locking "Tuning-3" is not available. In the "Tuning-2" mode, CB locks the signals from the detectors and passes the signal from the test generator **TG** located in the input circuitry and generates a signal with frequency of 512 Hz. In this mode, for each detector, 10 spectra are recorded in the energy analyzer **EA**. From the output of **A $\Sigma$** , via the buffering amplifier, the information is fed to the testing equipment. Simultaneously, the signal is fed to the slope discrimination circuitry in which the delay line **DL1**, the rising slope discriminator **RSD**, and the pulse presence discriminator **PPD** pass the signals with amplitude greater than 0.38 V and generate the signal "Prohibition by Slope". The **A $\Sigma$**  output signal is fed also to the high-level discriminator **HLD** whose threshold voltage is 4 V. It generates the signal "Prohibition by amplitude". The signals "Prohibition by Slope" and "Prohibition by amplitude" go to the X/Z IGB and to the control blocks of the analogue-to digital converter **ADC**.

ADC operates by the following principle. The signal from **A $\Sigma$**  formed in the pulse formatter **PF** is fed to the zero detector **ZD** and to the sample & hold device **S&H** which memorizes the amplitude of the input signal in the capacitor **C**. **ZD** generates the signal "Start of conversion" upon strobbing it with a signal with frequency  $f = 1$  MHz. From the output of S&H the signal is fed to the end-of-conversion discriminator **ECD** where the signal "End of conversion" is generated. If a charged particle is registered, the current generator **CG** is switched on by the block of switches **BS** controlled by the "Z decision" and the capacitor in S&H, quickly allowing input circuitry to register the next signal. If an X-ray phenomenon is registered, the BS controlled by the "X-ray decision" permits operation of CG which discharges capacitor C by the pseudologarithmic law. The maximum conversion time is 32 ms. The operation frequency of the conversion counter **CC** is  $f = 1$  MHz. It is controlled by the conversion permission block **CPB**. CPB is reset by the zero circuit **ZC**. CC is switched on by the signal "X-ray decision" and off by the signal "End of conversion". The ZC block generates a signal by the signals: "End of conversion", "End of rewriting in microprocessor", and "Z decision". The reset signal turns CC and the detector number register **DNR** in start position. Five-bit information for the amplitude of the signal goes to the input buffer of the microprocessor from the output

of the CPB. The microprocessor starts rewriting the information provided by the signal "Information is ready" in the digital information readiness block **DIRB**. The "Information is ready" signal is blocked by the signals "Start of orientation" and "End of orientation" coming from the command decoder to the information permission block **IPB**. As exact coordination of the observed phenomena with onboard time is necessary, a device for time registration with accuracy of 1 ms is made.



The whole information coming from the above described analyzers and intensimeters is memorized in the RAM device in a given sequence, depending on the character of the observed X-ray phenomena. By a command transmitted from the satellite's service system, the information is reformatted and translated to the onboard type recorder. After transmitting the whole information, the device automatically starts working in the mode transmitted by the ground-based station and written in the command memory.

The described complex of a controlled orientated platform "Podsolnuh-P" and a spectrometer "Podsolnuh-D" gives the possibility to observe and analyze all known X-ray phenomena in the energy range 2-24 Kev, accounting for their specific features.

## REFERENCES

1. Rao, D.N., L.J.Glen, D.Taylor. Nucl. Instr. And Meth., No 100, 1972.
2. Filipov, L., V.Markov, Ch.Bliznakov, V.Genov. Analysis of X-ray Bursts. Adv.Space Res., vol.6, No 4, p.109-112.
3. Filipov, L., V.Markov, Ch.Bliznakov, V.Genov. A Device for Energy and Intensity Analysis of Data from X-ray Telescope. Acta Astronautica, vol.17, No 1, p.141-142.

# ISOPERIMETRICAL TASK FOR OPTIMIZATION OF THE CUMULATIVE CHARGE FOR PSEUDOMETEORITE PARTICLES

*Hristo Hristov, Victor Baranov\**

*Defense Advanced Researches Institute, Sofia*

*\*Tula State University, Tula, Russia*

A factor enhancing the effect of pseudometeorite particles when the shell of a space body is fired at in laboratory conditions is the maximal utilization of the net volume of the charge forming an elongated cumulative cloud of particles. Moreover, the cloud should also have maximal velocity and the needed length, with size and mass restrictions on the cumulative charge.

The symmetry of the cumulative charge structure with respect to the axis  $Ox$  reduces the solution of the problem for optimization with respect to the dynamic load factor to determination of the maximal area of a rotating figure  $ABCD$  about the axis  $Ox$  (fig.1). The figure  $ABCD$  is limited by the straight lines  $x=0$ ,  $x=H$  and the plane curves  $y = \Phi(x)$  and  $y = \varphi(x)$ . The function  $y = \Phi(x)$  is known; while rotating, it describes the internal surface of the cumulative charge shell, while  $y = \varphi(x)$  describes the external surface of the cumulative charge lining. The rotation of  $ABCD$  determines the volume occupied by the explosive substance.

The physics of the process of formation of a high-velocity cloud of pseudometeorite particle imposes on the function  $y = \varphi(x)$  the following restrictions: it should be smooth, continuous, and it should have positive first and second derivatives; besides:

$$(1) \quad \varphi'(0) = \alpha_{\Gamma}; \varphi'(H) = \alpha_{XB},$$

where  $\alpha_{\Gamma}$  and  $\alpha_{XB}$  are local static apex angles satisfying the condition for a continuous, discrete, or disperse cumulative jet of cloud particles [1, 2].

The boundary conditions are:

$$(2) \quad y(A) = \varphi_0; y(B) = \varphi_H.$$

The cumulative charge length of the line profile is unknown. It can be determined as a function of the cumulative cloud length [3].

The length of a plane curve is determined by expression [4]:

$$(3) \quad L = \int_0^H \sqrt{1 + \varphi'^2} dx.$$

The following problem is formulated: among all functions  $y = \varphi(x)$ , satisfying conditions (1), (2) and (3), it is necessary to select the one for which the area  $S_D$  of the figure  $ABCD$  attains maximum value:

$$(4) \quad S_D = \int_0^H (\Phi - \varphi) dx.$$

For the purpose, Euler's equation [5] must be solved for function:

$$J^* = \varphi + \lambda^* \sqrt{1 + \varphi'^2}$$

where  $\lambda^*$  is a Lagrangian multiplier.

Using intermediate integral [5]

$$J - J'_{\varphi'} \varphi' = C_1$$

we obtain [5]:

$$\varphi + \lambda \sqrt{1 + \varphi'^2} - \lambda \frac{\varphi'}{\sqrt{1 + \varphi'^2}} \varphi' = C_1.$$

Then, we transform [5]:

$$\varphi + \frac{\lambda}{\sqrt{1 + \varphi'^2}} = C_1;$$

$$\lambda^2 = (1 + \varphi'^2) (C_1 - \varphi)^2;$$

$$\varphi'^2 = \frac{\lambda^2}{(C_1 - \varphi)^2} - 1;$$

$$\frac{d\varphi}{dx} = \pm \frac{\sqrt{\lambda^2 - (\varphi - C_1)^2}}{\varphi - C_1}.$$

But  $\varphi > 0$ , then:

$$\frac{(\varphi - C_1) d\varphi}{\sqrt{\lambda^2 - (\varphi - C_1)^2}} = dx;$$

$$\sqrt{\lambda^2 - (\varphi - C_1)^2} = x + C^2;$$

$$(x + C_2)^2 + (\varphi - C_1)^2 = \lambda^2.$$

Equation (6) is the equation of a circumference, i.e. the solution of the problem is a circumference arc. Since the arc length is not determined by the problem's condition, we take into account conditions (1). The center of the wanted circumference with radius  $\lambda$  is determined as the interception point  $O_1$  of normals  $\eta_\Gamma$  and  $\eta_{XB}$  to the tangents of function  $\varphi(x)$  at points  $A$  and  $B$  respectively where, for geometrical reasons related with the given structure, the radius  $\lambda$  is equal to:

$$(7) \quad \lambda = \frac{\sqrt{H^2 + (\varphi_H - \varphi_0)^2}}{2 \sin(\alpha_{XB} - \alpha_\Gamma)}.$$

Besides:

$$C_1 = \frac{\cos \alpha_\Gamma}{2 \sin(\alpha_{XB} - \alpha_\Gamma)} \sqrt{H^2 + (\varphi_H - \varphi_0)^2};$$

$$C_2 = C_1 \operatorname{tg} \alpha_\Gamma.$$

As a result, an analytical expression for the cumulative charge line profile is obtained, ensuring maximal utilization of the free design space and accounting for the physics of the process and the additional integral condition (3).

The problem is a simple example of the use of variation calculus in cumulative charge optimization. It should be noted that here, the effect's optimization on the parameter of maximal utilization of the net volume is partial. To provide adequate description of the process, its kinematics and dynamics must be taken into account as well.

## REFERENCES

1. N.A.Zlatin. About Maximum Speeds of a Solid Condensed Cumulative Charge Jet. - Problem of Mathematics and Mechanics. Novosibirsk, Science, 1983.
2. S. K. Godunov, A. A. Deribass, I.V. Mali. About Influencing Viscosity of a Material on Process of Formation of a Spray at Impact of Metallical Laminas. - Physics of Combustion and Detonation. Novosibirsk, Science, 1975, N°1, 3-18.
3. The Artillery Ammunitions. Ed. G.M.Tretjakov, Military Technition Union, Sofia, 1973, p. 452.
4. S.V.Frolov, R.J. Shostack. A Course of Mathematics, High School, Kiev, 1973, №1, p.480.

5. J.B.Zeldovitch, A.D. Mishkis. Members of Applied Mathematics. Moscow. Science, 1967, p.646.

**ISOPERIMETRICAL TASK  
FOR OPTIMIZATION OF THE CUMULATIVE CHARGE  
FOR PSEUDOMETEORITE PARTICLES**

*Hristo Hristov, Victor Baranov\**

The isoperimETRICAL task for optimization of the cumulative charge of pseudometeorite particles on the parameter of maximal utilization of net volume is formulated and an analytical solution in the form of an equation of a circumference is obtained for the cumulative charge lining profile.

**ИЗОПЕРИМЕТРИЧНА ЗАДАЧА  
ЗА ОПТИМИЗАЦИЯ НА КУМУЛАТИВЕН ЗАРЯД  
ЗА ПСЕВДОМЕТЕОРИТНИ ЧАСТИЦИ**

*Христо Христов, Виктор Баранов*

Формулирана е изопериметрична задача за оптимизация на кумулативен заряд за псевдометеоритни частици по параметър - максимално използване на полезния обем и е получено аналитично решение във вид на уравнение на окръжност за образуващата на профила на кумулативната облицовка.

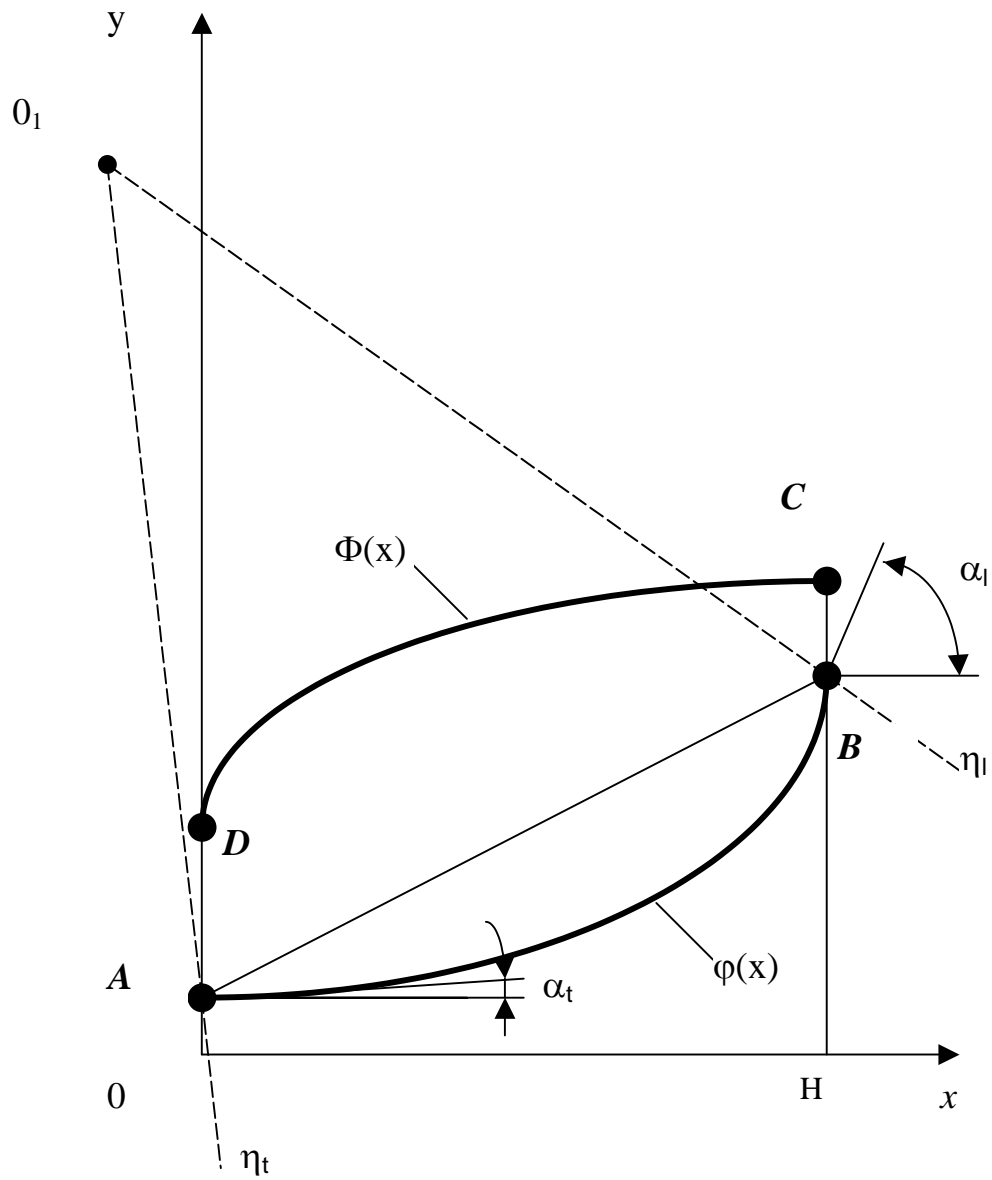


Fig.1. The diagram of cumulative line profile definition  $y = \varphi(x)$ .

# NON-LINEAR OSCILLATOR UNDER EXTERNAL SYNCHRONIZING INFLUENCE: COMPARISON OF PERTURBATION AND CANONICAL METHODS OF ANALYSIS

Vladimir Damgov\*, Petar Georgiev\*\*

\* Space Research Institute, Bulgarian Academy of Sciences

\*\* Department of Physics at the Technical University - Varna

## INTRODUCTION

The analysis of oscillations and vibrations is usually reduced to the problem of a non-linear oscillator, subjected to external periodic influence (perturbation). With the development of perturbation methods, two main directions have formed: canonical (Hamiltonian) methods and non-canonical (non-Hamiltonian) methods.

The development of these two main directions as well as an overview of the principal methods of analysis of perturbed nonlinear oscillator are given in [1].

The present work compares the results obtained by different perturbation methods. It is shown that the solutions using action-angle variables (obtained through canonical transformations) and those obtained using Kuzmak's method produce equivalent results.

## GENERATING SOLUTION

Consider a generalized non-linear oscillator described by the following system of equations:

$$(1) \quad \begin{cases} \frac{dx}{dt} - p = 0 \\ \frac{dp}{dt} + f(x, T) = \mu F_v \left( \frac{dx}{dt}, x, t, T \right) \end{cases}$$

where  $0 \leq \mu \ll 1$  is a small parameter,  $T$  is secondary scaling /slow time/,  
 $T = T_0 + \mu t$ ,  $T_0 = \text{const}$ ,  $dT/dt = \mu$ .

Let  $\mu F_v$  depend on  $t$  primarily through the phase /quick/ variable, such that:

$$(2) \quad \frac{d\gamma(t)}{dt} = \Gamma(t) \quad \frac{d\Gamma(t)}{dt} = O(\mu)$$

/the latter means that  $(1/\mu)(\Gamma(t)/dt)$  is limited in the neighborhood of  $\mu = 0$ /

In (2)  $\Gamma$  is the circular frequency of external influence,  $2\pi/\Gamma(t)$  is the period of external influence.

We are looking for a solution of (1), synchronous with the external influence, i.e. with  $\gamma(t)$  which has circular frequency:

$$(3) \quad \Omega(t) = \frac{m}{n} \Gamma(t) \quad m, n = 1, 2, 3, \dots, \quad \frac{d\Omega(t)}{dt} = O(\mu)$$

The period of the generating solution in the non-autonomous regime is:

$$\Pi_{or}(t) = \frac{2\pi}{\Omega(t)}$$

The following substitution is made:  $\frac{m}{n} \frac{d\gamma(t)}{dt} = \Omega(t) = \frac{2\pi}{\Pi_{or}(t)}$ . The frequency of the oscillations in

the autonomous regime is  $\omega(E, T) = \frac{2\pi}{\tilde{T}(E, \tilde{\Phi})}$  where  $E = \text{const}$  is an integration constant and  $\Pi(E, T)$  is the corresponding oscillation period.

That yields for the non-autonomous regime/in the presence of synchronizing influence/:

$$(4) \quad \frac{d\Psi}{dt} = \Omega(t) = \xi(E, T) \omega(E, T); \quad \Pi_{or}(t) = \frac{\Pi(E, t)}{\xi}$$

where  $\xi = \begin{cases} 1, & \text{in the absence of frequency lock - on} \\ \frac{\Omega}{\omega}, & \text{in the presence of frequency lock - on} \end{cases}$

We represent the frequency  $\Omega$  in an asymptotic series:

$$(5) \quad \Omega(t) = \Omega_0(T) + \mu [\Omega_1(T) + W_1(t, T)] + \mu^2 [\Omega_2(T) + W_2(t, T)] + \dots$$

This means that:

$$(6) \quad \left\{ \begin{aligned} \Psi(t) &= \Psi_1(t) + \hat{I}(\mu), \\ \xi(E, t, T) &= \xi_0(E, T) + \hat{I}(\mu) \\ \ddot{I}_{or}(t) &= \frac{\ddot{I}(\hat{A}, \hat{D})}{\xi_0(E, T)} + \hat{I}(\mu) \end{aligned} \right.$$

Let's now consider the generating solution in non-autonomous regime by making the substitution:

$$(7) \quad \mu = 0, \quad T = T_0 = const, \quad E(T) = const, \quad \Omega = const$$

Then  $\Omega = \Omega_0(T) = \xi_0(E, T)\omega(E, T) = const$  and the solution of the system (1) is sought to be in the form:

$$(8) \quad \left\{ \begin{aligned} x &= x_d[E, t+t_0, T] = x_a[E, (t+t_0)\xi(E, T), T] \\ p &= p_d[E, t+t_0, T] = p_a[E, (t+t_0)\xi(E, T), T] \end{aligned} \right.$$

where  $x_A$  and  $p_A$  are solutions of the system /1/ in the autonomous case [1].

$$E = \frac{1}{2}p^2 + V(x, T), \quad V(x, T) = \int_0^x f(x', T) dx' \text{ is the potential energy.}$$

The functions /8/ satisfy the generating system when condition (7) is satisfied, i.e.

$$(9) \quad \left\{ \begin{aligned} \frac{dx}{dt} &= \xi(E, T)p \\ \frac{dp}{dt} &= -\xi(E, T)f(x, T) \end{aligned} \right.$$

A new integration constant A is introduced:  $t_0 = A/\Omega$ . Then

$$\Psi + A = (t + t_0)\omega(E, T)\xi = (t + t_0)\Omega.$$

We introduce the new functions:

$$(10) \quad \left\{ \begin{aligned} x_c[E, \Psi + A, T] &= x_d[E, \frac{\Psi + A}{\Omega}, T] \\ p_c[E, \Psi + A, T] &= p_d[E, \frac{\Psi + A}{\Omega}, T] \end{aligned} \right.$$

From (4), (9) and (10) follows the system of equations:

$$\begin{aligned} \Omega \frac{\partial x_c(E, \Psi + A, T)}{\partial(\Psi + A)} - \xi(E, T)p_c &= 0 \\ \Omega \frac{\partial p_c(E, \Psi + A, T)}{\partial(\Psi + A)} + \xi(E, T)f(x_c, T) &= 0 \end{aligned}$$

or, equivalently:

$$(11) \quad \mathbf{Y}_{or} \begin{bmatrix} 0 \\ \Omega \end{bmatrix} + \begin{bmatrix} -\xi p_c \\ \xi f \end{bmatrix} = 0$$

where:

$$(12) \quad \mathbf{Y}_{\text{or}}(E, \Psi + A, T) = \begin{bmatrix} \frac{\partial \alpha_c(E, \Psi + A, T)}{\partial E} & \frac{\partial \alpha_c(E, \Psi + A, T)}{\partial(\Psi + A)} \\ \frac{\partial \hat{p}_c(E, \Psi + A, T)}{\partial E} & \frac{\partial \hat{p}_c(E, \Psi + A, T)}{\partial(\Psi + A)} \end{bmatrix} = \begin{bmatrix} \frac{\partial \alpha_c(E, \Psi + A, T)}{\partial E} & \frac{\xi}{\Omega} p_c \\ \frac{\partial \hat{p}_c(E, \Psi + A, T)}{\partial(\Psi + A)} & -\frac{\xi}{\Omega} f(x_c, T) \end{bmatrix}$$

and  $\det \mathbf{Y}_{\text{or}} = -\frac{\xi}{\Omega}$  (the condition for the applicability of the perturbation method is:  $\mathbf{Y}_{\text{or}} \neq 0, \infty$ ).

## PERTURBING IN ENERGY-ANGLE VARIABLES

Below we solve the perturbed equation (1) applying the method of varying coefficients: we assume  $E = E(t)$  and  $A = A(t)$ . We seek a solution of the form:

$$\begin{cases} x = x_c[E(t), \Psi(t) + A(t), T] \\ p = p_c[E(t), \Psi(t) + A(t), T] \end{cases}$$

From here and (11) it follows:

$$\begin{bmatrix} \frac{dx}{dt} \\ \frac{dp}{dt} \end{bmatrix} = \mathbf{Y}_{\text{or}} \begin{bmatrix} \frac{dE}{dt} \\ \Omega(t) + \frac{dA}{dt} \end{bmatrix} + \mu \begin{bmatrix} \frac{\partial x_c}{\partial T} \\ \frac{\partial p_c}{\partial T} \end{bmatrix}$$

Substituting in (1) and taking into account (11) gives:

$$(13) \quad \begin{bmatrix} \frac{dE}{dt} \\ \frac{dA}{dt} \end{bmatrix} = \mathbf{Y}_{\text{or}}^{-1} \begin{bmatrix} -\mu \frac{\partial x_c}{\partial T} \\ -\mu \frac{\partial p_c}{\partial T} + \mu F_v \end{bmatrix} - \begin{bmatrix} 0 \\ \frac{\xi - 1}{\xi} \Omega \end{bmatrix},$$

where from (12) it follows:

$$\mathbf{Y}_{\text{or}}^{-1} = \begin{bmatrix} f(x_c, T) & p_c \\ \frac{\Omega}{\xi} \frac{\partial \hat{p}_c(E, \Psi + A, T)}{\partial E} & -\frac{\Omega}{\xi} \frac{\partial \alpha_c(E, \Psi + A, T)}{\partial E} \end{bmatrix}$$

The system of equations (13) can be written in the form:

$$(14) \quad \begin{cases} \frac{dE}{dt} = \mu G_r(E, \Psi + A, T, \mu) \\ \frac{dA}{dt} = \mu G_s(E, \Psi + A, T, \mu) - \frac{\xi - 1}{\xi} \Omega \end{cases}$$

We seek a solution having the asymptotic form (5) and (6) and also:

$$(15) \quad \dot{A} = \dot{A}_1(\hat{O}) + \mu [\dot{E}_1(T) + U_{r1}(tT)] + \mu^2 [\dot{E}_2(T) + U_{r2}(tT)] + \dots$$

$$(16) \quad A = A_1(\hat{O}) + \mu [A_1(T) + U_{s1}(tT)] + \mu^2 [A_2(T) + U_{s2}(tT)] + \dots$$

The condition is that  $U_{rk}$  and  $U_{sk}$ ,  $k = 1, 2, 3, \dots$  should not contain secular terms, i.e.:

$$(17) \quad \left\langle \frac{\partial}{\partial t} U_{rk}(tT) \right\rangle_t = 0, \quad \left\langle \frac{\partial}{\partial t} U_{sk}(tT) \right\rangle_t = 0, \quad k = 1, 2, 3, \dots,$$

where  $\langle \rangle$  means average with respect to time  $t$ .

Substituting (15) and (16) in (14) we expand in series with respect to  $\mu$ . In front of  $\mu^1$  we get:

$$\begin{cases} \frac{dE_o(T)}{dT} + \frac{\partial U_{r1}(tT)}{\partial t} = G_{r1} \\ \frac{dA_o(T)}{dT} + \frac{\partial U_{s1}(tT)}{\partial t} = G_{s1} - \frac{1}{\mu} \frac{\xi - 1}{\xi} \Omega \end{cases}$$

On the right-hand side appear  $E_o(T)$ ,  $\Psi_o(T)$ ,  $A_o(T)$ ,  $\Omega_o(T)$ ,  $\xi_o[E_o(T), T]$ . Averaging with respect to time  $t$  and taking into account (17) gives:

$$(18) \quad \begin{cases} \frac{dE_o}{dT} = \langle G_{1r} \rangle_t \\ \frac{dA_o}{dT} = \langle G_{1s} \rangle_t - \frac{1}{\mu} \frac{\xi_o - 1}{\xi_o} \Omega \end{cases}$$

In addition to these equations expression (4) should also be considered. Then  $U_{r1}$  and  $U_{s1}$  can be found in analogy with the asynchronous case, described in [1]. Synchronization or frequency lock-on will be observed when condition  $\frac{dA_o}{dT} = 0$  is satisfied from which it follows that:

$$(19) \quad \langle G_{1s} \rangle_t - \frac{1}{\mu} \frac{\xi_o - 1}{\xi_o} \Omega_o = 0$$

From equations (4), (18) and (19) we find  $E_o, A_o, \xi$ .

Eventually, the initial approximation (18) is determined to have the form:

$$(20) \quad \left[ \begin{array}{c} \left\langle \frac{dE}{dt} \right\rangle_t \\ \left\langle \frac{dA}{dt} \right\rangle_t \end{array} \right] = \left\langle \mathbf{Y}^{-1} \left[ \begin{array}{c} -\mu \frac{\partial x_c}{dT} \\ -\mu \frac{\partial p_c}{dT} + \mu F_v \end{array} \right] \right\rangle - \left[ \begin{array}{c} 0 \\ \frac{\xi - 1}{\xi} \Omega \end{array} \right],$$

where all the initial approximations have been substituted in.

## PERTURBATION IN ACTION-ANGLE VARIABLES

We will first determine the generating system of Hamilton's canonical equations. The corresponding Hamiltonian has the form :

$$\hat{E} = K_a(x, p, T) = K_c \left[ H(x, p, T) T \right]$$

where  $K_c(H, T) = \int_0^H \xi(H', T) dH'$ . The integral is taken at  $T = \text{const}$ . Here:

$$(21) \quad H = H(x, p, T) = \frac{1}{2} p^2 + V(x, T) = E,$$

$\xi(H, T)$  is the corresponding detuning in the presence of synchronizing influence.

The canonical system of Hamilton's equations has the form:

$$\begin{cases} \frac{dx}{dt} = \frac{\partial K_a(x, p, T)}{\partial p} = \frac{\partial K_c(H, T)}{\partial H} \frac{\partial H(x, p, T)}{\partial p} = \xi(E, T) p \\ \frac{dp}{dt} = -\frac{\partial K_a(x, p, T)}{\partial x} = -\frac{\partial K_c(H, T)}{\partial H} \frac{\partial H(x, p, T)}{\partial x} = -\xi(E, T) F(x, T) \end{cases}$$

We look for a generating function  $W_{or}(x, J, T)$  such that the new momentum  $\bar{p}$  is a constant, which we denote by  $J$ , i.e.  $J = \bar{p}$ . The new coordinate  $\Psi = \bar{x}$  represents angle. Then:

$$(22) \quad p = \frac{\partial W_{or}(x, J, T)}{\partial x} \quad \Psi = \frac{\partial W_{or}(x, J, T)}{\partial J}$$

The new Hamiltonian  $\bar{k}$  coincides with the old Hamiltonian  $\bar{k}(J, \Psi, T) = K(x, \rho, T)$ . The period with respect to  $\Psi$  must be:  $P_o = 2\pi$ . Then, from Hamilton's canonical equations it follows that:

$$\frac{\partial \Psi}{\partial t} = \frac{\partial \bar{K}(J, \Psi, T)}{\partial J} = \text{const}$$

$$\frac{\partial J}{\partial t} = -\frac{\partial \bar{K}}{\partial \Psi} = 0, \quad J = \frac{1}{2\pi} \oint \frac{W_{or}}{\partial x} dx$$

The circular frequency in the generating system is also determined as  $\frac{d\Psi}{dt} = \Omega_c(J, T) = \xi_c(J, T) \omega_c(J, T)$ , where  $\omega_c(J, T)$  is the circular frequency in the autonomous system at  $\mu = 0$ ,  $\xi_c(J, T) = \xi(E, T)$ . The oscillation period in the generating system is respectively:

$$\dot{T}_{or}(J, T) = \frac{2\pi}{\Omega_c(J, T)} = \frac{\dot{T}(E, T)}{\xi_c(J, T)}, \text{ where } \Pi(E, T) \text{ is the autonomous system period.}$$

Taking into account (21) and (22) gives:

$$W_{or}(x, J, T) = \pm \int_0^x \sqrt{2E - 2V(x', T)} dx'$$

$$\Psi = \int_0^x \frac{\omega_c}{\pm \sqrt{2E - 2V(x', T)}} dx = \Omega_c t + \text{const}$$

We now express  $x, p$  through the variables  $J, \Psi$ :

$$(23) \quad \begin{cases} x = x_f(J, \Psi + A, T) = x_c(E(J, T), \Psi + A, T) \\ p = p_f(J, \Psi + A, T) = p_c(E(J, T), \Psi + A, T) \end{cases}$$

The generating system is then represented as:

$$\begin{cases} \frac{dx}{dt} = \xi_c(J, T) p \\ \frac{dp}{dt} = -\xi_c(J, T) F(x, T) \\ \frac{d\Psi}{dt} = \Omega_c(J, T) \end{cases}$$

$$\text{or in the following matrix form: } \mathbf{Z}_{or} \begin{bmatrix} 0 \\ \Omega_{,b} \end{bmatrix} + \begin{bmatrix} -\xi p_t \\ \xi f(x, T) \end{bmatrix} = 0,$$

$$\text{where } \mathbf{Z}_{or}(J, \Psi + A, T) = \begin{bmatrix} \frac{\partial x_f(J, \Psi + A, T)}{\partial J} & \frac{\partial x_f(J, \Psi + A, T)}{\partial(\Psi + A)} \\ \frac{\partial p_f(J, \Psi + A, T)}{\partial J} & \frac{\partial p_f(J, \Psi + A, T)}{\partial(\Psi + A)} \end{bmatrix}$$

and  $\det \mathbf{Z}_{or} = -1$  (the condition for applicability of the perturbation method in this case is  $\mathbf{Z}_{or} \neq 0, \infty$ ).

We now solve the perturbed system of equations (1). The perturbation is non-Hamiltonian. For this reason we approach it with the averaging method. We try to find a solution by varying the constants (23):

$$(24) \quad \begin{bmatrix} \frac{dx}{dt} \\ \frac{dp}{dt} \end{bmatrix} = \mathbf{Z}_{or} \begin{bmatrix} \frac{dJ}{dt} \\ \Omega_o(t) + \frac{dA}{dt} \end{bmatrix} + \mu \begin{bmatrix} \frac{\partial x_f}{\partial T} \\ \frac{\partial p_f}{\partial T} \end{bmatrix}$$

Substituting (24) in (1) we get:

$$(25) \quad \begin{bmatrix} \frac{dJ}{dt} \\ \frac{dA}{dt} \end{bmatrix} = \mathbf{Z}_{\text{or}}^{-1} \begin{bmatrix} -\mu \frac{\partial x_f}{\partial T} \\ -\mu \frac{\partial p_f}{\partial T} + \mu F_v \end{bmatrix} - \begin{bmatrix} 0 \\ \frac{\xi_c - 1}{\xi_c} \Omega_c \end{bmatrix}$$

where:

$$\mathbf{Z}_{\text{or}}^{-1} = \begin{bmatrix} \frac{\xi_c}{\Omega_c} f(x_f, T) & \frac{\xi_c}{\Omega_c} p_f \\ \frac{\partial p_f}{\partial J} & -\frac{\partial x_f}{\partial J} \end{bmatrix}$$

The system of equations (25) can be written in the form:

$$(26) \quad \begin{cases} \frac{dJ}{dt} = \mu G_v(J, \Psi + A, tT, \mu) \\ \frac{dA}{dt} = \mu G_w(J, \Psi + A, tT, \mu) - \frac{\xi_c - 1}{\xi_c} \Omega_c \end{cases}$$

We now seek an asymptotic expansion:

$$(27) \quad \begin{cases} \Omega_c(T) = \Omega_o(T) + \mu[\Omega_1(T) + W_1(t, T)] + \mu^2[\Omega_2(T) + W_2(t, T)] + \dots \\ J(T) = J_o(T) + \mu[J_1(T) + U_{v1}(t, T)] + \mu^2[J_2(T) + U_{v2}(t, T)] + \dots \\ A(T) = A_o(T) + \mu[A_1(T) + U_{w1}(t, T)] + \mu^2[A_2(T) + U_{w2}(t, T)] + \dots \\ \xi_c(J, T) = \xi_o(J, T) + O(\mu) \end{cases}$$

where  $U_{vk}(tT)$ ,  $U_{wk}(tT)$ ,  $k = 1, 2, 3, \dots$  do not contain secular terms, i.e.

$$\left\langle \frac{\partial}{\partial t} U_{vk}(tT) \right\rangle_t = 0, \quad \left\langle \frac{\partial}{\partial t} U_{wk}(tT) \right\rangle_t = 0, \quad k=1, 2, 3, \dots$$

We substitute (27) into (26) and expand in a series with respect to the powers of  $\mu$ . We average with respect to time  $t$ . In front of  $\mu^1$  we get:

$$\begin{cases} \frac{dJ_o}{dT} = \langle G_v \rangle_t \\ \frac{dA_o}{dT} = \langle G_w \rangle_t - \frac{1}{\mu} \frac{\xi_o - 1}{\xi_o} \Omega \end{cases}$$

Then we find  $U_{v1}$  and  $U_{w1}$  etc.

We get frequency lock-on or synchronization when  $\frac{dA_o}{dT} = 0$ .

Finally, we obtain the following system of equations:

$$(28) \quad \begin{cases} \frac{dI_o}{dT} = \langle G_v \rangle_t \\ \langle G_w \rangle_t - \frac{1}{\mu} \frac{\xi_o - 1}{\xi_o} \Omega = 0 \\ \frac{d\Psi}{dt} = \Omega_c(T) = \xi \omega_c \end{cases}$$

Equations (28) determine  $J_o, A_o, \xi_o$ .

The initial approximation has the form:

$$(29) \quad \left[ \begin{array}{c} \left\langle \frac{dI}{dt} \right\rangle_t \\ \left\langle \frac{dA}{dt} \right\rangle_t \end{array} \right] = \left\langle \mathbf{Z}_{\text{or}}^{-1} \left[ \begin{array}{c} -\mu \frac{\partial x_f}{dT} \\ -\mu \frac{\partial p_f}{dT} + \mu F_v \end{array} \right] \right\rangle - \left[ \begin{array}{c} 0 \\ \frac{\xi_c - 1}{\xi_c} \Omega_c \end{array} \right].$$

## COMPARISON WITH KUZMAK'S METHOD IN MATRIX FORM

Above, in the consideration of a synchronous non-linear oscillation when using the non-canonical /non-Hamiltonian/ perturbation method in energy-angle variables as well as when using the canonical approach in action-angle variables, we assumed the detuning  $\xi$  in the system to be a known function. Here, on the contrary,  $\xi$  will initially be considered as an independent variable and any definite substitutions will only be made at a later stage.

We again consider a generating system in the form (9) where  $\xi = \text{const}$  is for now an independent parameter.

The solution of (9) is represented in the form:

$$(30) \quad \left\{ \begin{array}{l} x = x_a \mathbb{E} [t + t_0, \xi T] \\ p = p_a \mathbb{E} [t + t_0, \xi T] \end{array} \right.$$

We introduce an angle variable  $\Psi$  and the integration constant  $\alpha$  according to the expressions:

$$t = \frac{\Psi}{\omega(E, T)}; \quad t_0 = \frac{\alpha}{\omega(E, T)}, \quad \text{where } \omega(E, T) = \frac{2\pi}{\Pi(E, T)} \text{ is the circular frequency in the generating}$$

solution,  $\Pi(E, T)$  is the period in time  $t$ . Let  $\theta = \Psi + \alpha$  and  $\mathbf{N} = \begin{bmatrix} 1 & 0 \\ 0 & \xi \end{bmatrix}$  ..

We introduce the matrix  $\Xi_g = \Xi \mathbb{E} [t + t_0, \xi T]$  such that it satisfies:

$$(31) \quad \Xi_g \mathbf{N} = \begin{bmatrix} \frac{\partial x_a \mathbb{E} [t + t_0, \xi T]}{\partial E} & \frac{\partial x_a \mathbb{E} [t + t_0, \xi T]}{\partial (t + t_0)} \\ \frac{\partial p_a \mathbb{E} [t + t_0, \xi T]}{\partial E} & \frac{\partial p_a \mathbb{E} [t + t_0, \xi T]}{\partial (t + t_0)} \end{bmatrix}$$

We will work with the functions:

$$\left\{ \begin{array}{l} x_b(E, \theta, \xi, T) = x_a \mathbb{E} \left[ \frac{\theta \xi}{\omega(E, T)}, T \right] \\ p_b(E, \theta, \xi, T) = p_a \mathbb{E} \left[ \frac{\theta \xi}{\omega(E, T)}, T \right] \end{array} \right.$$

Let:

$$\mathbf{Y}_g = \mathbf{Y}(E, \theta, \xi, T) = \begin{bmatrix} \frac{\partial x_b \mathbb{E} [\theta, \xi, T]}{\partial E} & \frac{\partial x_b \mathbb{E} [\theta, \xi, T]}{\partial (\theta \xi)} \\ \frac{\partial p_b \mathbb{E} [\theta, \xi, T]}{\partial E} & \frac{\partial p_b \mathbb{E} [\theta, \xi, T]}{\partial (\theta \xi)} \end{bmatrix}$$

From (9), taking (30) into account, we obtain the following variational equation:

$$(32) \quad \frac{\partial}{\partial t} (\Xi_g \mathbf{N}) + \xi \mathbf{B} (\Xi_g \mathbf{N}) = 0,$$

where  $B = \begin{bmatrix} 0 & -1 \\ \frac{\partial F(x,T)}{\partial x} & 0 \end{bmatrix}$ .

Apart from this, the quantity (31) can be represented also in the form:

$$(33) \quad \underline{E}_g N = Y_g H N [1 - \xi(t - t_0) Q],$$

where  $H = \begin{bmatrix} 1 & 0 \\ 0 & \omega \end{bmatrix}$ ,  $Q = \begin{bmatrix} 0 & 0 \\ \frac{\partial \ln \Pi(E, T)}{\partial E} & 0 \end{bmatrix}$

We now solve the system of equations (1). It is expressed in the following equivalent form:

$$(34) \quad \begin{cases} \frac{dx}{dt} - \xi p = (1 - \xi) p \\ \frac{dp}{dt} + \xi f(x, T) = \mu F_v + (\xi - 1) x(x, T) \end{cases}$$

We seek a solution in the form:

$$(35) \quad \begin{cases} x = x_b [E(T), \Psi(T) + A(T)T] + \mu U_{1a}(t, T) \\ p = p_b [E(T), \Psi(T) + A(T)T] + \mu U_{2a}(t, T) \end{cases}$$

where  $t_0 = \frac{A}{\Omega}$  and also:

$$(36) \quad \frac{d\Psi(t)}{dt} = \Omega(t) \quad \xi(E, t, T) = \frac{\Omega(t)}{\omega(E, T)}$$

In this way we initially found  $\underline{E}$  and only then considered the constant period functions  $x_b, p_b$ .

Having /35/ as a basis to stand on we can write:

$$(37) \quad \begin{bmatrix} \frac{dx}{dt} \\ \frac{dp}{dt} \end{bmatrix} = Y_g \begin{bmatrix} \mu \frac{dE}{dT} \\ \Omega + \mu \frac{dA}{dT} \end{bmatrix} + \mu \begin{bmatrix} \frac{\partial x_b}{\partial T} \\ \frac{\partial p_b}{\partial T} \end{bmatrix} + \mu \frac{\partial U_a}{\partial t} + \mu^2 \frac{\partial U_a}{\partial T},$$

where we have introduced the notation:  $U_a(t, T) = \begin{bmatrix} U_{a1}(t, T) \\ U_{a2}(t, T) \end{bmatrix}$

We look for a solution by representation with an asymptotic series:

$$\begin{cases} \Psi(t) = \Psi_0(t) + \mu \Psi_1(t) + \mu^2 \Psi_2(t) + \dots \\ \Omega_b(t) = \Omega_0(T) + \mu [\Omega_1(T) + \omega_1(t, T)] + \mu^2 [\Omega_2(T) + \omega_2(t, T)] + \dots \\ A(T) = A_0(T) + \mu A_1(T) + \mu^2 A_2(T) + \dots \\ E(T) = E_0(T) + \mu E_1(T) + \mu^2 E_2(T) + \dots \\ \xi(E, t, T) = \xi_0(E, T) + O(\mu) \\ \mu U_a(t, T) = \mu U_1(t, T) + \mu^2 U_2(t, T) + \dots \end{cases}$$

where  $U_k(t, T) = \begin{bmatrix} U_{k1}(t, T) \\ U_{k2}(t, T) \end{bmatrix}$ ,  $k = 1, 2, 3, \dots$

From (9) and (35) it follows:

$$(38) \quad \mathbf{Y}_g \begin{bmatrix} 0 \\ \Omega \end{bmatrix} + \begin{bmatrix} -\xi \mathbf{p}_b \\ \xi \mathbf{f}(x_b, T) \end{bmatrix} = 0$$

Substituting /37/ in /34/ and taking into consideration /38/ we get:

$$\mu \left[ \frac{\partial \mathbf{U}_a}{\partial t} + \xi \mathbf{B} \mathbf{U}_a \right] + \mu \mathbf{Y}_g \begin{bmatrix} \frac{dE}{dT} \\ \frac{dA}{dT} \end{bmatrix} + \mu \begin{bmatrix} \frac{\partial x_b}{\partial T} \\ \frac{\partial p_b}{\partial T} \end{bmatrix} = \mu \begin{bmatrix} 0 \\ \mathbf{F}_v \end{bmatrix} + (\xi - 1) \begin{bmatrix} -\mathbf{p}_b \\ \mathbf{f}(x_b, T) \end{bmatrix} + \mathcal{O}(\mu^2)$$

Developing in a series in the powers of  $\mu^k$ ,  $k=1,2,3, \dots$  we get in front of  $\mu^k$ :

$$(39) \quad \frac{\partial \mathbf{U}_{\hat{e}}(tT)}{\partial t} + \xi \mathbf{B} \mathbf{U}_{\hat{e}}(tT) = \hat{\mathbf{O}}_{\hat{e}}, \quad \hat{e} = 1, 2, 3, \dots$$

where  $\Phi_k = \begin{bmatrix} \Phi_{k1} \\ \Phi_{k2} \end{bmatrix} \quad k = 1, 2, 3, \dots$

In particular, in front of  $\mu^1$  we get:

$$(40) \quad \frac{\partial \mathbf{U}_1(tT)}{\partial t} + \xi \mathbf{B} \mathbf{U}_1(tT) = \hat{\mathbf{O}}_1,$$

where

$$(41) \quad \Phi_1 = -\mathbf{Y}_g \begin{bmatrix} \frac{dE_o(T)}{dT} \\ \frac{dA_o(T)}{dT} \end{bmatrix} + \begin{bmatrix} -\frac{\partial x_b}{\partial T} \\ -\frac{\partial p_b}{\partial T} + \mathbf{F}_v \end{bmatrix} + \frac{(\xi_o - 1)}{\mu} \begin{bmatrix} -\mathbf{p}_b \\ \mathbf{f}(x_b, T) \end{bmatrix}$$

The solution of (39) and, in particular of (40), is sought by variation of the constants.

Let:

$$(42) \quad \mathbf{U}_{\hat{e}}(tT) = \mathbf{\Xi}_g \mathbf{N} \mathbf{V}_{\hat{e}}$$

where  $\mathbf{V}_k(t, T) = \begin{bmatrix} \mathbf{V}_{k1}(t, T) \\ \mathbf{V}_{k2}(t, T) \end{bmatrix}$ .

Taking into account (32) from (39) it follows:  $\frac{\partial \mathbf{V}_{\hat{e}}(tT)}{\partial t} = (\mathbf{\Xi}_g \mathbf{N})^{-1} \hat{\mathbf{O}}_{\hat{e}}$

and, taking into account (33),

$$(43) \quad \mathbf{V}_{\hat{e}}(tT) = \mathbf{V}_{\hat{e}}(0T) + \int_0^t \mathbb{1} + (t+t_o) \mathbf{Q} \mathbf{N}^{-1} \mathbf{H}^{-1} \mathbf{Y}_g^{-1} \hat{\mathbf{O}}_{\hat{e}} dt'$$

Below, for brevity, the index "k" is omitted. From (43) it follows that:

$$(44) \quad \mathbf{V}_{\hat{e}}(tT) = \mathbf{V}_{\hat{e}}(0T) + \int_0^t \mathbb{1} + (t+t_o) \mathbf{Q} \left\{ \frac{\partial}{\partial t'} [\mathbf{K}_1 + \mathbf{D}(Tt')] \right\} dt'$$

where  $\mathbf{K}_1$  and  $\mathbf{D}(T)$  have been introduced through the relations:

$$\int_0^t \mathbf{N}^{-1} \mathbf{H}^{-1} \mathbf{Y}_g^{-1} \Phi dt = \mathbf{K}_1 [\Psi(t), T] + \mathbf{D}(T)t,$$

$$\mathbf{D}(T) = \left\langle \mathbf{N}^{-1} \mathbf{H}^{-1} \mathbf{Y}_g^{-1} \hat{\mathbf{O}} \right\rangle_t$$

at  $\mathbf{K}_1 [\Psi(0), T] = 0$

Integrating (44) by parts we obtain:

$$\mathbf{V}_k(t, T) = \mathbf{V}_k(\mathbf{0}, T) + [1 + (t + t_0)\mathbf{Q}]\{\mathbf{K}_1[\Psi(t), T] + \mathbf{D}(T)t\} - \mathbf{Q}\left\{\mathbf{K}_2[\Psi(t), T] + \mathbf{L}(T)t + \frac{\mathbf{D}(T)t^2}{2}\right\}$$

where  $\mathbf{L}(T) = \left\langle \mathbf{K}_1 \right\rangle_t$ .

$$\int_0^t \mathbf{K}_1[\Psi(t'), T] dt = \mathbf{K}_2[\Psi(t), T] + \mathbf{L}(T)t \text{ at } \mathbf{K}_2[\Psi(0), T] = 0.$$

Substituting in (42) and taking into account (33) as well as the fact that  $\mathbf{Q} = 0$ , we get:

$$\mathbf{U}(t, T) = \mathbf{Y}_g \mathbf{H} \mathbf{N} \left\{ -\frac{\mathbf{Q} \mathbf{D} t^2}{2} + [ -\mathbf{Q} \mathbf{V}(0, T) + \mathbf{D}(T) - \mathbf{Q} \mathbf{L}(T) ] t + [(1 - t_0 \mathbf{Q}) \mathbf{V}(0, T) + \mathbf{K}_1 - \mathbf{Q} \mathbf{K}_2] \right\}$$

The matrix function  $\mathbf{U}$  will be periodic with respect to  $t$  under the condition that  $\mathbf{Q} \mathbf{D} = 0$  and  $\mathbf{D}(T) = \mathbf{Q} [\mathbf{L}(T)] + \mathbf{V}(0, T)$  for the satisfaction of which it is sufficient to do the substitution:

$$(45), (46) \quad \mathbf{D} = 0, \quad \mathbf{V}(0, T) = -\mathbf{L}(T).$$

Then we get:

$$\mathbf{U}(t, T) = \mathbf{Y}_g \mathbf{H} \mathbf{N} [\mathbf{K}_1 - \mathbf{Q} \mathbf{K}_2 + (1 - t_0 \mathbf{Q}) \mathbf{V}(0, T)]$$

The condition (45) is equivalent to:

$$(47) \quad \left\langle \mathbf{Y}_g^{-1} \hat{\mathbf{O}}_{\hat{e}} \right\rangle_t = 0, \quad \hat{e} = 1, 2, 3, \dots$$

and, in particular, to the first order ( $\mu^1$ ). When  $k=1$ , from (41) and (47) it follows that:

$$(48) \quad \left[ \left\langle \frac{d\hat{A}_i(\hat{O})}{d\hat{O}} \right\rangle_t \right] = \left\langle \mathbf{Y}_g^{-1} \left[ \begin{array}{c} -\frac{\partial x_b}{\partial T} \\ -\frac{\partial p_b}{\partial T} + F_v \end{array} \right] \right\rangle_t - \left[ \begin{array}{c} 0 \\ \frac{\Omega_c (\xi_c - 1)}{\mu \xi_c} \end{array} \right].$$

In this way we eventually obtained the system of equations (36), (46) and (47).

## CONCLUSION

The analysis of the results obtained above leads to the important conclusion that: first, the initial approximation (29) obtained in action-angle variables is equivalent to the initial approximation (20) obtained in energy-angle variables; and, second, the equations obtained by Kuzmak's method are equivalent in first approximation  $/\mu^1/$  to the corresponding equations obtained by the non-canonical perturbation approach in energy-angle variables /see equations (48) and (20)/. The obtained results support the idea, particularly in the context of the analysis of a non-linear oscillator under external synchronizing influence, that the non-canonical /non-Hamiltonian/ and the canonical /Hamiltonian/ methods do not differ in principle. We must note at this point that, in the theory of nonlinear oscillations, a number of other methods exist that are not, even in first approximation, absolutely equivalent to the three methods presented above.

## REFERENCES

I. Damgov V., P. Georgiev. Non-linear oscillator under external asynchronous influence: comparison of perturbation and canonical methods of analysis. Aerospace Research in Bulgaria, V.16, 2000.

# NON-LINEAR OSCILLATOR UNDER EXTERNAL SYNCHRONIZING INFLUENCE: COMPARISON OF PERTURBATION AND CANONICAL METHODS OF ANALYSIS

Vladimir Damgov\* and Peter Georgiev\*\*

\* Space Research Institute at the Bulgarian Academy of Sciences

\*\* Department of Physics at the Technical University, Varna

Abstract. The term “Synchronous action” here encompasses all cases of frequency lock-on, frequency multiplication and division, phenomena of synchronization at commensurable frequencies. A non-canonical /non-Hamiltonian/ perturbation approach is presented for the study of non-linear oscillator under external synchronous action in “energy-angle” variables. The iteration constants of the initial solution are introduced to be the new variables. By applying consistently the method of canonical transformations and multiplying functions, a canonical approach in “action-angle” variables for analysis of the same system under similar conditions is developed. Both approaches are characterized by the transition, in the very beginning, to functions with constant period, and only then the necessary functional matrices are introduced. The same problem is studied on the basis of a version of Kuzmak’s method developed in a matrix form, for the case when, in the very beginning of the study, the system detuning is regarded to be an independent parameter. The conclusion is formed, on the basis of the performed analysis, that the equations and the first approximation of the respective solutions when using the three basic approaches mentioned above are equal to each other. In particular, this conclusion is a contribution to the idea that there is no principal difference between the non-canonical /non-Hamiltonian/ and the canonical /Hamiltonian/ methods. However, attention is drawn to the fact that some of the other existing analytical methods developed in the frames of the Theory of Non-linear Oscillations could not give, even in the first approximation, a complete coincidence with the solution obtained using the three approaches mentioned above.

# ON THE EXPECTED OBSERVATIONAL BEHAVIOUR OF THE ACCRETION FLOW IN A CLOSE BINARY

**Maria M. Dimitrova**

Here is presented one idea about the origin of the quick non-periodic or quasi-periodic oscillation of the X-ray luminosity in close binary systems. It is shown that a change in the inflow gas stream can produce those variations in the inner part of the flow.

As it is well known, nearly all X-ray binaries involving mass exchange between the two components display quick quasi-periodic or non-periodic oscillations with different amplitudes and time scales [1-3]. We are talking about variations with small amplitudes that cannot be identified as individual events, such as bursts, eclipses, etc.

So far, most of authors believe that these variations are produced as a result of some instabilities at the inner boundary of the accretion flow [1, 3-5].

Our studies on the behaviour of a gas flow with variable inflow parameters [6] revealed that such variations of the inflow parameters travel along the spiral shock fronts and, as a result, variations in the X-ray luminosity at the inner boundary of the flow are produced.

Based on the two-dimensional model described in [7], involving the full energy-exchange equation [8], a series of calculations are made, attempting to describe the influence of such exchanges in inflow gas debit through the inner Lagrangean point over the X-ray luminosity.

The calculations are made for a close binary, containing a compact object with mass  $\dot{I}_1 = 1.5 M_o$ , a star that is filling its Rosh lobe with mass equal to  $\dot{I}_2 = 4 M_o$ , a distance between the components  $R_{12} = 10^{11}$  cm and an accretion rate equal to  $10^{-9} M_o$  per year.

As a base, the steady state reached by the flow after some orbital periods was used. Calculations are made, where for about five seconds, the accretion rates increase respectively 2, 4, 6, 8, and 10 times. In Figs.1-3, the behaviour of X-ray luminosity is shown during the first 30 seconds, after these increases in the last three cases.

As it is seen in the figures, the increase in the inflow accretion rate produced quasi-periodic oscillations accompanying the increase of X-ray luminosity.

The described model, however, is very far from the possibility to be base for modelling of the luminosity that we can observe. It rather aims to study the structure of the accretion flow and its stability.

The model is only a first step in trying to determine the influence of the different physical parameters in the flow on the produced luminosity. It attempts to emphasize the most important details in a future three-dimensional model which will calculate radiation production and its interaction with the gas flow.

The X-ray luminosity  $L_x$  calculated here is integral both by frequency and by space distribution. Moreover, in these calculations we assume that the whole gravitational energy of the gas fallen onto the surface of the compact object is converted to X-ray luminosity.

To be able to calculate the observation behaviour of the object we must know the frequency and the space distribution of this luminosity, and to give an account of the interaction between this luminosity and the gas flow.

Nevertheless, we can provide quality estimation.

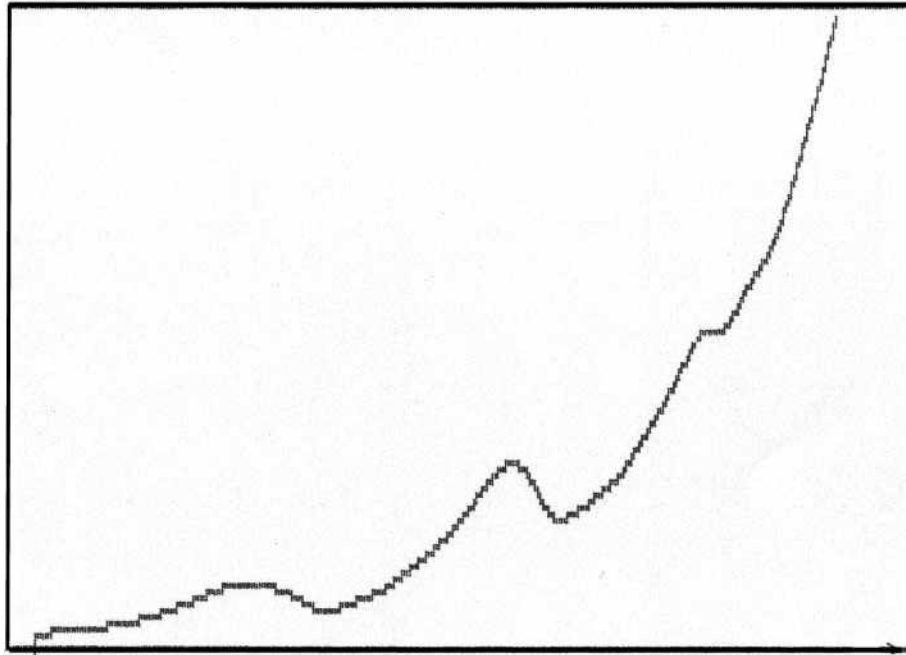


Fig. 1 The behaviour of X-Ray luminosity on the compact object surface during the first 30s after a 6 time increase of the inflow accretion rate

First, the calculated variations in X-ray luminosity shown in Figs. 1-3 provide an idea of the possible origin of the same kinds of quick variations observed in most of the X-ray binaries, as a product of the exchange in the inflow gas stream parameters. These curves are calculated as a product of a one-time increase in the accretion rate at the first Lagrangean point. The same behaviour was observed after the changes of the inflow gas direction [6].

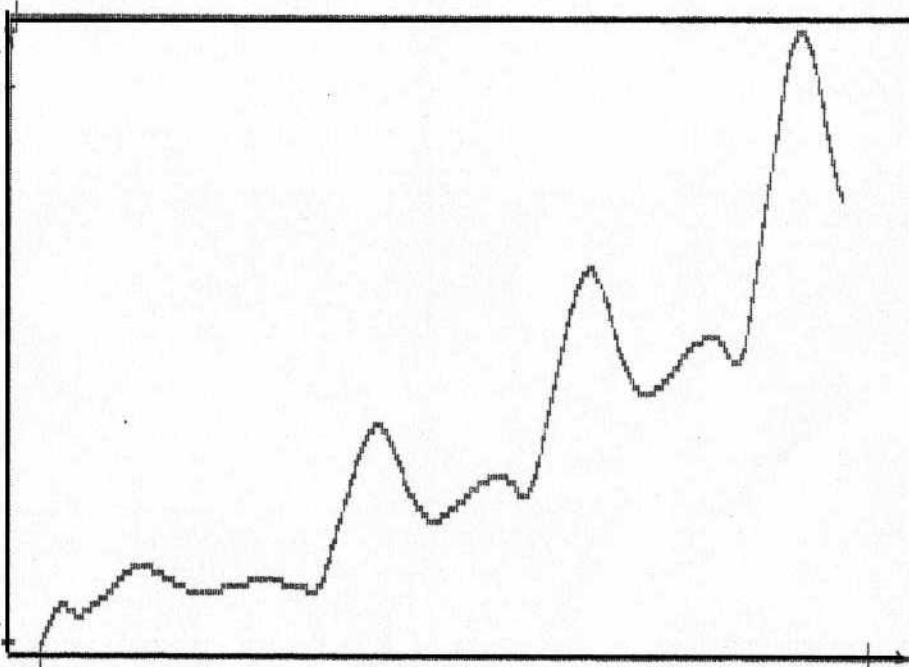
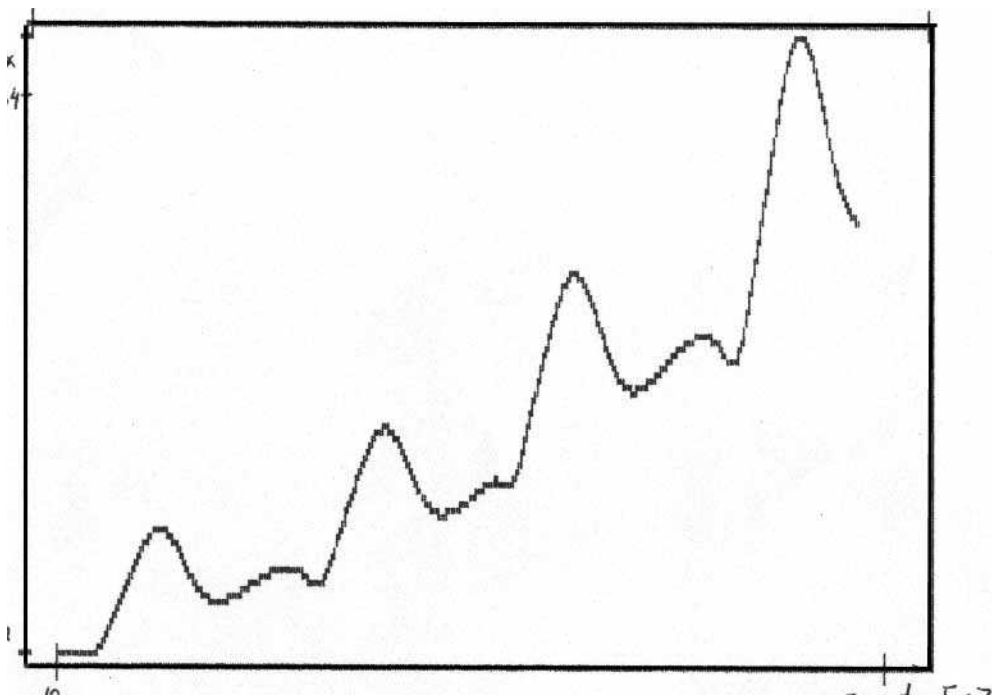


Fig.2 The behaviour of X-Ray luminosity on the compact object surface during the first 30s after a 8 time increase of the inflow accretion rate



inflow  
; that  
oo.

Fig. 3 The behaviour of X-Ray luminosity on the compact object surface during the first 30s after a 10 time increase of the inflow accretion rate

To be comparable with the observations, such variability must be calculated by a model admitted for the physical activity of the companion star.

The second prediction of our model is that, because of the non-uniform disk thickness, when the object is observable at low angle with respect to the binary plane, we must observe some kind of eclipses of the central X-ray luminosity.

A more detailed study on these issues will be carried out in the future.

#### References:

1. I. van der Klis, "Rapid aperiodic variability in X-ray binaries", 1993, AIAP-1993-009
2. White, N.E., Astron. and Astrophys. review, 10.2.1989
3. Hayakawa S., Physics Reports, v.121, N 6, 1985
4. Collins, T.G.B., H.L. Helfer, H.M. van Horn, Ap.J. 508, p. 159, 1998
5. Collins, T.G.B., H.L. Helfer, H.M. van Horn, A&A, 193, p. 5205, 1998
6. Dimitrova, M.M., *Àãðíêîñì-âñêè èçñëääááíèÿ â Áúëääðèÿ*, 13, ñ. 19, 1997
7. Dimitrova, M.M., *Àãðíêîñì-âñêè èçñëääááíèÿ â Áúëääðèÿ*, 13, ñ. 27, 1997
8. Dimitrova, M.M., *Àãðíêîñì-âñêè èçñëääááíèÿ â Áúëääðèÿ*, 15, ñ. 3, 1999

# THE INFLUENCE OF THE INFLOW GAS TEMPERATURE ON THE EFFICIENCY OF THE ACCRETION ENERGY PRODUCING

**Maria M. Dimitrova**

*Space Research Institute of the BAS, 6 Moskowska str., Sofia, BULGARIA*

It is not yet fully investigated the influence of the inflow gas parameters on the structure, stability, complete behaviour of the gas stream in close binary systems. Most of the authors are not pay attention on these parameters at all.

In our previous papers [1-2]we shown that the velocity and its direction acts very strong on the complete behaviour of the accretion flow.

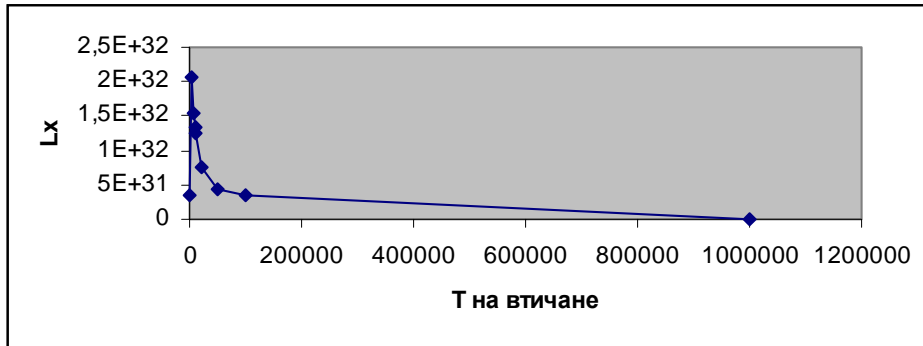
During last years some author [4-6] shows, that these parameters are in fact the boundary conditions in the equation system, describing the gas dynamic. And, therefore, they are very important parameter, that can change hole picture.

In this paper we are investigate the influence of the temperature in the first Lagrangian point of the gas stream in close binary system on the produced x-ray luminosity at the inner part of the flow. We are made these investigation numerically, using 2D model, described in our previous works [1-3]. It was used the full energy-transfer equation [3].

We are used the following binary system parameters:  $M_{ns} = 1,5 M_{\odot}$ ,  $M_2 = 4 M_{\odot}$ ,  $R_{21} = 10^{11}$  sm., debit of the inflow gas equal to  $10^{-9} M_{\odot}/\text{year}$ , the inflow angle equal to  $30^{\circ}$ . We made calculation for the inflow gas temperatures and respectfully fined the x-ray luminosity at the inner part of the flow after reaching the steady state, as follows in Table 1:

Table 1

inflow gas temperature [°K]	x-ray luminosity [erg/s]
$10^3$	$3,426 \cdot 10^{31}$
$5 \cdot 10^3$	$2,0601 \cdot 10^{32}$
$7,5 \cdot 10^3$	$1,5484 \cdot 10^{32}$
$9 \cdot 10^3$	$1,3426 \cdot 10^{32}$
$10^4$	$1,244 \cdot 10^{32}$
$2 \cdot 10^4$	$7,625 \cdot 10^{31}$
$5 \cdot 10^4$	$4,2842 \cdot 10^{31}$
$10^5$	$3,426 \cdot 10^{31}$
$10^6$	$1,55 \cdot 10^{28}$



The same results are shown on the Fig 1.

Figure 1

As it is seen, the inflow gas temperature acts very strong on the efficiency of the energy producing in the accretion flow. More than this, if the inflow temperature is less than  $10^3$  °K, the steady state solution can not be reached in our model. If the temperature is very high, unfortunately, the efficiency decrease. In optimal case of temperatures between  $10^3$  K and  $10^5$  K, the efficiency varies 100 times.

As a conclusion we can say that all the parameter of the inflow gas stream plays very important role in the dynamically behaviour of the stream as a hole. And it is necessary these parameters to be included in all investigations.

## References

1. Dimitrova, M.M., Аерокосмически изследвания в България, 13 , с. 27, 1997
2. Dimitrova, M.M., Аерокосмически изследвания в България, 13 , с. 19, 1997
3. Dimitrova, M.M., Аерокосмически изследвания в България, 15 , с. 3, 1999
4. Feng Yuan, arXiv:astro-ph/9907317, 1999
5. Yuan, F., Peng, Q., Lu, J., Wang, J., arXiv:astro-ph/0002068, 2000
6. Feng Yuan, arXiv:astro-ph/0002069, 2000

# **ВЛИЯНИЕ НА ТЕМПЕРАТУРАТА НА ВТИЧАЩАТА СЕ ГАЗОВА СТРУЯ ВЪРХУ ЕФЕКТИВНОСТТА НА ЕНЕРГООТДЕЛЯНЕТО ПРИ АКРЕЦИЯ**

**М.М. Димитрова**

## **РЕЗЮМЕ**

На базата на двумерен числен модел на акреционното течение в тясна двойна звездна система е изследвано влиянието на температурата на втичащата се газова струя върху продуцираната Рентгенова светимост от повърхността на компактния обект. Показано е, че тази температура е от съществено значение за ефективността на енергоотделянето при акреция. Като се имат предвид резултатите от предишни изследвания на зависимостта на динамиката на течението от останалите параметри на втичащата се газова струя, следва да се заключи, че всички тези параметри са от съществено значение и не бива да се пренебрегват.

# **First Successful Space Seed-to-Seed Plant Growth Experiment in the SVET-2 Space Greenhouse in 1997**

*Tania Ivanova, Svetlana Sapunova, Plamen Kostov,  
Ivan Dandolov*

*Space Research Institute, Bulgarian Academy of Sciences, 1113 Sofia, Bulgaria*

## **1. Introduction**

The effect of microgravity on plant growth is an important research area since plants could eventually be a major contributor to biological life support systems (BLSS) in future long term space missions. On space stations orbiting the Earth, Moon, or other planets, and in spacecrafts making long journeys, supplementing the food that is carried along from the Earth with food that can be grown in space, would be a great weight-saving benefit. In addition plants can provide a service now performed by sophisticated equipment to scrub the carbon dioxide in the atmosphere expelled when the crew breathes. At present the oxygen necessary for breathing has to be replaced by onboard supplies carried from the Earth. Plants that use carbon dioxide in their metabolism and expel oxygen as a waste product can potentially take on the task of regenerating the atmosphere and eliminating excess humidity from the environment. And, not to be underestimated, is the up-lifting psychological effect of caring for and nurturing a garden, so far away from the greenery of the Earth. With the goal of studying this important link of a future BLSS in mind a Russian-Bulgarian group started working in 1984 on the project and created the first Space Greenhouse (SG) named SVET. Greenhouse modules were designed and tested on Earth by Bulgarian scientists from the Space Biotechnology Department of the Space Research Institute, Bulgarian Academy of Sciences.

## **2. Brief description of the early experiments in SVET SG**

Some unique onboard experiments in the field of fundamental gravitational biology have been conducted in the SVET SG. The first major advance was made in June 1990 when the equipment was launched to the MIR Orbital Station (OS) inside the Krystal module and the first space experiment began [1]. The first fresh vegetables (radishes and Chinese cabbage) were produced in space during this experiment. Although plants grew during the 54-day period, a delay in the stages of development of the space plants was observed [2]. The fresh 23- and 54-day and dried 29-day plants returned to Earth were less of the size of the ground control plants that had been grown under the same lighting conditions as onboard MIR OS. Physiological and chemical analyses showed that the space plants were exposed to significant moisture and nutrient stress [3]

In 1994, NASA, the U.S. Space Agency, and the Russian Space Agency signed an agreement to conduct a number of joint SHUTTLE-MIR missions. According to this agreement a number of experiments on the "Greenhouse" Project were planned by the Utah State University (USU) and the Institute of BioMedical Problems (IBMP), Moscow, that were carried out in the SVET SG equipment [4]. Wheat, as an important agricultural crop and primary candidate for a future plant-based BLSS was used in the beginning. To achieve the ultimate goal, growing up of plants "from seed to seed" in microgravity, a

series of flight and earth experiments were conducted, the most important being: a 3-month space experiment on MIR OS in 1995 termed “Greenhouse 2a” and a 6-month one in 1996-1997, termed “Greenhouse 2b” when mature wheat plants were harvested.

The “Greenhouse 2a” experiment was conducted on MIR OS between Aug. 10 and Nov. 9, 1995. Seeds of *Super-dwarf* wheat plants were planted in the SVET-2 SG[5]. Plants were sampled at 5 stages: on the 14th, 19th, 35th, 53rd and 74th day from planting and final harvest was on the 90th day. The plants were disoriented since, due to the Mylar mirror, the light was coming from all directions. The most interesting results were that the plants remained vegetative throughout the experiment, no flower formation was observed in any of the samples that were studied and some mature plants had as many as 18 leaves instead of the usual 8 leaves plus an ear.

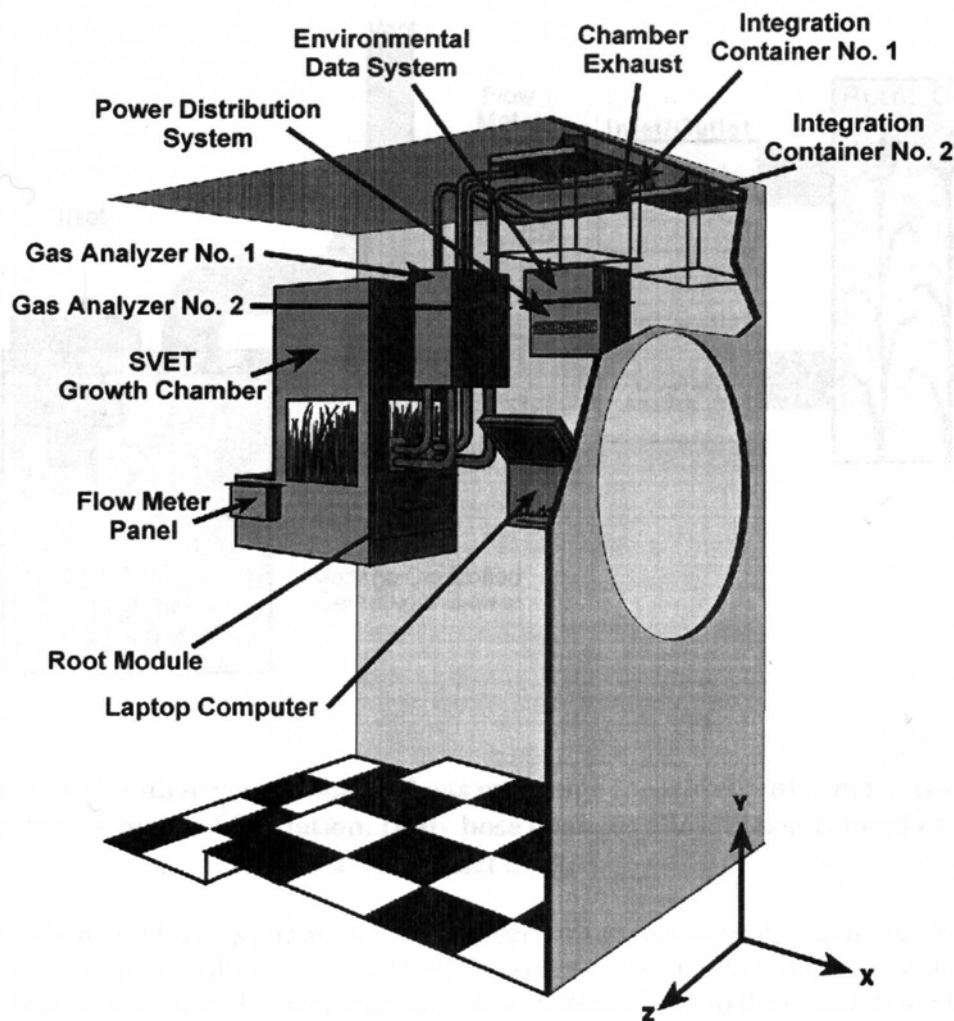
The “Greenhouse 2b” experiments were conducted on MIR-NASA-3 program from Aug. 10, 1996 to Jan. 17, 1997. Healthy plants of *Super-dwarf* wheat were grown through a complete life cycle [6]. The seeds were sown on 10 August 1996 by astronaut Shannon Lucid and plants were sampled at 4 stages: on the 43rd, 61st, 74th and 85th day. U.S. astronaut John Blaha harvested the first crop of healthy plants on 6 December 1996 and said he collected about 400 seeds! Later we were disappointed - it turned out there were 297 heads but not a single seed (all the heads were sterile). Our plants produced far more biomass and additional drying of the biological material showed that the absolute content of the dry material in the plant biomass was 95.6% - that is far more than in any other plant experiments. A second crop was planted with seeds brought from Earth a few hours after the harvest, and when the Shuttle Atlantis docked with MIR OS in mid-January 1997 (on 42nd day) that crop was harvested green, frozen in liquid nitrogen, and returned to Earth for investigation.

Ground studies were initiated to replicate the conditions on MIR OS to try to isolate the cause of the plant sterility. There is a list of about a dozen things that could have caused the sterility of the heads, only one of which is microgravity. Prof. Frank Salisbury from USU – the principal investigator of the study believes the likely culprit for the plants heads sterility to be the gas, *ethylene*, in the cabin atmosphere of MIR OS. Ethylene, a gaseous plant hormone, is known to produce male sterility (lack of valuable pollen) in wheat, and the preliminary observations revealed a lack of pollen in well-formed but unopened anthers in the wheat flowers (which were arrested in their development). There was an excessive amount of tillering (branching) in the plants (hence the many heads), and this is a well-known symptom of excess ethylene. Various species of fungi produce ethylene, and there is much fungus growth in MIR and even in SVET-2 SG (apparently not directly harmful to vegetative growth and head formation of the wheat). Thus, a strong circumstantial case exists for ethylene as the cause of the lack of seed formation. Ethylene is not normally measured in the cabin atmospheres of spacecraft because it is harmless to humans until concentrations reach about 85 % in the atmosphere, but plants are sensitive to ethylene in the parts-per-billion range.

The scientists from NASA reached a decision to make an attempt with another plant species, *Brassica Rapa* plants, in the next “seed-to-seed” experiments conducted on MIR OS in 1997.

### 3. Equipment used in 1997 experiment

The basic SVET SG equipment including all life support systems necessary to provide normal plant growth was used in these experiments but it was upgraded and extended under Bulgarian-American contract. A new generation SVET-2 SG with considerably improved technical characteristics was developed to satisfy the increased requirements of the experiments [7]. A new brighter Illumination Unit and updated Root Modules (RM) were developed, delivered to the station and mounted in the SVET Growth Chamber existing onboard the MIR OS (Fig. 1).



The RM were charged with a new kind of “substrate, the so-called “turface”. It was not dressed beforehand with nutritives and mineral salts as the “Balkanine” used in the “GH-2” [8]. But 1 gram of special Osmocote pellets was to be added to each plant row as a nutritive supply. The Gas Exchange Measurement System (GEMS) designed and built in USU (under the direction of Dr. Gail Bingham) was added to the basic SVET equipment to extend the range of environmental parameters that were monitored [9]. It included the Gas

Analyser System with two infrared Gas Analysers that provide all the measurements of H<sub>2</sub>O and CO<sub>2</sub> concentrations and differences and the Environmental Data System with sensors for soil moisture, air and leaf temperature, light, and cabin air pressure. GEMS was controlled by the Laptop Computer, collecting all data on disk. Controlling the moisture within the RM has always been a problem of utmost importance (the Flow Meter Panel was added). To solve this problem USU developed sophisticated system including sixteen soil moisture sensors inserted into the RM to measure distributed water content both on the surface and in depth of the substrate. But even though that was sophisticated and provides indisputable possibilities to monitor the moisture distribution in the substrate volume the rather simpler measurements of the two Bulgarian-design sensors were the ones that were used to control the moisture level.

#### 4. Description of the 1997 Experiments

These experiments were again addressed to the problem of “seed-to-seed” cycling in microgravity. They were planned by the Louisiana State University (LSU), IBMP and USU and were carried out between 27 May and 31 September 1997 under the direction of Dr. Mary Musgrave from LSU on the MIR-NASA-5 Program. The species *Brassica rapa* which derive from the economically important mustard family and have a very short life cycle were used in the experiments. The experiments were carried out by the astronaut Michael Foale (M.F.) who was launched on MIR OS on May 15 by the STS-84 mission of the joint Russian-American project MIR-SHUTTLE [10]. Along with Foale aboard Atlantis were *Brassica rapa* seeds and associated experiment hardware. Hardware transported included all supplies required to collect biological samples, equipment for pollination and operation with the seeds as well as Bulgarian equipment for SVET-2 SG (three RM and new lamps for the Illumination Unit).

The goal of the experiments was to study a plant’s entire life cycle in microgravity and better understand the effects of microgravity on plant reproduction. It was approached with the hypothesis that the microgravity environment caused a reduction in the storage reserves available to support reproductive events. The plan was for three successive plantings of *Brassica rapa*, beginning with planting of 52 seeds launched from the ground on STS-84 - the so-called “Earth seeds” (E1 seeds). These plants take about 14 days to flower after planting and the plan was for Foale to spend seven days to pollinate them. After 45 days plants were to be harvested. Seeds produced in space from this first planting on MIR OS were to be collected, dried and used in the second growth cycle. This second set of seeds was called “Space 1” (S1 seeds). Seeds generated in space from the second planting on MIR OS, the S2 seeds were to be collected and planted in the third planting in space, along with Earth seeds and S1 seeds. The experimental data would aid in determining the effects of space flight on plant growth, reproduction, metabolism, and production. By studying the chemical, biochemical, and structural changes in plant tissues, we hoped to understand how processes such as photosynthesis, respiration, transpiration, stomatal conductance, and water use were affected by the space station environment.

From May 21 to May 26, 1997 the greenhouse hardware was assembled on board the MIR OS and prepared for the experiment operations. After that "Program 1" was run to test the SVET-2 SG hardware. On May 29 M.F. started "Program 2" on the Control Unit adding water for initial substrate moistening. This program was performed two times to provide sufficient water to the two RM cells K1,2 of the SVET-2 SG. The seeds were planted on May 31. They were in cellophane strips on a sticky tape about a millimetre in

size. He placed them into the wick, about 13 per row. After planting the seeds M.F. started "Program 3" for long vegetation. The Illumination Unit was switched to a program in a cycle of 23 hours on and one hour off.

The first sprouts were visible on June 2. As the seeds started to germinate, about 50% of them grew along the wick because M.F. had placed them fairly deep down into the wicks. When they finally popped up above the wick he teased them up with tweezers and the light, through phototropic action, drew the plants upwards, toward the lamps. Overall, about 80% of the seeds germinated. On June 6 when the plants had grown about three or four centimetres M.F. placed the leaf bags over. They allowed to measure CO<sub>2</sub> and humidity levels of the air entering and exiting each bag. In a matter of a week or so the plants started to grow one or two primary leaves, and then flower buds. After about four weeks, when the plants were about five centimetres, the buds produced a plethora of yellow flowers, which had pollen on the stamens. On June 16 the leaf bags were removed and four plants were harvested and fixed for ground analysis.

Pollination procedures were started on the next day (June 17). There is only a day's or two days' window in this very rapid growth cycle when the flower is ripe to give pollen. That is why pollination was carried out over a period of about a week. Throughout the week before June 18, only cell K1 was yielding mature plants for pollination. On June 23 M.F. reported that cell K2 started producing flowers and should be pollinated an additional week. He also reported that seed pods, known as siliques, in cell K1 appeared to be "lumpy" which he believed was indicative of seed development.

After finishing the pollination procedures the leaf bags were put back on in order to measure CO<sub>2</sub> over the plants again. The second harvest and subsequent fixation was scheduled to occur five days after the first harvest but it was postponed to allow more time for pollination activities.

Experiment operations continued normally until the space accident of June 25 during the docking of a supply ship Progress 234 that collided with the MIR OS causing subsequent Spektr depressurisation. Almost all science on board MIR OS was affected. Due to power constraints, normal lighting operations for the experiment were interrupted for a few days and plants experienced 72 hours of darkness. The Krystall module was totally unpowered. Then, to save the experiment, M.F. powered the SVET-2 SG from the base block using a long extension cord. It was a pretty hard environment for that experiment. At that time to assess the effect on the plants and advise M.F. on future operations the scientists from LSU created the same conditions for the control plants growing on Earth. The ground-based laboratory plants exhibited reduced seed weight and had a higher percentage of undeveloped seeds than plants that continued in the light. However, it is not believed that the irregular lighting schedule seriously impacted the study. Daily observations and photography sessions continued despite the power constraints. Unfortunately the leaf bags were stored in Spektr at the time of the collision. So they were not usable and the experiment had to go on without gas-exchange measurements.

On Earth the cycle is about four weeks. It took longer in space, because the conditions were harder on MIR OS at that time. The temperatures were not quite so constant, they were down even in the 5°C range, CO<sub>2</sub> concentrations ranged 15-20 times above normal levels on Earth and it slowed down things. After six weeks, some pretty long seed pods (just like pea pods) grew in the place where the flowers were. They seemed to be full of seeds.

Seeds (S1 seeds) were collected just before the final harvest, which occurred on

July 21. Seed pods were placed into little vials with desiccant, while the rest of the plants were put into formaldehyde, so they could be studied later on Earth. Space produced S1 seeds were a total of 15 or 20. They were tiny, half a millimetre in size. They were smaller than Earth seeds and not as strong. The preliminary report said that the seeds had similar structures to Earth seeds and that they looked viable. Unfortunately the S1 seeds were so weak and flimsy that only a few of them were worth even planting.

The “second planting” was performed on July 23, 1997. Six or seven of the S1 seeds were replanted together with Earth seeds so that there were half space seeds and the other half, original Earth seeds in the first row. The Earth seeds sprouted and were reported to be approximately 1 cm tall on July 30. Some of the S1 seeds sprouted too, but by that time they had not appeared above the wick material. Both Earth and S1 seeds continued to grow and later, on August 6, they were reported to be approximately 2.5 to 3.0 cm tall.



The pollination procedures for the plants germinated from Earth produced seeds were started on August 9 and were performed daily for eight days thereafter due to various stages that the plants were at. Pollination for the S1 seed germinated plants would be scheduled as these plants matured. The first fixation of samples from the second harvest was completed on August 14. The Earth plants produced siliques and on August 27 they were 3-5 cm long. Both the space plants and the Earth plants that did not produce siliques were collected and placed into a chemical preservative solution on August 29. On September 3, 1997, the Earth plant seed pods appeared healthy and were reported to be 5-6 cm long and 6 mm wide. They were harvested on September 13. The final harvest for the second planting (S1,2 seeds) was performed on September 16.

Only four of the space produced seeds germinated, out of the six or seven that were planted. There were 4 space plants on orbit - a total of four space seeds matured into “space plants” but M.F. thinks only two of them actually ended up producing a viable plant that grew up (see Fig.2). These second generation plants were smaller than the first. A cause for this is likely to be the small size of the S1 seeds. In the conditions of this hard environment in SVET-2 SG with difficulties in substrate moistening and the uncertainty of how the seed gets the nutrient through the wick it is supposed that the seed that is bigger is

always favoured to do better because how much built-in carbohydrate material that seed has, determines how far it gets going. If the environment was more favourable and the soil - very nutritious, then it would not matter too much, how strong the seed was. Irrespective of this result, the germination of the space seeds and subsequent plant maturation were major experimental milestones since these events had never before occurred on-orbit.

The third planting was performed on September 17 with the seeds collected from the September 13 harvest (S1,2 seeds). The Greenhouse experiment operation concluded with the final harvest for the third planting performed on September 30 and the hardware was subsequently disassembled. The Greenhouse hardware and all preserved plant samples were returned to Earth on STS-86.

A total of three successive generations of plants were grown and harvested during the MIR-NASA-5 mission. On-orbit seed germination of seeds and maturation of plants that were themselves grown in space has never been accomplished before and this was a great success of the science.

#### 5. Some environmental conditions during the 1997 experiment

One of the vital parameters for plant development is the substrate moisture SM1,2, measured in the two separate cells K1 and K2 of RM and maintained within defined (set up by the astronauts) threshold levels (SMT) by the Control Unit (CU) of SVET-2 SG [11]. On Fig.3 are shown the substrate moisture (SM2) and temperature (ST2) values in the second cell K2 of RM as well as the necessary water consumption (WC2). The data has been received through the telemetry system during the first month of the 1997 experiments. During the first two days from the start of the experiment (29 and 30 May 1997) the astronauts run Program 2 for initial substrate moistening of RM twice, each time supplying 30 water doses (relying on our experience of 1996).

When starting Program 3, SMT was set to 50 % to provide a good and regular substrate moistening in the whole RM volume (close to the full soil moisture capacity when the water distribution velocity is highest). Such a moisture level creates favourable conditions for better water movement and good aeration of the root zone at the same time. In space metrology, a method has been adopted for calibration of the substrate moisture measurement sensors SM1,2 accepting as 100% moisture level the moisture of a volume filled with substrate and flooded. For that reason, the full soil moisture capacity has different values for different media (substrates) and varies between 45% and 65%. During the initial period of moistening when evaporation is relatively small (only from the surface of RM and without plant transpiration) the American sensors have indicated moistening of the whole volume and the SMT was reduced by 5% (to 45%). During the first days of germination the seeds placed in the wicks (connected to the pipes of the hydrosystem) were pretty well moistened.

When Program 3 was restarted during the 6<sup>th</sup> day of the experiment the necessary threshold of 45% was not set up and the result was an abundant water supply in the substrate volume. This raised the water content in RM to such a level that during the following week it was not necessary to supply even a dose of water (there was no value measured under 45%). On the 14<sup>th</sup> day SMT was raised to 50%, the automated system reacted immediately and supplied continuously water doses, maintaining SM2 regularly in these limits, compensating the evaporation. On the 25<sup>th</sup> day the SMT was reduced again to 45% to dry the plants and mature the seeds, but on the 27<sup>th</sup> day the experiment was stopped (temporarily) and the TMS information - definitively due to the collision.

From the measured substrate temperature values (ST2) it is clear that the temperatures maintained on MIR OS have been comparatively high during the first 2 weeks – within 27-28°C, and they have returned to normal during the next two weeks (22-23°C). The substrate temperatures being in direct dependence on the environmental air onboard the MIR OS are only 1-2°C lower (due to the evaporation).

## 6. Conclusion

After the failure of the idea of producing wheat seeds in space during the “Greenhouse 2” experiment the success of the 1997 experiment stimulated the scientists to continue conducting wheat plant experiments aimed at carrying out a complete life cycle (“seed-to-seed”) under microgravity.

As a third experiment (“Greenhouse 3”) in the consecution of wheat plant experiments in February 1998 the American scientists made an unsuccessful attempt to grow *Super-dwarf* wheat on MIR OS in another greenhouse equipment (“Astroculture”). Unfortunately the equipment failed and the experiment was interrupted.

The next experiment (“Greenhouse 4”) was carried out in the SVET-2 SG on MIR OS between November 1998 and February 1999 by the Russian 26 crew (astronaut S. Avdeev). Healthy plants of wheat (a variety of *Apogey*) were grown through a complete life cycle. This variety has been developed by scientists of USU specially for greenhouses and is distinguished for its ability to form seeds in high ethylene concentrations. The *Apogey* wheat reaches average height which is important for the conditions of space flight. The seeds were sown on 18 November 1998. Only 8 of them germinated because of problems with the program for substrate moistening. After solving these problems the seeds were sown again on 30 November. In the beginning of December they started to germinate and grew good sprouts. Later, about 15 January, plants started to form ears and on February 26 the life cycle was completed and the plants were harvested. The first wheat seeds were produced under microgravity conditions in this experiment. Some of the plants were dried for chemical and biochemical analysis.

The next wheat plant experiment (“Greenhouse 5”) was started onboard the MIR OS in the SVET-2 SG equipment by the Russian 27 crew. On 3 March 1999 the astronauts soaked 40 seeds (30 of them were Earth produced and the rest of 10 - space produced). The goal was already sprouting seeds to be planted in SVET-2 SG. All the seeds germinated and on 9 March were sown in the RM. The program for initial substrate moistening passed and the crew completed successfully the 3-month experiment.

Reliable equipment and biotechnology were created and considerable experience in conducting of plant experiments was gained in the 1990’s. Certainly, these experiments will be continued in the next 21<sup>st</sup> Century on the International Space Station (ISS): Russia is interested in a new updated version of SVET-3 SG; NASA is developing two suites of equipment - the Gravitational Biology Facility (Plant Research Unit) and Centrifuge Facility; ESA - Biopack and SGH. ESA and NASA signed an agreement for joint use of all life science facilities on ISS.

## References

1. I v a n o v a, T.N., Yu.A.Bercovich, A.L.Mashinskiy, G.I.Meleshko. The First Vegetables Have been Grown up in the "SVET" Greenhouse by Means of Controlled Environmental Conditions. *Microgravity Quarterly* (ISSN 0958-5036), Vol. 2, 2, 1992, 109-114.
2. I v a n o v a, T.N., I.W.Dandolov. Moistening of the Substrate in Microgravity. *Microgravity Science and Technology* (ISSN 0938-0108), Volume V (3); October, 1992, 151-155.
3. I v a n o v a, T., S.Sapunova, I.Dandolov, Y.Ivanov, G.Meleshko, A.Mashinskiy and Y.Berkovich. "SVET" Space Greenhouse Onboard Experiment Data, Received from "MIR". Station and Future Prospects. *Advances in Space Research* (ISSN 0273-1177), Vol. 14,11, 1994, 343-346.
4. I v a n o v a, T.N., S.M.Sapunova, P.T.Kostov. New Biotechnological Experiment Greenhouse SVET-2 for the MIR-SHUTTLE'95 Mission. *ACTA VET. BRNO* (ISSN 0001-7313), vol.65, 1, 1996, 5- 9.
5. S a l i s b u r y, F.B., G.W.Bingham, W. F. Campbell, J. G. Carmen *et al.*, Growth of super-dwarf wheat on the Russian space station MIR, *26th Intern. Conf. on Environmental Systems*, Monterey, CA, 8-11 July 1996 (SAE 961392).
6. I v a n o v a, T.N., P.T.Kostov, S.M.Sapunova, I.W.Dandolov, F.B.Salisbury, G.E.Bingham, V. N.Sytchov, M.A.Levinskikh, I.G.Podolski, D.B.Bubenheim, G.Jahns. Six-Month Space Greenhouse Experiments - a Step to Creation of Future Biological Life Support Systems. *Acta Astronautica* (ISSN 0094-5765), Vol. 42, Nos. 1-8, 1998, 11-23.
7. I v a n o v a, T., P.Kostov, S.Sapunova, G.Bingham, S.Brown. Equipment for the Greenhouse SVET'95 Project and Some Optimisations for Future Experiments on board the MIR Orbital Complex. *Аерокосмически изследвания в България* (ISSN 0861-1432), 1998, 14, 46-49.
8. I v a n o v a, T., I.Stoyanov, G.Stoilov, P.Kostov, S.Sapunova. Zeolite Gardens in Space. *NATURAL ZEOLITES Sofia'95*. Proceedings of the Sofia Zeolite Meeting' 95, 18-25 June 1995 (ISBN 954-642-015-8), G. Kirov et al. (eds), PENSOFT, 1997, 3-10.
9. B i n g h a m, G.E., T.Ivanova, P.Kostov, S.Sapunova et al. Plant Growth and Plant Environmental Monitoring Equipment on the Mir Space Station: Experience and Data from the Greenhouse II Experiment, *26th Intern. Conf. on Environmental Systems*, Monterey, CA, 8-11 July 1996 (SAE 961364).
10. F r e e m a n, M. Research on Mir Advances Growing Plants in Space. *EIR Science & Technology* (ISSN 0273-6314), Vol. 25, 41, 1998, 26-35.
11. I v a n o v a, T.N., P.T.Kostov, S.M.Sapunova, H.S.Dobrev, I.W.Dandolov. Sensors and Methods for Measurement of the Environment parameters in "SVET" Space Greenhouse. *Compt. rend. Acad. Bulg. Sci.* (ISSN 0861-1431), 45, 11, 1992, 55-58.

# RESULTS OBTAINED ONBOARD THE INTERCOSMOS-19 SATELLITE USING THE P4 DEVICE

G.Gdalevich\*, S.Chapkanov, T.Ivanova, M.Petrunova, V.Markov

*\*Space Research Institute, Russian Academy of Sciences  
Space Research Institute, Bulgarian Academy of Sciences*

*A b s t r a c t: Albeit the P4 device was in operation to the 236<sup>th</sup> orbit only, the results obtained by means of the cylindrical probe and the spherical ion trap compared with other measurement data provided to determine:*

- 1. The fidelity of the charged particles concentration probe measurement [1];*
- 2. The possibility of low-frequency wave excitation in the main ionospheric trough (MIT) and the auroral region [2,3,4];*
- 3. The low-frequency wave propagation along the magnetic field below the MIT level [5];*
- 4. To verify experimentally the interrelation between magnetospheric and ionospheric processes [6].*

*A survey of the papers referred to and the main results obtained using the P4 device is made.*

## **1. Fidelity of the charged particles concentration probe measurement.**

Some instruments for measurement of the charged particles concentration were placed onboard the IK-19 satellite: the IS-338 ionospheric station [7], two spherical ion traps, a cylindrical Langmuir probe (the P4 device) [8], and the KM-3 device measuring electron concentration every 4 sec along with its primary function – to measure the electron plasma temperature by a high-frequency method [9]. The measurement methods used in all these instruments were analyzed and the experimental data obtained from them was compared every several orbits, so as to check the fidelity of the charged particles concentration probe measurement [1]. It should be noted that concentration measurement accuracy depends on the ion-probe plasma frequency.

The results of the measurement of the electron concentration  $n_e$  by the Langmuir probe are shown in Fig.1 (curve 2); curve 1 represents the ion-probe data  $n_i$  (IS-338); curve 3 – the device KM-3  $n_e$  data with data correction compared to the ion-probe; curve 4 –  $n_i$  data from the spherical ion trap with a “floating” potential.

Universal Moscow Time (UT); Magnetic Latitude (MLAT); Local Time (LT); and Satellite Altitude (ALT) are given along the x-axis.

It becomes evident from [1] that the data from the spherical ion trap with a “floating” potential has the highest resolution time. Concentration variations according to ion-probe and ion trap data are cophasal and have a similar pattern although the concentration values exceed the possible measurement error being most likely relevant to the partial trap “occultation” (due to the solar batteries) by the plasma flow, arising as a result of the satellite’s flight. Therefore, the Langmuir probe data is used for comparison only and the ion trap with a “floating” potential data is used to follow the fine structure of plasma concentration variations.

The ionospheric station data allows to measure  $n_e$  at a distance of 5-8 km in the presence of distinct trails on the ionogram. Taking this into account, when the Langmuir probe measurement error is about 10%, it can be maintained that the results obtained in the satellite’s neighbourhood by the Langmuir probe and the ion-probe coincide.

The spatial variations of heat plasma density and the fluctuations of the magnetic component of the field of low-frequency plasma radiation with a frequency of 15 kHz in the MIT neighbourhood depending on  $D_{st}$  are given in Fig.2.  $D_{st}$  is the variation during the plasma storm of March 9–11, 1979 (22:04 LT). The following symbols are used in the figure: 1 – MIT boundary near the equator, 2 – concentration minimum, and 3 – MIT boundary near the pole.

## **2. Possibility of low-frequency wave excitation in the MIT and auroral region.**

Experimental data is analyzed statistically in [2]. The correlation coefficients of the measured mutually perpendicular electromagnetic field components (the magnetic and electric components  $B_x$

and  $E_y$ , respectively) are measured. The correlation coefficient is quite low at ELF-frequencies, tending to unity at frequency of 15 kHz.

The low correlation coefficient at lower frequencies may be attributed to the fact that wave field structure at low frequencies is more complex compared to the field structure at higher frequencies. The ion plasma components are of great importance to wave propagation: there are waves of different kinds with different amplitudes and different wave vector orientations.

The low correlation coefficient at ELF-frequencies shows that the waves are, generally, electrostatic. It is known that electrostatic waves cannot propagate at great distances away in the ionospheric plasma. Therefore, it can be asserted that excitation of such waves occurs in a highly non-homogeneous medium [3,4].

### 3. Verification of the quasi-longitudinal propagation of low-frequency waves at mean latitudes in the high ionosphere.

As the direction diagram is large enough, the signal level practically does not change within a wide enough corporal aerial angle. In this connection, at first approximation, the  $B_x$  and  $E_y$  satellite components obviously coincide with the total wave amplitude. In this case, the relation between the magnetic and electric component amplitudes of the noise field at quasi-longitudinal wave propagation is:

$$(1) \quad B_x/E_y = 3.336 n_o$$

where  $B_x$  is magnetic field induction,  $E_y$  – electric field strength in nT/ $\sqrt{\text{Hz}}$  and  $\mu\text{V}/\text{m}\sqrt{\text{Hz}}$  respectively, and  $n_o$  – wave refraction index at quasi-longitudinal propagation.

$$(2) \quad n_o = \omega_{oe}^2 / \omega(\omega_{be}\cos\theta - \omega)$$

where  $\omega$  and  $\omega_{oe}$  are the circular and plasma frequencies

$$\omega_{oe} = 4\pi n_o / \omega$$

$\omega_{be}$  – electron gyro-frequency,

$\theta$  - the angle between the wave normal direction and the geomagnetic field vector  $B_o$ .

The results from the calculations using formulae (1) and (2),  $\cos \theta$ , the amplitude to amplitudes  $B_x$  and  $E_y$  ratio, and the measured values of  $n_e$  are shown in Fig 3.

It is evident that the values of  $n_e$  practically coincide with the calculated ones. This gives a reason to maintain the theory of quasi-longitudinal propagation of low-frequency waves at mean latitudes in the high ionosphere.

### Conclusion

Albeit the P4 device was in operation to the 236<sup>th</sup> orbit only (later the device resumed operation), the electron concentration data obtained by it generally coincides with the ionospheric station IS-338 data. The ion concentration data can be used when  $n_e = n_i$ ; the spherical ion trap with a “floating” potential data has the highest resolution time and therefore, it is used to follow the fine structure of plasma concentration variations.

### References:

1. Гдалевич, Г. Л., В. Д. Озеров, В. Ф. Губский, В. В. Афронин, С. К. Чапкынов, Т. Н. Иванова, М. Х. Пегрунова, Ц. П. Дачев, Я. Шмилауэр, К. Кубат, Г. В. Васильев, Л. П. Гончаров, М. Д. Флигель, Ю. В. Кушнеревский, Ю. Н. Шаулин, А. Т. Карпачев. Локальная концентрация ионосферной плазмы по данным различных методов на спутнике ИНТЕРКОСМОС-19. — Българско геофизично списание, т. IX, N 2, 1983, 27-38.

2. Linkhter, Ja. I., V. I. Larkina, G. L. Gdalevich,. Small-scale fluctuations of magnetic and electric components of the ELF and VLF wave fields in the sub-auroral topside ionosphere: characteristics of the wave field. – Journal of Atmospheric and Terrestrial Physics, Vol. 54, N 10, 1992, pp. 1311-1320.
3. Гдалевич, Г. Л., Н. И. Ижовкина, В. М. Ларкина, Я. И. Мехтер. Амплитудно-частотные характеристики ОНЧ и КНЧ-полей в неоднородной плазме субавроральной ионосферы. — Космические исследования, М., т. 32, вып. 4-5, 1994, 165-169.
4. Алтынцева, В. И. В. Ф. Губский, В. И. Ларкина. Экспериментальное доказательство квазипродольного распространения низкочастотных волн на средних широтах в верхней ионосфере. - Космические исследования, М., т. 25, вып. 3, 1987, 464-465.
5. Гивишвили, Г. В., Н. А. Коченова, Л. Н. Лещенко, М. Д. Флигель. Об одной экваториальной аномалии в ночной области F ионосферы. УДК 551.510.535.2., М., 1986, 464-465.
6. Гдалевич, Г. Л., В. Ф. Губский, Ю. Н. Минеев, Е. Д. Толстая, В. М. Ларкина. Связь магнитосферных и ионосферных процессов во время геомагнитной бури по данным спутника ИНТЕРКОСМОС-19. Космические исследования, М., т. 37, N 1, 1999, 50-56.
7. Васильев, Г. В., Л. П. Гончаров, Ю. В. Кушнеревский, В. В. Мигулин, М. Д. Флигель. Спутниковая система импульсного зондирования ионосферы ИС-338. — Аппаратура для исследования внешней ионосферы, М. ИЗМИР АН СССР, 1980, 109-119.
8. Иванова, Т., М. Пегрунова, С. Чапкынов, Г. Л., Гдалевич, В. Ф. Губский. Прибор П4 для измерения концентрации и температуры электронов, а также концентрации положительных ионов. - Аппаратура для исследования внешней ионосферы, М. ИЗМИР АН СССР, 1980, 109-119.
9. Кубат, К., Я. Клас, Я. Шмилауэр, В. В. Афонин. Прибор КМ-3 для измерения электронной температуры и распределения скоростей тепловых электронов. - Аппаратура для исследования внешней ионосферы, М. ИЗМИР АН СССР, 1980, 120-135.

# DIRECT DETERMINATION OF IONOSPHERIC PLASMA STRUCTURAL PARAMETERS IN THE EXPERIMENT WITH A SPHERICAL ION TRAP

Maria Petrunova, Boncho Peev\*

Space Research Institute, 1000 Sofia

\*Solar Terrestrial Influences Laboratory, 1113 Sofia

## INTRODUCTION

The study of the properties of Earth-surrounding plasma is of great practical importance. Plasma structural parameters are determined by the direct probe method. The results of these studies complete the physical analysis of Earth-surrounding space and are related with space energy resources.

## THEORETICAL MODELS

At a thermal velocity of the ions significantly lower than the velocity of the satellite  $V_o$  (relative to the plasma), the mean energy of the ions of mass  $M_i$  that have reached the probe is  $\frac{1}{2} M_i V_o^2$ . By the change of the positive bias, conditions are created for reaching the probe by the ions with different energies (respectively masses) and a possibility for mass selection, thus providing to obtain data for the density and temperature of the different kinds of ions [1].

Figure 1a displays the dependence of the ion current on the voltage applied to a probe for definite types of ions. The data is taken from [1], a probe characteristic of ESRO-1 mass spectrometer: grid transparency 30%, for oxygen ions  $O^+$  with temperature 1000 K. To determine ion temperature, the second derivative of the current-voltage characteristics is used, Fig. 1b.

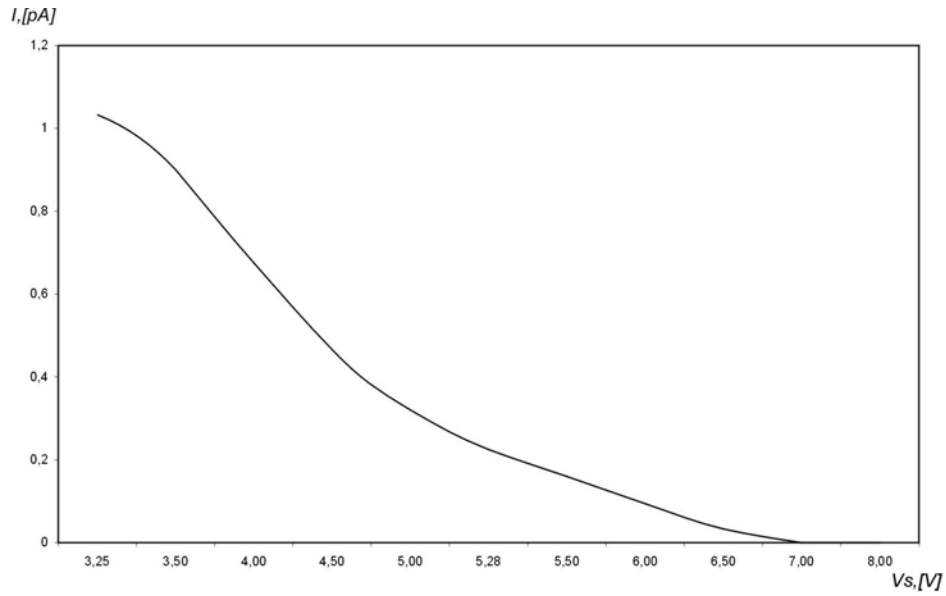


*Fig. 1a*

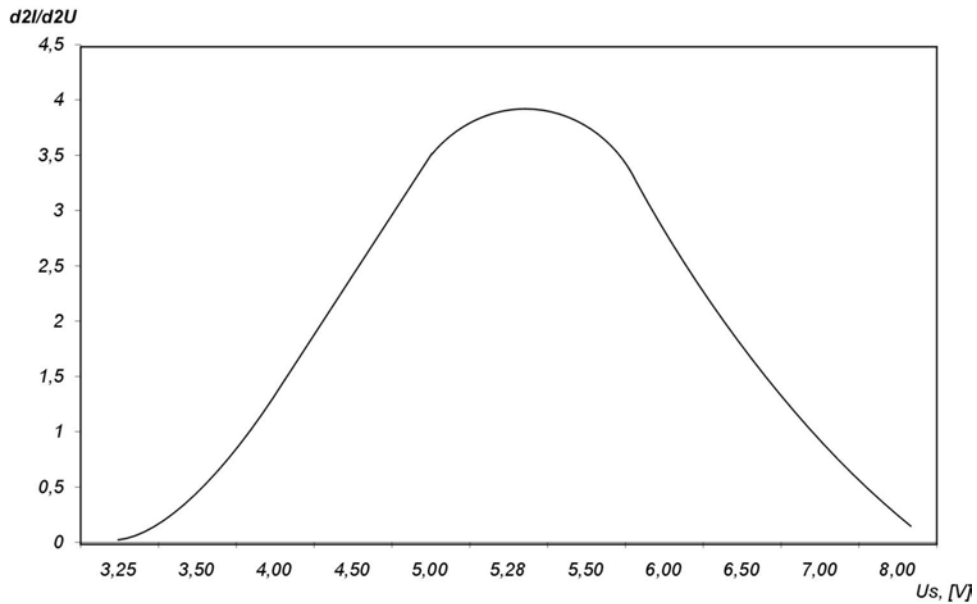


*Fig. 1b*

A spherical ion trap can be used as a measuring device that can determine the “mass number” of different types of positive ions at comparatively low mass resolution. In spite of this limitation, ion temperature can be determined, too [1]. Ion density is defined by the application of the result of Druyvestin (1930) who shows that the energy

distribution of charge carriers collected by a probe biased to a voltage  $V$  relative to the plasma in the retarding region is given by

$$(1) \quad \int (E) dE = \frac{1}{|U|^{1/2}} \frac{\partial^2 I}{\partial U^2} dU$$

$$(2) \quad N_i = \int_0^{\infty} f(E) dE$$

The form of the function  $\partial^2 I / \partial U^2$  for a spherical probe collecting current from plasma with drift velocity on which Maxwellian velocity distribution is superimposed has been studied by Medicus (1961, 1962) [2].

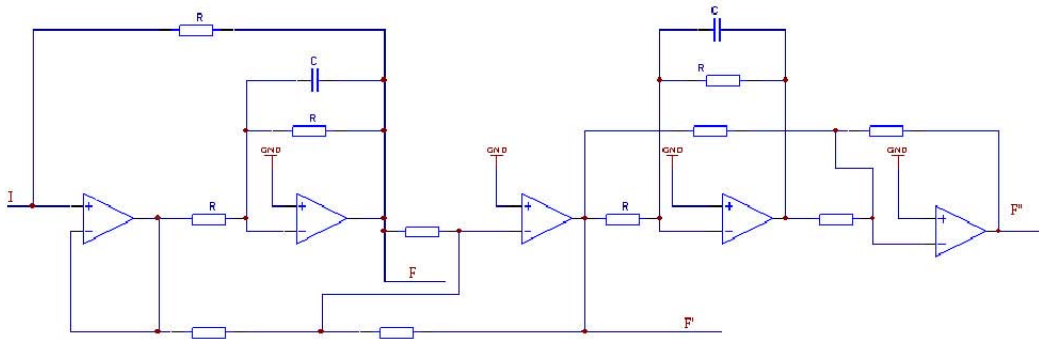
The analysis of the characteristics based on this theory is more convenient [1], [3]. The density  $N_i$  is obtained from the value of the second derivative function peak. The probe bias at which this maximum is obtained (detention bias) is used for the determination of  $M_i$ . The width of the second derivative function curve at level 0,5 is a “measure” of ion temperature  $T_i$ . On the basis of equations (1) and (2), the energy distribution  $E_i$  for ions of a given type can be also determined. The above-stated shows that, from the second derivative function of the probe current with respect to the voltage, almost all structural parameters of plasma ion components can be determined.

## DEFINITION AND SOLUTION OF THE PROBLEM

The accuracy and the potentials of SIT experiment can be increased if on board of the satellite the current-voltage characteristics and their derivatives are obtained [3] as continuous real-time functions. From the second derivative of the characteristics, the plasma structural parameters  $N_i$ ,  $M_i$ ,  $T_i$ ,  $E_i$  can be determined.

In the present work, we have suggested the solution of the problem for simultaneous obtaining of the current-voltage characteristics, its first and second derivatives as continuous real-time functions. This problem concerns the main amplifier in the circuit of a SIT probe experiment. This solution is a development of the authors' idea that has been published in [4]. The derivatives of the input function can be calculated by a differentiating circuit. The main differentiating circuits are not used for direct computation of a function derivative because of the high noise level and the operation instability.

Operation stabilization and noise reduction can be attained indirectly when the derivative is calculated by the function and its integral [5]. This idea has been further developed in the present work by using minimum hardware and has been applied in two steps for obtaining the second derivative of the input function. The indirect approach for calculating a function derivative is a process approximation which works in the low frequency region [5], [4]. The type of the circuit that implements the described approach at a double step application (calculation of the first and second derivatives in a continuous form) is shown in Fig. 2.



The main amplifier contains high impedance input operation amplifier operating in the non-inverting mode and an inverting integrator with a feedback loop. At these stages, the input current  $SIT$  is converted into a voltage and the first derivative of the input function is calculated. During the next stages, a similar circuit of an integrator and amplifier that calculates the second derivative of the function is applied. The described circuit has been analyzed by operating methods to determine the frequency range in which the approximation conditions  $f_{max} \ll 2_n RC$  are accomplished. Only the frequency determining elements are marked in the circuit. The obtained low-frequency range corresponds to the real experimental conditions.

The described circuit based on an indirect approach for calculation of the first and second derivatives of the input function as continuous real time functions has been experimented by means of a laboratory model. To simulate input functions, different in form (sinewave, triangular, orthogonal) voltage generators of amplitude of 0,35-3V have been used, at which stable operation has been observed.

## CONCLUSION

The above described solution of the problem provides an opportunity for the immediate real-time obtaining of the first and second derivatives of the

current-voltage characteristic as continuous functions by an approximation which operates in the low-frequency range. This makes it possible to determine directly the structural parameters  $N_i$ ,  $M_i$ ,  $T_i$ ,  $E_i$  of the plasma in a SIT probe experiment decreasing useless information which, in its turn, simplifies the technique of measurement.

## PERSPECTIVES

There are tendencies in the development of space technology for the next years to replace expensive space programs by smaller and cheaper programs that give faster results as well [6].

In many fields, intensive studies are carried out for the accomplishment and use of “distributed” systems of “micro-devices”. There are ideas to use “micro-satellites” as intelligent sensors for the simultaneous measurement at many points of ion concentration and temperature [6]. From this point of view, the suggested solution could be realized in a minimized version with a much lower power supply.

## SUMMARY

The paper presents a solution for real-time immediate obtaining of the first and second derivatives of the current-voltage characteristics in a probe experiment with SIT which provides opportunity for direct determination of plasma structural parameters. An indirect approach has been used by which noise effect is reduced and operation is stabilized with minimized circuitry. Possible prospects for development of the measurement technique are outlined.

## REFERENCES

1. Rait W.J., J. Blades, T.S. Bowling, A.P. Willmore, J. Physics Sci Instrum. 1973, 6, p.443.
2. Medicus G., J. Appl. Phys., 1962, 33, p. 3094.
3. Серафимов К., Космические исследования в Болгарии, изд.БАН, София, 1979, с. 247.
4. Петрунова М., Б. Пеев. Аерокосмически изследвания в България, 15, 1997.
5. Краме J., Application of operational amplifiers, Burr Brown Res. Corp., 1973, p. 78.

6. Robinson E., H. Helvajian, S. Janson Aerospace America, Oct. 1996, p. 38.

# LOWFREQUENCY ELECTRIC FIELD MEASUREMENT PROBES ON BOARD INTERCOSMOS - 24 - AKTIVEN SATELLITE

D.K.Teodossiev, M.S.Astrukova, R.G.Shkevov, G.K.Galev  
Space Research Institute, Bulgarian Academy of Sciences, 1113 Sofia

On 30 September 1989, from the Plesetsk launching site, the Intercosmos - 24 - AKTIVEN satellite was launched, with the following orbital parameters: apogee 2500 km, perigee 530 km, and orbital inclination 82.2°. The AKTIVEN Project envisaged measuring the parameters of undisturbed plasma and the characteristics of perturbations in the surrounding plasma caused by the actual impact on it from board of satellite. On board the major satellite, a powerful low-frequency transmitter with major frequency 9.8 kHz was installed, along with a neutral-gas injector: xenone. The spatial-time characteristics of the perturbed area were studied by the satellite-sub-satellite system (including space apparatus IK-24 and MAGION-2) whereas the distance between them could be partially controlled. The scientific equipment comprised a complex for measuring low-frequency electric field consisting of the devices: NVK-ONCh, ONCh-2, and ShASh. Six identical probes designed at the Space Research Institute (SRI) of the Bulgarian Academy of Sciences (BAS) acquired the input signal to all devices within the complex. The probes included sensitive elements - spheres with glass-carbon cover interacting with the surrounding plasma, and an input electronic block mounted within the spheres. To provide basis for comparison of the results, the similar electromagnetic wave complex KEM-1 on MAGION-2 satellite was furnished with probes with the same sensitive spherical elements designed and worked out in SRI - BAS.

## *Introduction*

The spherical form of the probes' sensitive elements is used in various devices for measuring electric fields on satellites, rockets, and balloons. A comprehensive theoretical study of the requirements and limitations for their use is provided in [1]. In the same work, the use of probes with carbon cover is thoroughly substantiated. A study of this type of probes operation in measuring the quasi-constant electric fields (DC), and alternating electric fields (AC) is provided in [5-11], whereas a large amount of experimental data for the operation of the satellites Injun-5, OGO-6, GEOS 1, GEOS 2, DE-A, DE-B, S3-3, and ISEE 1 is used. In accordance with the scientific program of the AKTIVEN Space Project, the requirement was set for the electric field to be measured within a wide frequency range: from 5Hz to 25kHz for the satellite, and from 0.01Hz to 100kHz for the sub-satellite. This presented serious requirements to the probes, too - to their surface qualities and to their structure. In the paper, some characteristics of the probes used on board of the Intercosmos 24 - AKTIVEN satellite are discussed.

## *Measurement Technique and Requirements to the Probes*

The devices NVK-ONCh, ONCh-2 and ShASh measured the electric field using the double-probe technique [1]. In this case, the input signal to the electronic blocks is given by expression (1):

$$(1) \quad \Delta U = \frac{\vec{E}' \cdot \vec{d} + (V_1 - V_2) + (WF_1 - WF_2)}{1 + R_1 / R + R_2 / R}$$

where  $E$  is the electric field in satellite coordinate system,  $d$  is the distance between the spheres' centers,  $V_1$  is the potential difference between sphere 1 and the surrounding plasma with infinite input impedance,  $V_2$  is the potential difference between sphere 2 and the surrounding plasma with infinite input impedance,  $WF_1$  is the work function for sphere 1, and  $WF_2$  is the work function for sphere 2,  $R$  is the input resistance of the preamplifier, and  $R_i$  ( $i = 1,2$ ) is the resistance of the plasma layer surrounding probes 1 and 2. Quantities  $V_1$  and  $V_2$  depend on plasma temperature  $T$  and concentration  $N$  at the measurement site; they change along the orbit and, generally, are difficult to determine. The targeted accuracy of measurement can be achieved by minimization of expression  $V_1 - V_2$ , i.e. by provision of the best possible conditions for location, operation and identity of the probes. For this reason, as sensitive elements, glass-carbon spheres were used featuring maximum symmetry. The probes were located at the far end of the rods projecting in front of the satellite and symmetrical to its velocity vector.

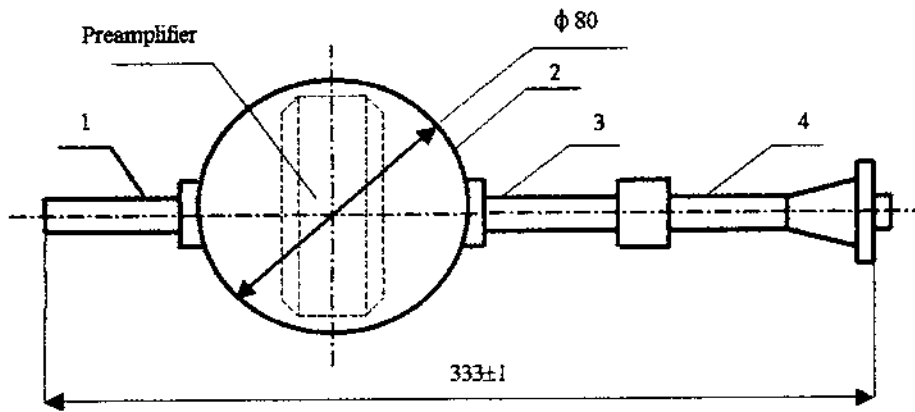


Fig. 1

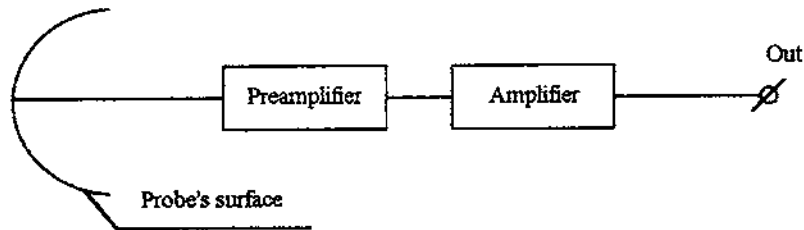


Fig. 2

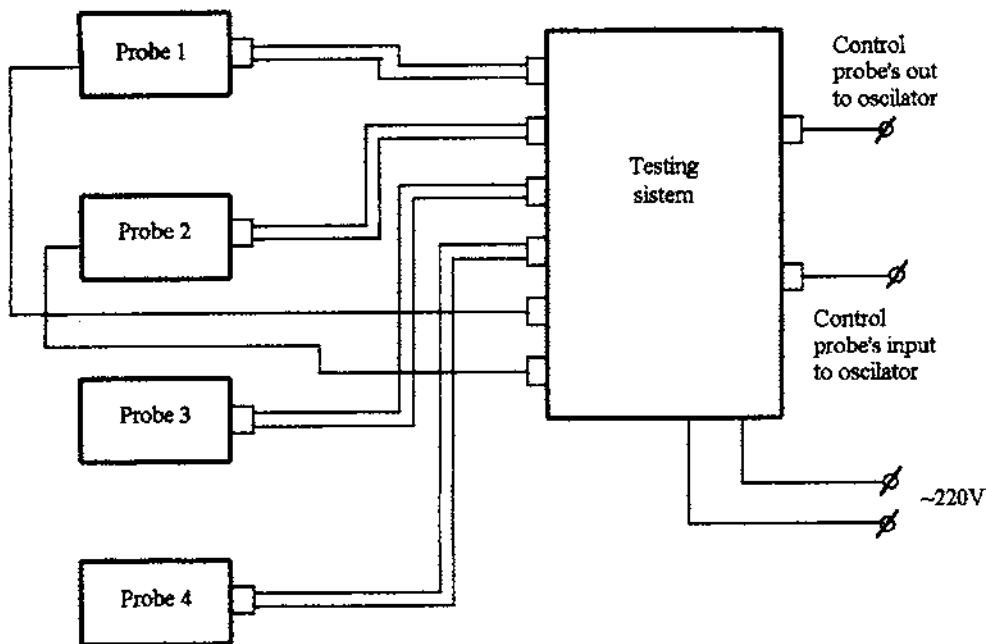


Fig. 3

The outer appearance of the probes is shown in Fig.1 where the notifications are as follows: symmetry axis (1), spherical sensitive element (2), bearing axis (3), antiphotoelectron axis (4), preamplifier (5).

The spherical irregularity of the sensitive elements of the probes influences the value of  $V$  thus producing systematic error. For this reason, special measures were taken to maximally reduce spherical irregularity. The results from the performed measurements revealed that spherical irregularity does not exceed 0.04 mm for each sphere.

The length of the bearing and symmetry axes is  $L = 2r = 80\text{mm}$  where  $r$  is the sphere's radius. The bearing and symmetry axes are electrically isolated from the collecting surface but their potential is equal to the sphere's potential. This provides for greater symmetry in the distribution of the electric potential in the probe-surrounding plasma. The symmetry axis aims to provide equal shading of the probe's collecting surface with different orientation of the satellite with respect to the sun.

The length of the antiphotoelectron axis is  $L = 2r = 80\text{mm}$ . It is also isolated from the other parts of the probes but its potential is strongly negative, about 10 V. As a result of this, it stops the photoelectrons that have left the satellite's surface, so the useful signal is determined mainly by the parameters of the surrounding plasma.

These structural features were selected to minimize the second term in expression (1) ( $WF_1 - WF_2$ ).

For the purpose, the spheres' surface was covered by glass-like carbon produced by a technology developed at BAS particularly for electrical field measuring devices [4]. Glass-carbon features uniform work function all over its surface. The measurements of both flat specimen and real probes revealed that this cover provides for a mean quadratic deviation of the work function  $WF$  less than 0.025 eV. Thus, the third term in expression (1) was minimized.

In the probes used so far for electric field measurement by the IESP device on board the IK-Bulgaria-1300 satellite [2], the preamplifiers were mounted within a box positioned in the end of the bearing axis, at the place where the axis is attached to the rod. The surface of the box was covered by special thermo-protection die providing normal temperature operation regime of preamplifier's (PA) board mounted in it. To improve preamplifiers' characteristics, preamplifiers (PA) of probes BVU.01 of device NVK-ONCh were mounted within the glass-carbon-covered spherical sensitive elements, on their operation surface.

The probes' structure was selected so as to leave enough room to mount the preamplifier within the sphere. This posed certain requirements for the features of the electronic elements used therein, such as operation within a definite temperature regime, consumed power etc. Laboratory measurements were made to evaluate the thermal conditions under which these elements are to operate. The reflection characteristics were studied of graphite specimen covered with glass-carbon produced by the same technology as the one used in working out the probes' spheres. The reflection characteristics of the specimen obtained when they were subjected to radiation of monochromatic light with wavelength from 200 nm to 2500 nm were used for theoretical evaluation of temperature within the sphere. The preamplifier mounted within the sphere had an output of 0.25W. The temperatures obtained ( $T_{\text{max}} = 40^\circ\text{C}$ ) lie within the allowed temperature range providing for the preamplifier's electronic components normal operation. Another means of overcoming the problem with the amplifier's temperature increase as a result of spheres temperature increase caused by the sun is to make the amplifier's thermal regime practically independent of the sphere's thermal status. This can be achieved by precise processing of the outer surface of the amplifier's box, i.e. by making it shining-smooth.

Probes BVU.01 constitute a part of the device NVK-ONCh. They are intended to measure the low-frequency electric fields by the double probe technique. The structure of probes BVU.01 is illustrated in Fig.1. The length of each probe without the connecting cable is  $333 \pm 1$  mm. Its mass without the cable and protective case does not exceed 0.3 kg. The probes are electrically connected to device NVK-ONCh by a 550 mm long cable and an RS-19 connector. The flow-chart of the electric part of probes BVU.01 is shown in Fig.2. These

are preamplifiers (PA) mounted on a round glass-textolite board with near-to-uniform distribution of electronic elements mass on it. The amplifiers preserve their operability with multiple shock 100 g loadings of the three axes. According to the Technical Mission of the device, the amplifiers should operate within the frequency range of 0.1 Hz to 25 kHz. The non-linearity of the amplitude-frequency characteristics of the PA within the range from 5 Hz to 25 kHz should not exceed 0.5 dB and the temperature range within which the PA preserves its characteristics is from  $-55^{\circ}\text{C}$  to  $+125^{\circ}\text{C}$ . Two versions of PAs were designed: one based on operation amplifiers LH 0042, and another, on LF 156. These amplifiers have a JFET input, input resistance of the order of  $10^{12} \Omega$ , low drift of the input signal ( $3\div 5 \mu\text{V}/^{\circ}\text{C}$ ), and low noise level of the input signal - about  $100 \text{ nV}/\text{Hz}^{1/2}$  at frequency 10 Hz. A thorough description of the circuit, its operation and the results from the study of the amplitude-frequency, dynamic, and noise characteristics of six BVU.01 probes with preamplifiers is given in [3].

### ***Conclusions***

The operability of probes BVU.01 with preamplifier was studied by Control-Measurement Instrumentation (CMI), the connection diagram being shown in Fig.3.

The probes' features were also verified upon the performance of climatic tests (temperature - with temperature  $\pm 80^{\circ}\text{C}$ ; moisture - with relative moisture 93% and temperature  $+40^{\circ}\text{C}$ ; and thermo - vacuum - with temperature  $\pm 80^{\circ}\text{C}$  and pressure about  $10^{-4} \text{ Pa}$ ), as well as upon the performance of vibro-mechanical tests with single 100 g loading. The device NVK-ONCh with probes BVU.01 operates successfully on board the IK-24-AKTIVEN satellite. The scientific results related therein are published in [13-15].

To illustrate the qualities of probes BVU.01 in Fig.4 are presented results from electric field measurements within the range from 300 Hz to 10400 Hz performed by the filter spectrum analyzer of ONCh-2 device during an active experiment. Active impact is indicated by arrow 2 in the upper left corner of Fig.4. Data refers to orbit No 1930 from 02.03.1990; it is analyzed in [13].

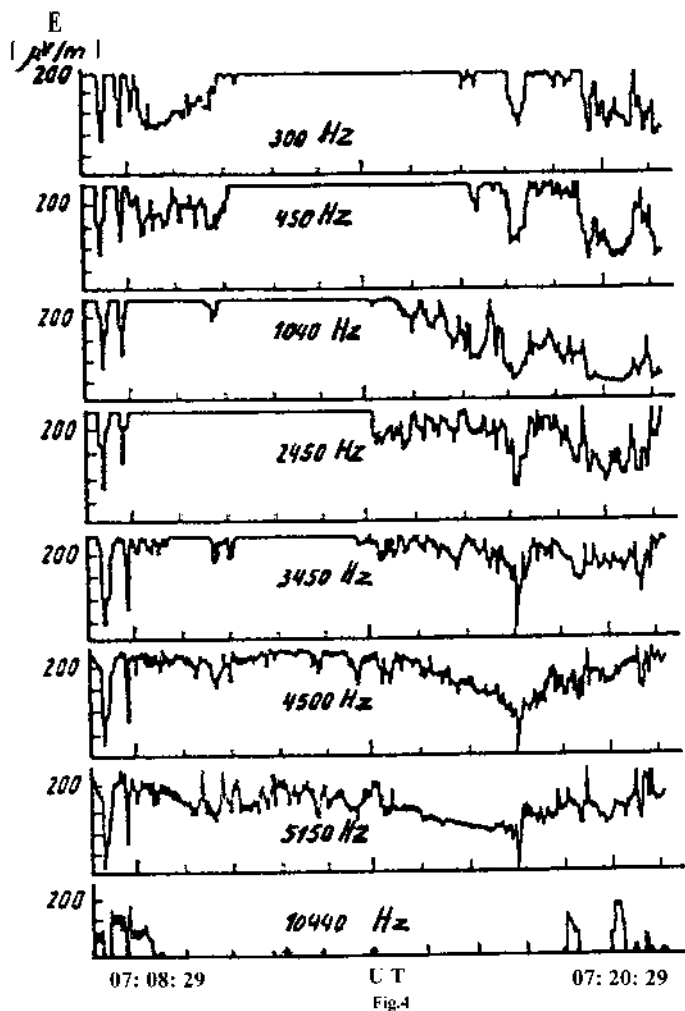


Fig.4

The results may be used as basis for further improvement of the probe complex for measurement of electric field by the double probe technique and its use in future space experiments.

#### REFERENCES:

1. U.V.Fahleson, M.C.Kelly and F.S.Mozer, Investigation of the operation of a DC electric field detector, Planet.Space Sci., v.18, pp.1551-1561, 1970.
2. G.Staney, M.Petrunova, D.Teodosiev, I.Kutiev, K.Serafimov, S.Chapkunov, V.Chmyrev, N.Isaev, P.Pushchaev, I.Pimenov and S.Bilichenko, An instrument for DC electric field and AC electric and magnetic field measurements aboard "Intercosmos-Bulgaria-1300" satellite, Adv.Space Res., v.2, No7, pp.43-47, 1983.
3. М.Аструкова, Р.Шкевов, Върху някои предусилватели и техния трансфер, IV Международен семинар "Философия, физика, космос", Кърджали, 10-30 май 1988 г.
4. Теодосиев Д., Печеняков И., Георгиев Й., Добрев Р., Петров П., Вълков Р., Станев Г., Метод за импрегниране и покриване на порьозни огнеупорни материали със стъкловодород, Авторско свидетелство No36107, 1981 г., България.
5. Fahleson U., Theory of electric field measurements conducted in the magnetosphere with electric probes, Space Sci.Rev., 1967, v.7, p.238.
6. Mozer F.S., Analyses of techniques for measuring DC and AC electric fields in the magnetosphere, Space Sci.Rev., 1973, v.14, No2, p.272.

7. Shawhan S.D., Gurnett D.A., Odem D.L., The plasma wave and quasistatic electric field instrument (PWI) for DYNAMICS EXPLORER-A, Space Sci. Instr., 1981, v.5, p.535.
8. Boyd R.L., Measurement of electric field in the ionosphere and magnetosphere, Space Sci.Rev., 1967, v.7, p.230.
9. Maynard N.C., Bielecki E.A., Burdick H.F., Instrumentation for vector electric measurements from DE-B, Space Sci.Instr., 1981, v.5, p.523.
10. Gurnet et al., Initial observation of VLF electric and magnetic fields with the Injun-5 satellite, J.G.R., 1969, v.74, No19, p.4631.
11. Mozer F.S., On the lowest altitude S3-3 observations of electrostatic shocks and parallel electric fields, GRL, 1980, v.7, No12, p.1097.
12. Stanev G.A. et al., An instrument for DC electric field and AC electric and magnetic field measurements aboard "Intercosmos-Bulgaria-1300" satellite, Adv.Space Res., 1983, v.2, p.43.
13. Гдалевич Ю., М.Михайлов, З.Клос, Л.Банков, М.Гушева, Эффекты, связанные с напуском нейтрального газа на спутнике "Интеркосмос-24", Геомагнетизм и аерономия, 1997, т.37, №6, стр.71-79.
14. Михайлов, Г.А.Михайлова, О.В.Капустина, КНЧ- и ОНЧ-электромагнитный фон во внешней ионосфере над сеизмоактивными районами (ИСЗ "Интеркосмос-24"), Геомагнетизм и аерономия, 1997, т.37, №4, стр.78-85.
15. Mikhailova, A.M.Golyavin and Yu.M.Mikhailov, Dynamic Spectra of VLF-Radiation in the Outer Ionosphere Associated with the Iranian Earthquake of June 21, 1990 (Intercosmos-24 Satellite), Geomagnetism and Aeronomy, 1991, v.31, No5, p.647-651.

## **LOWFREQUENCY ELECTRIC FIELD MEASUREMENT PROBES ON BOARD INTERCOSMOS - 24 - AKTIVEN SATELLITE**

D.K.Teodossiev, M.S.Astrukova, R.G.Shkevov, G.K.Galev

(A b s t r a c t)

In the paper, the probes used for low frequency electric field measurement on board "Intercosmos-24-AKTIVEN" are presented. The reasons for using amorphous carbon in the structure of the BVU.01 probes are analyzed. Amorphous carbon is a know-how technology of the Space Research Institute at the Bulgarian academy of Sciences. The mechanical structure and flow-chart, as well as the probes connection with the ground-based testing system are drawn. The characteristics of the probe electronic parts are discussed. The results from the actual measurements of the electric field in space plasma during active experiments are shown. Conclusions about reliability tests and probes operation in space are made.

# **ON THE CONTACT POTENTIAL DIFFERENCE AND THE METHODS FOR ITS MEASUREMENT FOR THE PURPOSES OF SPACE TRIBOLOGY**

Medy Astrukova

Space Research Institute, Bulgarian Academy of Sciences, 1113 Sofia

## ***Introduction***

In this work, a review is made of some of the existing scientific theories for the contact potential difference and the methods for its measurement. Grounds are also provided explaining why one of these methods is most widely used in practice, for the purposes of space tribology including.

The theory of the contact potential difference has numerous applications in many scientific fields like biophysics, biochemistry, electrochemistry etc. In engineering, it is accounted for in electrovacuum units, highvacuum units in particular, as well as in solid rectifiers, crystal detectors ,etc.

In modern space research, space materials, and space tribology, the measurement and reading of the contact potential difference, respectively the work function, is of great importance. For example:

1. In probe methods, the measurement of electron and ion temperature and electrostatic field by the “double probe” method is related accordingly with the use of flat and spherical probes (sensors), and probes with carbonglass cover. The material, geometry, and surface state of these probes, respectively the change and reading of the work function, is of crucial importance for the precision of space measurements.
2. In space tribology, the choice of material for instrumentation operating in bare space (scanner driving mechanisms, probe supporting mechanisms, antennae, solar batteries etc.) is related with the specific tribological processes in high vacuum [1]. The state of the material’s surface at contact (friction, wearing rate, structural modifications, etc.) is judged by the magnitude of the contact potential difference, respectively the work function of the given material.

In this aspect, the reading of the magnitude of the contact potential difference, respectively the work function, appears to be, on the one hand, an

indicator of the precision of measurement in space experiments, and on the other hand, an indicator of the magnitude and direction of surface change, and of the best couple of heterogeneous metals from the viewpoint of space tribology, i.e. one that would be characterized by low wearing intensity, high reliability, and operational longevity.

### *Theory*

The theory of the contact potential difference is based on the phenomenon “electrization” [2] discovered by *Al. Volta*, according to which, when two heterogeneous conductors (metals) come in touch, contact potential difference appears. Later, the scientists *Kelvin*, *Lodge*, *de la Riva*, and others developed the theory further, until two arguing theories appeared, the physical theory supported mainly by *Kelvin*, and the chemical theory supported mainly by *de la Riva*, and modified later by *Lodge*. The argue was focused on the problem where exactly appears the contact potential difference. While *Volta*, *Kelvin*, and the supporters of the physical theory argued that it appeared at the very place of contact, *de la Riva*, *Lodge*, and other supporters of the chemical theory argued that the contact potential difference is the result of the chemical reactions taking place on the metal surface.

The further studies aimed at proving the existence of the contact potential difference, and particularly the experiments for production of chemically very pure metals by the high vacuum technique dealt a severe blow at the chemical theory. Nowadays, the modern electronic theory of metals and semiconductors proves definitely that at the place of contact of heterogeneous metals, contact potential difference appears, and that the phenomenon is of purely physical, to put it still more precisely, of purely electro-dynamical nature. Authors [5], by using the *Fermi - Dirak* statistics, show that the energy ( $\varepsilon$ ) distribution of the electrons within the metal is expressed by the formula:

$$(1) \quad f_{(\varepsilon)} = \frac{1}{\exp\left(\frac{\varepsilon - W_i}{kT}\right) + 1},$$

where  $W_i$  is the ultimate energy value or *Fermi's* ultimate energy value, and  $k$  is *Boltzman* constant.

*Al. Volta* was the first to order the metals in sequence [2], to be later supplemented and expanded [3, 4]:

+ Zn, Pb, Sn, Fe, Cu, Ag, Au, graphite, MnO<sub>2</sub> –

+ Cs, Rb, K, Na, Li, Al, Zn, Cd, Pb, Bi, Fe, Cu, Ag, Au, Pt, C –

Each metal from the above sequence is characterized by a quantity  $G$ , called “galvanic value” [2], which is constant for the given metal and determines its position in the sequence. This quantity increases starting from the noble metals and proceeding in the direction of the metals that are readily oxidized. At contact, the metals in the left hand side of the sequence are more positively electrified.

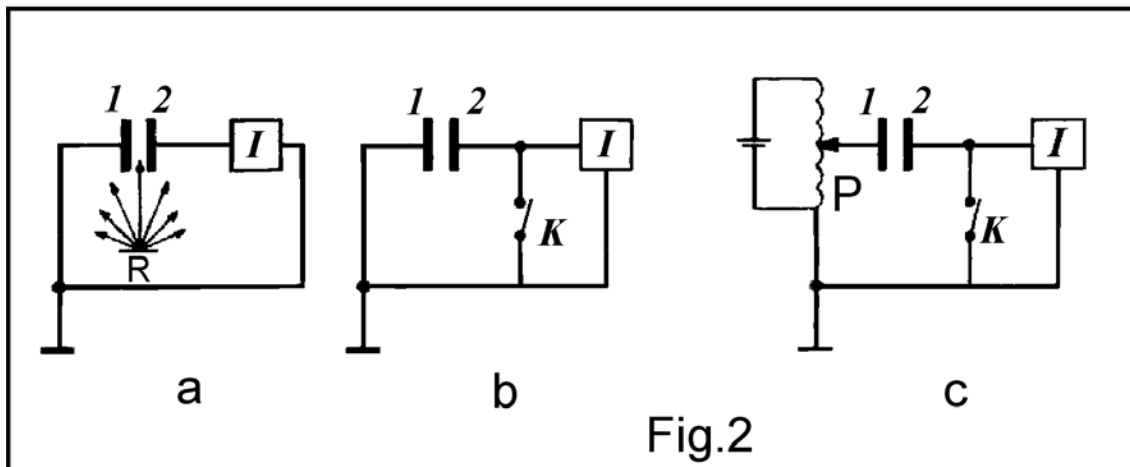
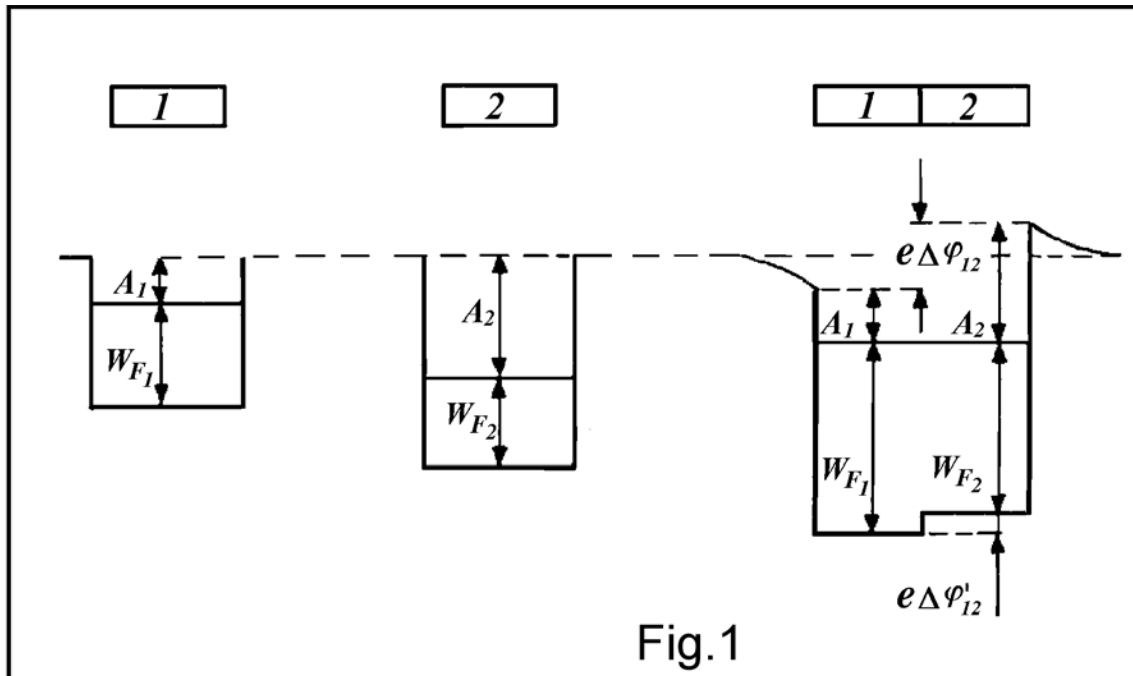
The *Fermi* levels of metals 1 and 2 at contact and individually are illustrated in Fig.1. The work function, respectively the electron's potential energy, is mathematically expressed by the equation:

$$(2) \quad W_p = -e\varphi$$

where  $W_p$  is the potential energy of the electron,  $e$  - the charge of the electron, and  $\varphi$  - the potential of the electron at a given point. At contact, a state of equilibrium is established, the condition for equilibrium between two heterogeneous contacting metals being expressed as follows:

$$(3) \quad \varphi_1 - G_1 = \varphi_2 - G_2 ,$$

$$(4) \quad \varphi_1 - \varphi_2 = G_1 - G_2 .$$



Equation (4) is in compliance with the modern interpretation of the phenomenon of the contact potential difference as difference of the metals work function:

$$(5) \quad \Delta\phi_{12} = -\frac{A_1 - A_2}{e},$$

where  $\Delta\phi_{12}$  is also known as external contact potential difference. It has different values for different couples of metals. They vary from tenths of volts to several volts. The internal contact potential difference  $\Delta\phi'_{12}$  is not the subject of this work.

In chemical thermodynamics, the problem for the contact potential difference is perceived as a change of the thermodynamic or electrochemical potential in transportation of charges from one point of the system to another [2]. It is not difficult to see the coincidence with the electrostatic definition of the contact potential difference in purely electrostatic phenomena, and that this definition fits and is appropriate for all cases from the theory of the contact potential difference, i.e. in the state of equilibrium, between a definite point from the surface of a given metal and another nearby point from the surface of another metal, a contact potential difference exists, respectively a difference in the metals work function .

### *Methods of measurement*

There are several different methods of measurement of the contact potential difference.

The principle of measurement of the ionization method is illustrated in Fig.2a, where 1 and 2 are metal plates (e.g. copper and zinc) which are connected to the indicator  $I$  (electrometer). One of the plates is grounded.  $R$  is a small amount of radioactive substance, ionizing the air between the plates, where contact potential difference is created, equal to the work function of both studied metals which is directly measured by the indicator. The method is convenient, it does not require a complex structure but its use is quite limited, because of the measurement error due to ionizing of the surrounding gas, and the method's inapplicability in high vacuum which provides for the maximum cleanness of the studied surface.

The photoelectric method is based on the photoelectric effect. The magnitude of photoemission is different for the different metals; it is related with the magnitude of the contact potential difference between them, respectively the difference between their work functions. The method has been named after the latter circumstance. However, it is inapplicable, too, much like the ionization method, because it does not allow for the correct determination of the contact potential difference, being related with drawing of the  $V - A$  characteristics, the saturation current characteristics ,etc.

The only difference between the thermoelectron and the photoelectric measurement method is the different electron source. Here again,  $V - A$  characteristics are drawn to read the contact potential difference, the method of shifting the characteristics is used, and the saturation current is read. In some of the configurations, the shift of the characteristics is effected by the use of magnetic field which reduces the anode current to a magnitude corresponding to the saturation current. It is at this moment that the difference in anode tensions is read which is different for the different metals. This method is also inaccurate. The magnitude is read graphically, and not immediately. Moreover, movable parts are used to replace the anodes.

The most widely used method is the capacitor one. The principle of measurement is presented schematically in Fig.2b. Between metal plates 1 and 2, contact potential difference, respectively difference in the work function, is established. The plates are charged by:

$$(6) \quad q = U_{12}C_1$$

where  $C_1$  is the capacity between the plates. Since the plate 1 is grounded, the charge appears on plate 2. With increase of the distance between the plates, changing the capacity  $C_1$  to  $C_2$ , charge  $q$  provokes potential difference  $U$  which is measured by the indicator  $I$ . Mathematically, this is expressed by the equation

$$(7) \quad U' = \frac{q}{C_1 + C_n}$$

where  $C_n$  is the capacity of conductor and indicator. From here, it is easy to calculate the contact potential difference  $U_{12}$ :

$$(8) \quad U_{12} = U' \frac{C_2 + C_n}{C_1}$$

In the above version, the method is inaccurate because it relies on the precise determination of the distance between the plates and the specific capacity of the system. *Kelvin* avoids this inconvenience (Fig. 2c), [2]. By the use of potentiometer  $P$ , such tension can be chosen that would

compensate for the contact potential difference between metal plates 1 and 2 until the indicator shows zero. And last, *Zisman* [6] introduces vibrating (mechanically or electronically) plates. Thus, the capacitor method with vibrating capacitor assumes its most effective and refined version. It becomes the basic method for development of modern techniques for measurement of contact potential difference.

### *Conclusions*

1. While, with the ionization and thermoelectron method for measurement of the contact potential difference between two heterogeneous metals, the ultraviolet emission and the heating to high temperatures provides inaccurate data, resulting from the change of the chemical composition on the surface of the studied material, respectively to change in the work function, with the capacitor method with vibrating capacitor, the measurement can be done in any type of medium: air and vacuum. The surface of the metal plates can assume any form and size, as much as the size of a vacuum friction trace which is important to vacuum tribology and which substantially increases the potentials of the measurement method. The measurement accuracy is high ( up to one tenth volts on an area a little bit greater than two square millimeters). The values of the measured quantity can be read continuously.

2. Based on the theory of the contact potential difference, modern measurement techniques can be developed to be applied not only in electrochemistry and high vacuum instrumentation, but in modern space instrumentation vacuum tribology, space technologies and space materials. Determination and forecast of the compatibility of space-used materials becomes reality.

### *References*

1. *Zisman*, Rev. Sci. Instr. vol.3, p.367, 1932.
2. Бете и Зоммерфельд, Электронная теория металлов, ОНТИ, 1938.
3. М. Царев, Контактная разность потенциалов, Москва, 1955.
4. Ю. Симеонова, М. Аструкова и др., Характерни особености на трибологичните процеси във висок вакуум, Контакт`97, София, 1997г.
5. Иванчев и др., Физика, Техн., 1975г.

6. Хр. Попов, Ст. Станев и др., Физика, 1993г.

**ON THE CONTACT POTENTIAL DIFFERENCE  
AND THE METHODS FOR ITS MEASUREMENT  
FOR THE PURPOSES OF SPACE TRIBOLOGY**

(S u m m a r y)

Medy Astrukova

Space Research Institute , Bulgarian Academy of Sciences, 1113 Sofia

A brief review is made of some of the major definitions, quantities, and ratios from the theory of the contact potential difference. Some methods for its measurement are described, greatest attention being paid to one of them which is most widely applied and having the greatest advantages in the field of space tribology.

# EVALUATION OF THE ATMOSPHERIC OPTICAL CHARACTERISTICS IMPACT ON THE SOLAR CORONA OBSERVATION

*Kalinka Bakalova, Vitchko Tsanev\**

*Solar-Terrestrial Influences Laboratory, Bulgarian Academy of Sciences, 1113  
Sofia*

*\*Institute of Electronics, Bulgarian Academy of Sciences, 1113 Sofia*

## Introduction

The present study of the atmospheric optical characteristics is stimulated by the necessity to account for their influence on the spectral images of the corona taken during the total solar eclipse from 11 August 1999. Nevertheless, the approach is common to various methods of coronal observations – e.g. during eclipses or using coronagraphs. We are mostly interested in the optical properties of the atmosphere that determine the transfer of direct and single scattered coronal radiation during a total solar eclipse. The final aim of the present study is to determine the restrictions on observations due to the atmosphere by comparison between the direct and single scattered components in the coronal measurements under various circumstances including the direction of the beam, the solar zenith angle and the altitude of observation.

The solar corona, when there are appropriate conditions for observation, could be considered as an extended light source of dimensions up to 22 solar radii  $R_{\odot}$  [1] and a corresponding angular radius not exceeding  $6^{\circ}$ . That is why the angular radius of the optical field of view is confined to  $6^{\circ}$  in our computations, supposing that the optical axis of the photograph instrument is pointing to the Sun. As far as every beam bearing specific information from the corona is projected onto a particular point in the picture, the polar coordinates of this point are in one-to-one correspondence with the direction of the beam. All possible directions of observation inside the view field are defined by the polar angle  $\theta$  about the optical axis and the azimuth angle  $\varphi$  measured in the image plane which is normal to the optical axis. Each view line has a different zenith angle  $z$  measured from the local vertical, expressed as follows

$$(1) \quad \cos(z) = \cos(\theta)\cos(z_{\odot}) - \sin(\theta)\sin(z_{\odot})\cos(\varphi)$$

where  $z_{\odot}$  is the solar zenith angle. The values of  $z$  vary in the range  $z_{\odot} \pm 6^{\circ}$ . The extreme quantities correspond to the peripheral points in the picture for which  $\varphi = 0^{\circ}$  or  $\varphi = 180^{\circ}$ . We reckon azimuth  $\varphi$  in the image plane from its intersection with Sun's vertical where  $z = \max$ . All further formulae hold true for monochromatic radiation, so the dependence on the wavelength is not explicitly shown. The numerical quantities in the figures refer to wavelength of  $0.55 \mu\text{m}$  and to atmospheric models for summertime at middle latitude [2]. The optical characteristics of aerosols are taken from the models in [3]. These do not confine the general use of considerations.

### Atmospheric transmittance and optical depth

We use the plane-parallel and horizontally homogeneous model of the atmosphere which is acceptable when the zenith angle  $z$  of the beam is not greater than  $75^\circ$ . In this case, the optical depth  $T$  of a slant path is a product of the optical depth  $T_0$  of the corresponding vertical path between the two altitudes  $h_1$  and  $h_2$  and the airmass factor  $m(z) = \sec(z)$ . Generally, we have

$$(2) \quad T(z) = T_0 m(z) , \quad T_0 = \int_{h_1}^{h_2} \alpha_e(h) dh .$$

Here,  $\alpha_e(h)$  is the vertical distribution of the coefficient of extinction, measured in  $km^{-1}$ . When the path encompasses the entire height of the atmosphere from sea level to the top of the atmosphere,  $h_1$  is equal to 0 and  $h_2$  is denoted by  $H_a$ . We can find the atmospheric transmittance along any slant path utilizing the Bouguer-Lambert's law

$$(3) \quad \tau(z) = \exp(-m(z) T_0) = \tau_0^{m(z)}$$

if  $\alpha_e(h)$  is known. In (3), the transmittance along the vertical path is denoted by  $\tau_0$ .

The distribution of the transmittance  $\tau(z(\theta, \varphi))$  for an arbitrary point  $(\theta, \varphi)$  in the image plane shows the directional dependence of the transfer through the medium of the radiance coming from a unit uniform light source. In other words,  $\tau(z(\theta, \varphi))$  is a multiplier modifying the space distribution of the coronal image. The airmass factor is an even function of the azimuth angle  $\varphi$  and  $\tau$  is mirror-symmetric about axis  $\varphi=0^\circ | 180^\circ$ .

It follows from formulae (1), (2), and (3) that for a given vertical stratification  $\alpha_e(h)$ , the Sun's zenith angle  $z_\theta$ , and altitude of observation  $h_1$ , the dependence of the transmittance on the direction of the beam is only geometrical. The behavior of the transmittance  $\tau(\theta)$  from the center to the periphery of the image (at the sea level) for different values of  $\varphi$  is presented in Fig. 1.

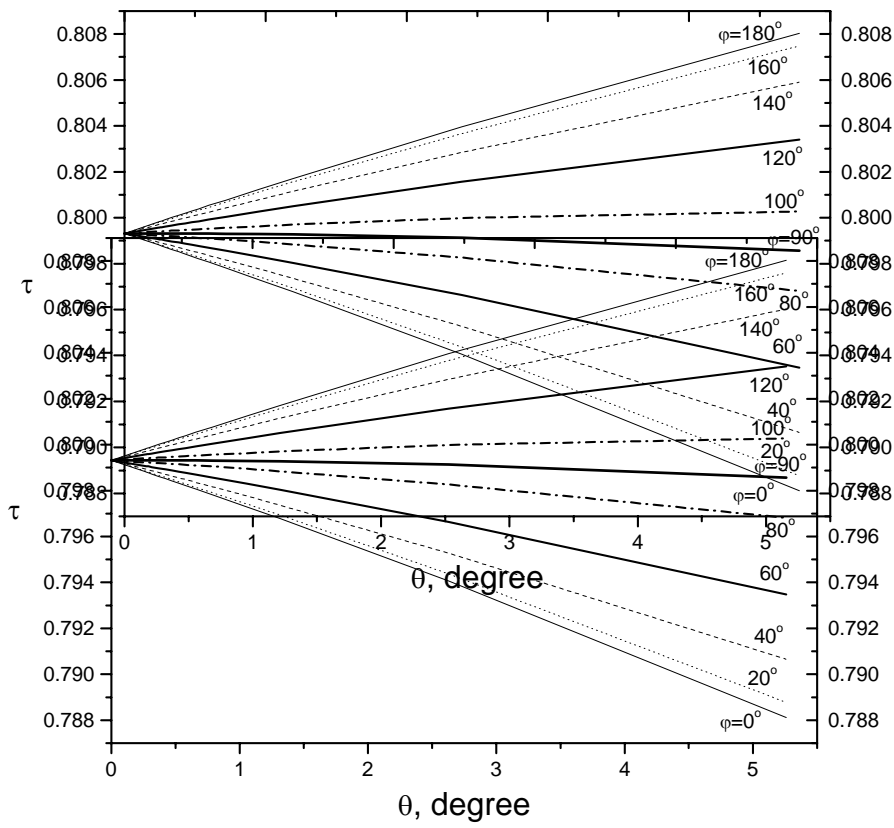


Figure 1. Distribution of the spectral transmittance  $\tau(\theta)$  (for  $\lambda=0.55 \mu\text{m}$ ) from the center to the periphery of the image for different values of  $\varphi$  through the entire atmosphere.

The transmittance decreases when  $\varphi$  varies from  $0^0$  to  $90^0$  and it grows up for  $90^0 < \varphi < 180^0$ . The transmittance practically keeps its value in the limits of the considered optical angle of view in the direction  $\varphi = 90^0$  which is normal to the Sun's vertical. For an arbitrary value of  $\theta$ , the transmittance has a minimum at  $\varphi = 0^0$  and is maximal for  $\varphi=180^0$ . This asymmetry of the transmittance distribution in the image plane is illustrated in Fig. 2 where  $\tau(\varphi)$  is shown for three values of the polar angle  $\theta$ . We have to mention that the asymmetry is stronger manifested at higher values of  $\theta$ .

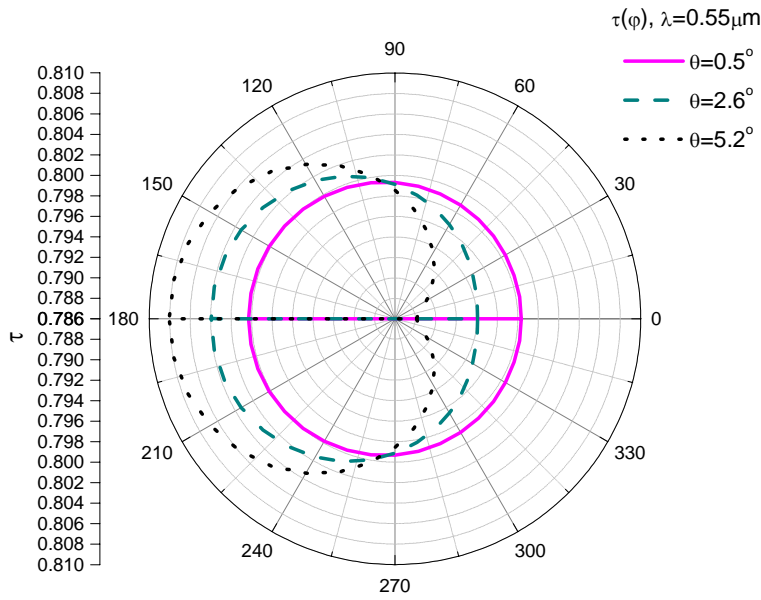


Figure 2. Asymmetry in the distribution of the transmittance  $\tau(\varphi)$  for three values of the angle  $\theta$ .

Computations of the dependence  $\tau(z(\theta, \varphi))$  for all possible directions inside the view field are necessary to account for the influence of the atmosphere on the transfer of the direct radiance from different parts of the corona. The measured radiance should be divided by  $\tau(z(\theta, \varphi))$  in order to obtain the real value. Strictly speaking, this is true only when the direct radiance exceeds significantly the background of the scattered light. Such a light source is the corona only near the solar limb because its radiance decreases rapidly along the radial direction (more than  $10^6$  times at distance of  $20R_{\odot}$  [1]).

#### Single scattering in the atmosphere

Scattered radiation is a parasitic additive component in the measurements. It restricts coronal observations. Determination of the Earth's atmosphere scattering properties is very important because it could be used to introduce some corrections in coronal measurements at greater distances from the solar limb.

The radiance of single scattered light is proportional to the irradiance (the surface density of the flux) from the source of initial radiation. The coefficient of proportionality describes the scattering capacity of the medium. In case of single scattering arising in the atmospheric stratum between altitude  $h_1$  and altitude  $h_2$ , it takes the form [4]

$$(4) \quad S_1(\theta, \varphi) = m(z) \int_{h_1}^{h_2} \tau(h_1, h)^{m(z(\theta, \varphi))} \tau(h, h_2)^{m(z_{\theta})} \beta(h, \theta) dh .$$

Here,  $\beta$  is the angular scattering coefficient of dimension  $\text{km}^{-1} \text{steradian}^{-1}$ . When the optical axis is pointing to the light source, the scattering angle is equal to the polar angle  $\theta$ .

The distribution of the function  $S_1$  in the image plane indicates the directional dependence of the single scattered radiance coming from a light source which gives unit uniform irradiance. The integral in (4) is practically independent of azimuth  $\varphi$ . There are some differences in the fourth significant digit when  $\theta$  exceeds  $5^\circ$ . That is why the asymmetry in the distribution of the single scattered radiance is due only to the airmass

factor  $m(z)$ . As distinct from the transmittance (see (3)), the scattered light is in direct

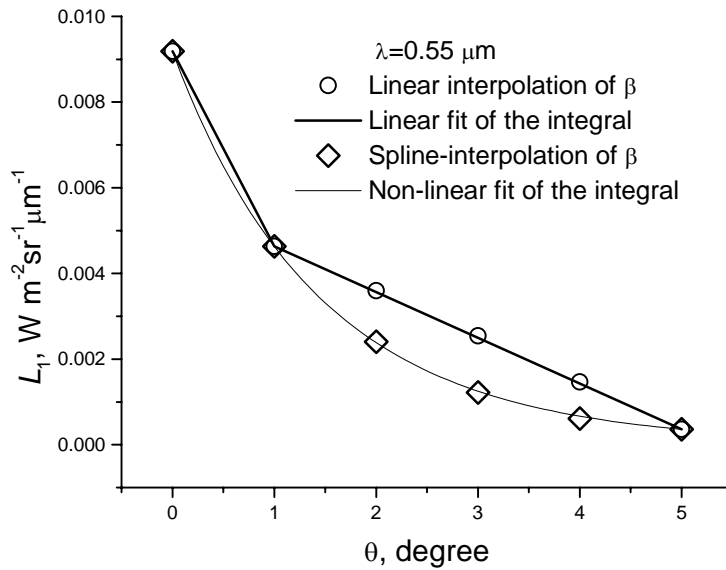


Figure 3. Radial distribution of single scattered coronal radiance

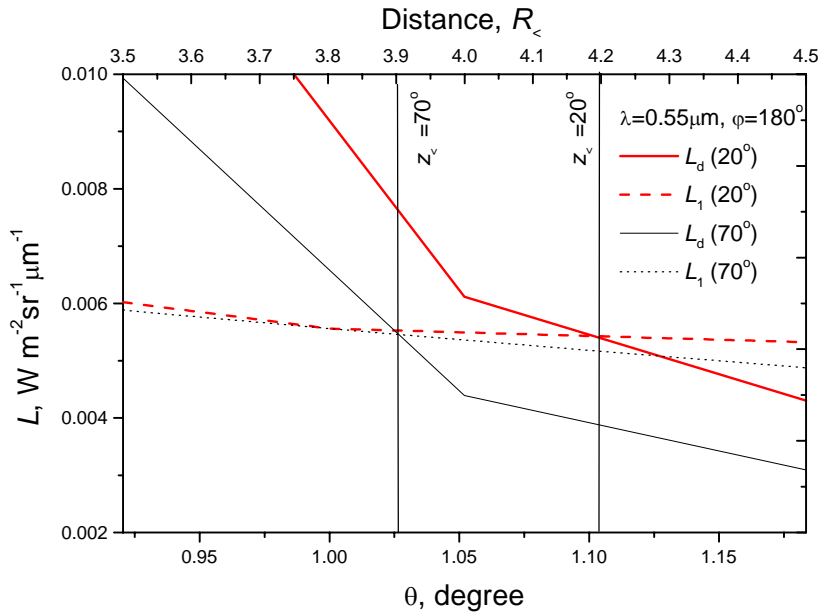
proportion to the airmass factor and is minimal for  $\varphi = 180^\circ$ . This direction is optimal for outlining the signal against the background from theoretical point of view.

The integrand in (4) consists of three multipliers. Two of them describe the transmittance of the atmosphere along the paths before and after the act of scattering that occurs at altitude  $h$ . The dependence of their product on the direction is negligible. Most important is the angular scattering coefficient  $\beta$  because the aerosols phase function is extremely extended in the forward direction. It varies by more than two orders in the considered range of angles between  $0^\circ$  and  $6^\circ$ . The basic problem in the evaluation of  $S_1$  comes from the limited data available in this range, namely at  $0^\circ$ ,  $1^\circ$ , and  $5^\circ$  angular degrees [3]. To make computations more precise we performed both linear and spline interpolation of the phase function in the range  $0^\circ$ - $180^\circ$  with step  $1^\circ$  for all 28 known altitudes [5]. As far as the procedure of preliminary spline interpolation is too labor-consuming and only a little part of the angular range is used, another approach is also tested. The computations of (4) are carried out for only 3 values of  $\theta$  ( $0^\circ$ ,  $1^\circ$ , and  $5^\circ$ ) for which the quantities of the phase function are tabulated. Later,  $S_1(\theta, \varphi = const)$  is determined by choosing an appropriate fitting function. The results from all mentioned methods of procedure are presented in Fig. 3. As an example, the amounts of the single scattered radiance  $L_1 = S_1 E_c$  from the corona during a total solar eclipse are taken. The quantity  $E_c$  is the irradiance caused by the corona. It turns out that only data elaborated for aerosol phase function could increase evaluation accuracy. The results obtained from the fit of the integral are identical to those from preliminary interpolation of the integrand  $\beta$  and thus time-consuming procedures can be avoided.

### Comparison between direct and single scattered radiance

We have already discussed the directional dependence of atmospheric optical characteristics during coronal observations. As a result of our theoretical models and computations we can evaluate and compare the amounts of direct and single scattered radiance in the radial direction under various circumstances. For example, it is important to evaluate the influence of the Sun's zenith angle during eclipses that occur at particular places (latitudes) and daytime. The distances where the direct and single scattered coronal radiance at sea level equalize for  $z_{\Theta} = 20^{\circ}$  and  $z_{\Theta} = 70^{\circ}$  are shown in Fig. 4. It could be inferred that the lesser the zenith angle  $z_{\Theta}$ , the better conditions for observation of the corona. On the whole, coronal observations at sea level are strongly influenced by the Earth's atmosphere and at distances of about  $4R_{\Theta}$  scattered skylight exceeds direct radiance.

Further, we are interested in the possibility for coronal observations at higher altitudes. As it could be expected, optical thickness and atmospheric scattering capacity decrease with growth of  $h_1$  because the medium gets thinner. This means better conditions for transfer of direct and lesser-scattered radiance. From computations using formulae (2) and (4) when  $h_2 = H_a$ , it follows that optical thickness decreases ten times Figure 4. Comparison between the direct  $L_d$  and the



single scattered  $L_1$  coronal radiance at sea level for two values of the Sun's zenith angle  $z_{\Theta}$ .

Figure 4. Comparison between the direct  $L_d$  and the single scattered  $L_1$  coronal radiance at sea level for two values of the Sun's zenith angle  $z_{\Theta}$ .

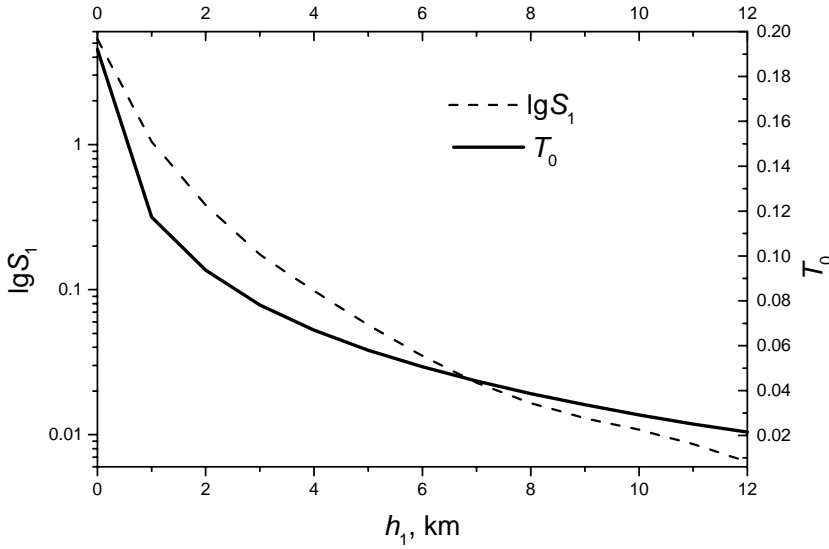
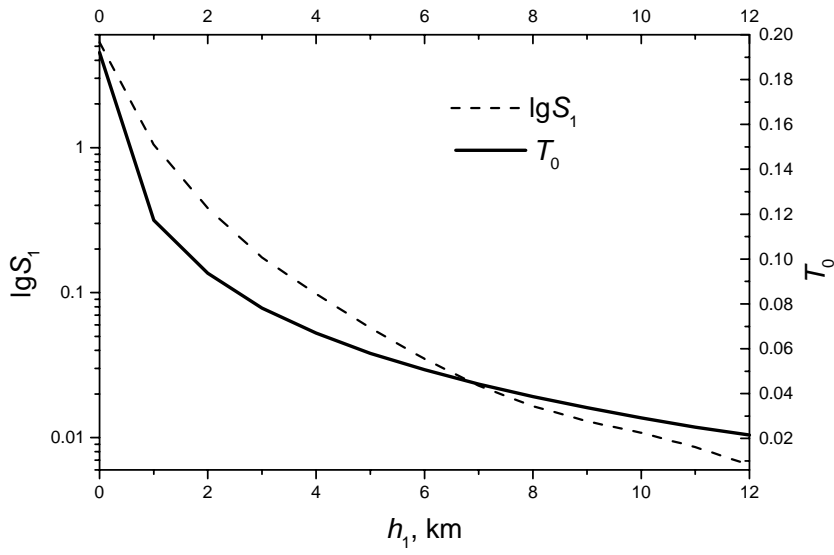


Figure 5. Vertical optical depth  $T_0(h_1, H_a)$  and scattering capacity  $S_1(h_1; \theta = 0, \varphi = 0)$  from altitude  $h_1$  to the top of the atmosphere  $H_a$ .

and scattering capacity by two orders at altitude  $h_1 = 12 \text{ km}$ . The behavior of the atmospheric characteristics ( $\lg S_1(h_1; \theta = 0, \varphi = 0)$  and  $T_0(h_1, H_a)$ ) is shown in Fig. 5. The distances at which direct and single scattered coronal radiance equalize more and more increase at higher altitudes. For example, with sea level observation, when  $z_\Theta = 31^\circ$  the cross point is at  $4R_\Theta$ , whereas, with  $h_1 = 1 \text{ km}$ , the cross point shifts to above  $5.5R_\Theta$  and with  $h_1 = 2 \text{ km}$  it shifts to above  $11R_\Theta$ . It is a good chance if the total solar eclipse can be observed at such a base altitude. The location of some cross points is denoted in Fig. 6. At aircraft's altitude of  $12 \text{ km}$ , the direct coronal radiance approaches the scattered one down to  $20R_\Theta$ . Practically, the entire corona could be observed in open-air conditions.

Figure 6. Comparison between the direct  $L_d$  and the single scattered  $L_1$  coronal radiance for

References:

1. Allen C. W. Astrophysical Quantities. London, Athlone Press, 1973.
2. Zuev, V. E., G. M. Krekov. *Recent problems of atmospheric optics. Vol. 2 Atmospheric optical models*. Leningrad, Gidrometeoizdat, 1986 (in Russian).
3. Krekov, G.M. , R.F. Rahimov. Optical models of the atmospheric aerosols. Publ. by IOA Sib. Branch of RAS, Tomsk , 1986 (in Russian).
4. Bakalova K., V. Tsanev. Influence of the single scattering on the spectral images of the corona during a total solar eclipse. *Comp. Rend. Acad. Bulg. Sci.*, **53**, No. 8, 2000.
5. Kirilov, K., K. Bakalova. Two-dimensional approximation of the spectral aerosol phase function stratification. *Comp. Rend. Acad. Bulg. Sci.* **53**, No. 9. 33-36, 2000.

# Using an orbital method and GPS measures of the ground control points in the georeference of the space images

N.Georgiev, R.Nedkov, D.Nedelcheva

## 1. Introduction

In works [1,2], the rectification and the precise georeference of space images are examined, analyzed and mathematically grounded. For this purpose, many additional settings and requirements are made for the quantities used in the mathematical model, namely: the necessary spatial orthogonal coordinate systems are defined; the coordinates of the ground control points (GCP)  $P_j$  ( $j = 1,2,\dots,8$ ) are determined by GPS measures; the Earth's /referent/ ellipsoid being assumed as projection plane is taken, with reading of the ellipsoid's heights (fig.1) [2]. In the present work, these settings will be accounted for, but the attention will be focused on the issues, related with the possibility of approximation and extrapolation of the orbital elements at the moment the image was taken  $t_k$ .

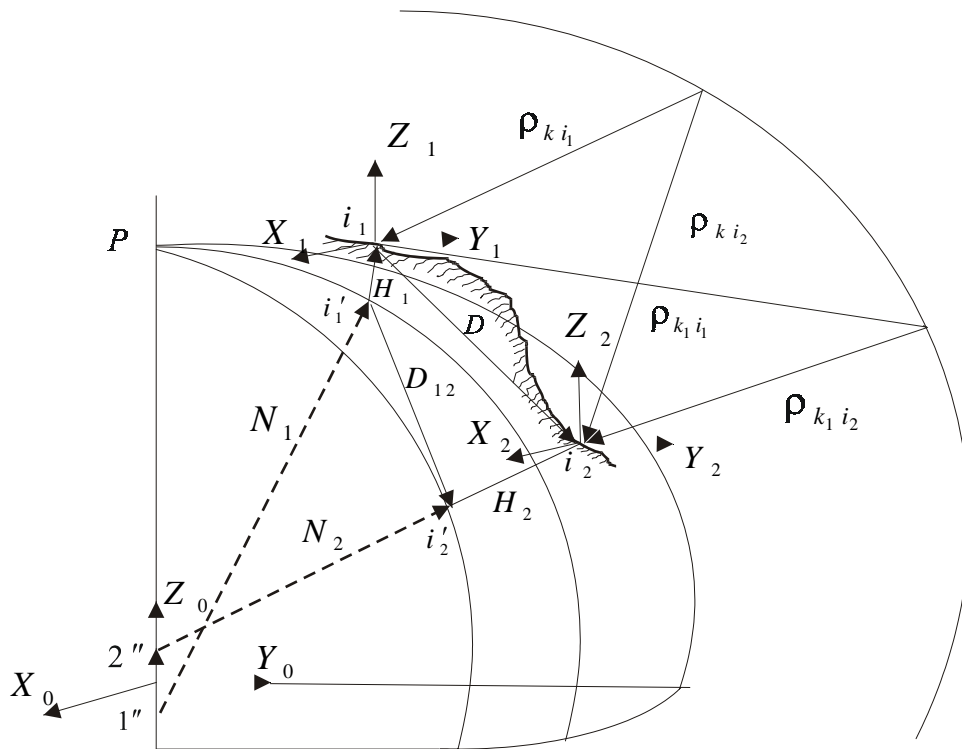


**Fig.1**

Each satellite is characterized in the space area by its initial elements for a given starting epoch  $t_0$ . These elements could be extrapolated and improved for the moment the image was taken  $t_k$  ( $k = 1, 2 \dots n$ ) with some of the experimental orbital or numerical methods, by using: Kepler's elements in the inertial coordinate system  $F = (i, \Omega, \omega, a, e, M)_0^T$ ; orthogonal inertial coordinates and components of velocity  $R = (x, y, z, \dot{x}, \dot{y}, \dot{z})_0^T$ ; spherical coordinates and components of velocities  $S = (\xi, \eta, \omega, \xi', \eta', \omega')_0^T$ ; or numerical integration of the fluxional equations of motion, and others [3, 4, 5, 6].

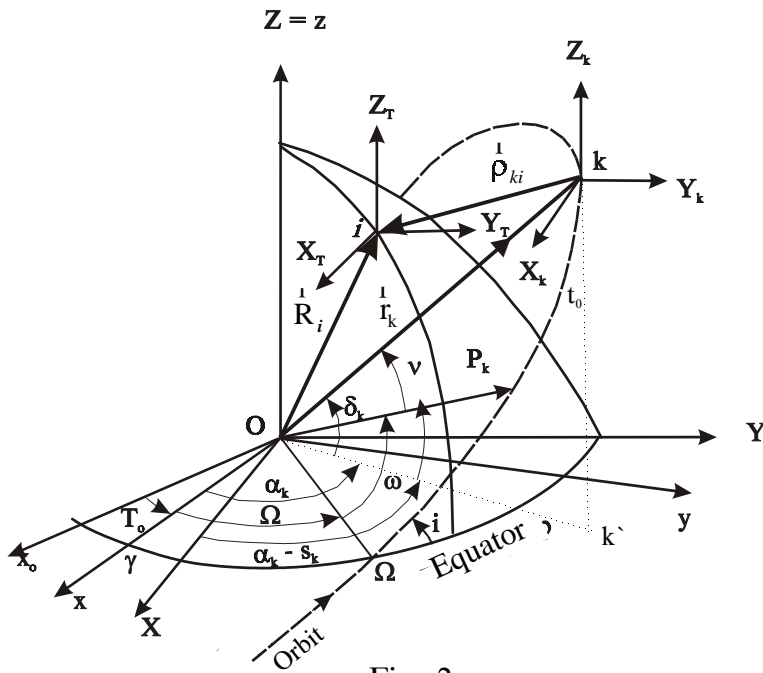


Fig. 2

We shall consider that in the first stage, by a chosen orbital method, an extrapolation of the initial elements of the satellite is made, and the initial quantities of the satellite at the moment of taking the picture  $t_k$  ( $k = 1, 2, \dots, n$ ) are determined. With these 'transferred' quantities and the of the known GCP determined by GPS coordinates, according to [2] fluxional specification of the coordinates of the satellite at the moment  $t_k$ , and the Oilers elements  $(\Omega, i, \omega)$  could be made.

With the quantities thus obtained way, the orthogonal coordinates of the necessary control points of the image (fig.2) in Greenwich coordinate system could be determined, i.e. the already known GCP of the area, by which the geometrical deformations could be eliminated.

## 2. Approximation and extrapolation of the satellite's orbit, for the moment of taking the image $t_k$ .

To solve the problem, the inter orbit of the satellites for short intervals of time in spherical coordinate system [4, 7, 8] will be used. This

way of extrapolation of the initial elements, provides a precise way of determination the spherical coordinates of the satellite  $S = (\xi, \eta, \omega, \xi', \eta', \omega')_0^T$  which was used in the INTERCOSMOS program while a specific software for processing was also made.

The relation between the inter spherical coordinates  $S_k = (\xi, \eta, \omega)_k^T$  and the rectangle coordinates  $r_k = (X, Y, Z)_k^T$  is given by [3, 4, 7]:

$$(1) \quad \begin{cases} X_k = \sqrt{(c^2 + \xi_k^2)(1 - \eta_k^2)} \cos \omega_k, \\ Y_k = \sqrt{(c^2 + \xi_k^2)(1 - \eta_k^2)} \sin \omega_k, \\ Z_k = c\sigma + \xi_k \eta_k. \end{cases}$$

To extrapolate of the orbit for the moment  $t_k$ , the expressions, providing to determine both the coordinates  $(\xi, \eta, \omega)_k$  and the components of the velocities  $(\xi', \eta', \omega')_k$  [4, 8] are used:

$$(2) \quad \begin{cases} \xi_k = \sum_{i=0}^n a_{0i} \tau_k^i, & \xi'_k = \sum_{i=0}^n i a_{0i} \tau_k^{i-1} \\ \eta_k = \sum_{i=0}^n b_{0i} \tau_k^i, & \eta'_k = \sum_{i=0}^n i b_{0i} \tau_k^{i-1} \\ \omega_k = \sum_{i=0}^n c_{0i} \tau_k^i, & \omega'_k = \sum_{i=0}^n i c_{0i} \tau_k^{i-1}; \end{cases}$$

$$(3) \quad \tau = \sum_{i=1}^n I_{oi} \Delta t_k^i, \quad \Delta t_k = t_k - t_0.$$

$\tau$  - is determined time;  $I_i \cong \xi_0^2 + c^2 \eta_0^2 + \varepsilon_0$ .

The coordinates obtained for the moment of taking the image  $t_k$ , must be corrected, accounting for the gravitational and non-gravitational disturbances [4, 10, 11]. By the used method, even the smallest disturbances, influencing the motion of the satellite could be determined, after which they are summed to the expressions:

$$(4) \quad \delta\xi = \sum_{i=1}^n \delta\xi_i; \quad \delta\eta = \sum_{i=1}^n \delta\eta_i; \quad \delta\omega = \sum_{i=1}^n \delta\omega_i;$$

producing:

$$(5) \quad \xi_k = \xi_{np} + \delta\xi; \quad \eta_k = \eta_{np} + \delta\eta; \quad \omega_k = \omega_{np} + \delta\omega .$$

We have the spherical coordinates and components of the velocity  $S = (\xi, \eta, \omega, \xi', \eta', \omega')^T$ , the inertial spatial coordinates  $r_k = (X, Y, Z)_k^T$ , according to eqs.(1) and components of the velocity  $(\dot{X}, \dot{Y}, \dot{Z})_k$  [4, (4.38)], of the satellite for the moment  $t_k$  from eqs.(1), and the measured GPS coordinates of the GCP  $R_i = (X, Y, Z)_i$ . Then

$$(6) \quad U_{ik}^0 = \begin{bmatrix} \gamma \\ \delta \\ \rho \end{bmatrix}_{ik} = \begin{bmatrix} \text{arctg} \frac{Y_k - Y_i}{X_k - X_i} \\ \arcsin \frac{Z_k - Z_i}{\sqrt{(X_k - X_i)^2 + (Y_k - Y_i)^2 + (Z_k - Z_i)^2}} \\ \sqrt{(X_k - X_i)^2 + (Y_k - Y_i)^2 + (Z_k - Z_i)^2} \end{bmatrix} .$$

By linearization of expressions (6) and taking into account the equation of floating differences, which is typical in using an orbital method, [4] we have:

$$(7) \quad U_{ik} + dU_{ik} = U_{ik}^0(X_k^0, Y_k^0, Z_k^0, X_i^0, Y_i^0, Z_i^0) + \frac{\partial U_{ik}^0}{\partial (X^0, Y^0, Z^0)_k} \cdot \frac{\partial (\xi, \eta, \omega)_k^0}{\partial (\xi_0, \eta_0, \omega_0, \xi_0', \eta_0', \omega_0')_k} \cdot d(\xi_0, \eta_0, \omega_0, \xi_0', \eta_0', \omega_0')_k + \frac{\partial U_{ik}^0}{\partial (X_i, Y_i, Z_i)} \cdot d(X_i, Y_i, Z_i) .$$

The equation of the floating differences after abbreviation by cancellation in expressions (7), is written in the form:

$$(8) \quad \mathbf{V}_{U_{ik}} = (\mathbf{A}_{ik} \mathbf{I}_k \mathbf{J}_k \mathbf{B}_{ik})_j \begin{pmatrix} d\mathbf{S}_{0j} \\ d\mathbf{R}_i \end{pmatrix} + \mathbf{L}_{U_{ik}} = (\mathbf{G}, \mathbf{B})_{kj} \begin{pmatrix} d\mathbf{S}_{0j} \\ d\mathbf{R}_i \end{pmatrix} + \mathbf{L}_{U_{ik}}; \quad \mathbf{P}_{U_{ik}},$$

where:

$$(9) \quad \mathbf{G}_{kj} = \mathbf{A}_{ik} \mathbf{I}_{kj} \mathbf{J}_{kj},$$

$$(10) \quad L_{U_{ik}} = U'_{ik} - U^0_{kj} (\mathbf{R}_i \mathbf{S}_{oj}, t_k - t_0) ,$$

$U'_{ik}$  - is determined from the coordinates of GCP -  $i$  ; and satellite -  $k$  ,

$U_{kj}$  - are extrapolated coordinates of satellite - $k$  ;

$$(11) \quad A_{ik} = -B_{ik} = \frac{\partial U^0_{ik}}{\partial (X^0, Y^0, Z^0)} = \begin{bmatrix} \frac{-\cos\gamma \sin\delta}{\rho} & \frac{\cos\gamma \sin\delta}{\rho} & \frac{\cos\delta}{\rho} \\ \frac{\sin\gamma}{\rho} & \frac{-\cos\gamma}{\rho} & 0 \\ \cos\gamma \cos\delta & \sin\gamma \cos\delta & \sin\delta \end{bmatrix}^0_{ik} = \begin{bmatrix} \frac{-\Delta x \Delta z}{s\rho^2} & \frac{\Delta y \Delta z}{s\rho^2} & \frac{s}{\rho^2} \\ \frac{\Delta y}{\rho^2} & \frac{-\Delta x}{\rho^2} & 0 \\ \frac{\Delta x}{\rho} & \frac{\Delta y}{\rho} & \frac{\Delta z}{\rho} \end{bmatrix}^0_{ik}$$

where:

$$(12) \quad \begin{cases} \Delta x_{ik} = X_k^0 - X_i & \Delta y_{ik} = Y_k^0 - Y_i & \Delta z_{ik} = Z_k^0 - Z_i , \\ \rho_{ik} = \sqrt{\Delta x^2 + \Delta y^2 + \Delta z^2} , \\ s_{ik} = \sqrt{\Delta x^2 + \Delta y^2} ; \end{cases}$$

$$(13) \quad \mathbf{I} = \frac{\partial (X_k^0, Y_k^0, Z_k^0)}{\partial (\xi, \eta, \omega)_k^0} = \begin{vmatrix} \frac{S_0}{F_0} \xi \cos \omega & -\frac{k_0}{F_0} \eta \cos \omega & -F_0 \sin \omega \\ \frac{S_0}{F_0} \xi \sin \omega & -\frac{k_0}{F_0} \eta \sin \omega & -S_0 \sin \omega \\ \eta & \xi & 0 \end{vmatrix}_k ,$$

for  $S_0, k_0, F$  we have the expressions:

$$(14) \quad S_0 = 1 - \eta_0^2 ; \quad k_0 = c^2 + \xi_0^2 ; \quad F_0 = \sqrt{S_0 k_0} ;$$

$$(15) \quad \mathbf{J} = \frac{\partial (\xi, \eta, \omega)_k^0}{\partial (\xi_0, \eta_0, \omega_0, \xi'_0, \eta'_0, \omega'_0)_k} = \begin{bmatrix} \frac{\partial \xi_k}{\partial \xi_0} & \frac{\partial \xi_k}{\partial \eta_0} & \dots & \frac{\partial \xi_k}{\partial \eta'_0} & \frac{\partial \xi_k}{\partial \omega'_0} \\ \frac{\partial \eta_k}{\partial \xi_0} & \frac{\partial \eta_k}{\partial \eta_0} & \dots & \frac{\partial \eta_k}{\partial \eta'_0} & \frac{\partial \eta_k}{\partial \omega'_0} \\ \frac{\partial \omega_k}{\partial \xi_0} & \frac{\partial \omega_k}{\partial \eta_0} & \dots & \frac{\partial \omega_k}{\partial \eta'_0} & \frac{\partial \omega_k}{\partial \omega'_0} \end{bmatrix} .$$

The values of the coefficients of matrix (12) are defined from [4, (4.18)].

The vectors  $d\mathbf{S}_{0k}$  and  $d\mathbf{R}_i$  have the form:

$$(16) \quad d\mathbf{S}_{0k} = (d\xi_0, d\eta_0, d\omega_0, d\xi'_0, d\eta'_0, d\omega_0)^T ,$$

$$(17) \quad d\mathbf{R}_i = (dX_i, dY_i, dZ_i)^T ,$$

$$(18) \quad \mathbf{S}_k^1 = \mathbf{S}_{0k} + d\mathbf{S}_k^1 ,$$

$$(19) \quad \mathbf{R}_i^1 = \mathbf{R}_i + d\mathbf{R}_i^1 .$$

In this case, when the GCP are defined by GPS measures ,  $d\mathbf{R} = 0$  could be placed in (19) , after which from eqs.(1) it is obtained :

$$(20) \quad \mathbf{V}_{U_{kj}} = \mathbf{G}_{kj} d\mathbf{S}_{kj}^1 + \mathbf{L}_{U_{kj}} ; \quad \mathbf{P}_{U_{ik}} .$$

The solution of the equation of floating differences (20), provides to obtain the unknown corrections  $ds$  from (16) and from (1) the values  $\mathbf{r}_k = (X^1, Y^1, Z^1)_k$  in inertial coordinate system which could be taken as a first approximation, namely:

$$(21) \quad \begin{cases} \xi_k^1 = \xi^0 + d\xi , \\ \eta_k^1 = \eta^0 + d\eta , \\ \omega_k^1 = \omega^0 + d\omega ; \end{cases}$$

$$(22) \quad \text{and from (1) it is obtained:} \quad \mathbf{r}_k = (X^1, Y^1, Z^1)_k .$$

### 3. Fluxional specification of the coordinates of the satellite for the moments $t_k$ and defining the Oiler's elements $(\Omega, i, \omega)$ .

Upon having obtained in first approximation the coordinates of the satellite  $(X^1, Y^1, Z^1)_k$  , in the moments of taking the image  $t_k$  ( $k = 1, 2 \dots n$ ) and having the defined coordinates  $(X_i, Y_i, Z_i)$  from the GCP, it is possible to accomplish the ultimate goal - time-coordinate georeference of the space image with the defining of the decode places and identified points (fig.1) in the Geenwich geocentric coordinate system OXYZ, firmly related with the rotating Earth. We will accept: that the beginning of the coordinate system O to coincide with the Earth's mass center or with the Earth's /referent/ ellipsoid center; the movement of the poles is accounted for.

Below we shall use the fundamental equation of space photogrammetry [2, 9, 12] (fig.2) for fluxional specification of the satellite orbit:

$$(23) \quad \rho_{ki} = -(\mathbf{r}_k - \mathbf{R}_i) \quad k=1,2,\dots,n \quad i=1,2,\dots,10$$

In each direction of the centric-satellite distance-vector  $\rho_{ki}^0$  to the GCP  $i$ , 'intersects' the topographic image in  $\bar{i}$ , which provides for the fundamental equation (22) to be presented in the form of the Greenwich coordinate system, by the expression (fig.2 and 3):

$$(24) \quad \begin{pmatrix} \bar{x}_{\bar{i}} \\ \bar{y}_{\bar{i}} \\ -f_t \end{pmatrix} = \frac{\Delta_{ki}}{\rho_{ki}} \mathbf{S}_k \mathbf{P}_k \begin{pmatrix} X_i - X_k \\ Y_i - Y_k \\ Z_i - Z_k \end{pmatrix},$$

where:

$\bar{x}_{\bar{i}}$   $\bar{y}_{\bar{i}}$   $f_t$  - are the coordinates in the topographic coordinate system of the space image (fig.3) ;

$\frac{1}{m} = \frac{\Delta_{ki}}{\rho_{ki}}$  - a scale coefficient ;

$\Delta_{ki} = \sqrt{x_k^2 + y_k^2 + f_t^2}$  - a scale factor ;

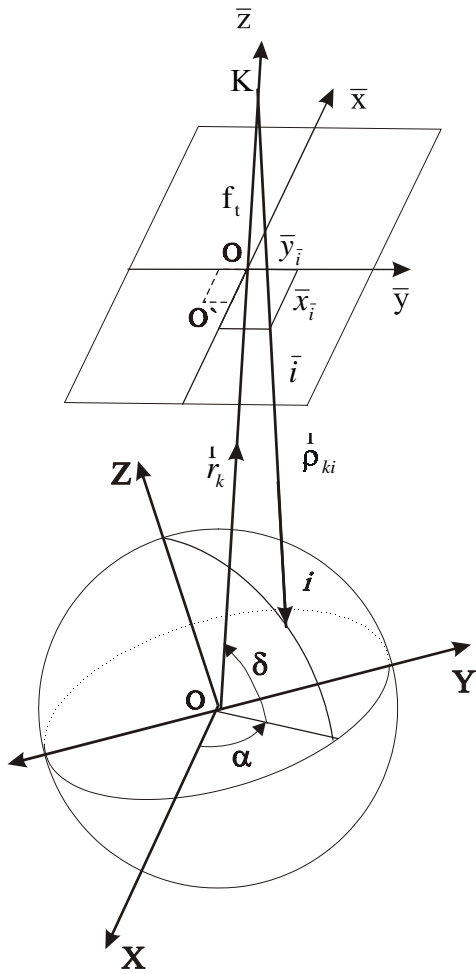


**Fig. 3**

$$(25) \quad S_k = \begin{vmatrix} \cos S & -\sin S & 0 \\ -\sin S & \cos S & 0 \\ 0 & 0 & 1 \end{vmatrix} \quad \text{- is a matrix for transformation in to Greenwich coordinate}$$

system.

For the orthogonal matrix  $P_k$  we have :

$$(26) \quad P_k = (P_0 P_i^*)^T$$

where  $P_0$  is an orthogonal matrix giving the orientation between the topographic and the star coordinate system ;

$P_i^*$  - operator giving the orientation of the star image towards the inertial.

$P_k$  in matrix form is:

$$(27) \quad \mathbf{P}_k = \begin{vmatrix} a_1 & a_2 & a_3 \\ b_1 & b_2 & b_3 \\ c_1 & c_2 & c_3 \end{vmatrix}$$

where  $a_i, b_i, c_i$  ( $i=1, 2, 3$ ) are the guiding cosines from the Euler's angles, which in [2, (14)] are given by the indexes:  $\Omega', i', \omega'$  .

Excluding the scale coefficient  $\frac{1}{m}$  , equation (24) could be written in colinear form :

$$(28) \quad \begin{cases} x_{ki} = -f_t \frac{a_1(X_i - X_k) + a_2(Y_i - Y_k) + a_3(Z_i - Z_k)}{c_1(X_i - X_k) + c_2(Y_i - Y_k) + c_3(Z_i - Z_k)} \\ y_{ki} = -f_t \frac{b_1(X_i - X_k) + b_2(Y_i - Y_k) + b_3(Z_i - Z_k)}{c_1(X_i - X_k) + c_2(Y_i - Y_k) + c_3(Z_i - Z_k)} \end{cases} .$$

The linearisation of the equation (24), respectively (28), for every pictured GCP  $i$ , on the topographical image  $\bar{i}$  with coordinates  $\bar{x}_{ki}$  and  $\bar{y}_{ki}$  yields:

$$(29) \quad \begin{aligned} \bar{u}_{ki} + d\bar{u}_{ki} &= \bar{u}_{ki}^0(\bar{x}_{ki}^0, \bar{y}_{ki}^0) + \frac{\partial \bar{u}_{ki}}{\partial(\Omega, i, \omega)_k} d(\Omega, i, \omega)_k + \\ &+ \frac{\partial \bar{u}_{ki}}{\partial(X, Y, Z)_k} d(X, Y, Z)_k + \frac{\partial \bar{u}_{ki}}{\partial(X, Y, Z)_i} d(X, Y, Z)_i \end{aligned}$$

where:

$\bar{u}_{ki} = (\bar{x}_{ki}, \bar{y}_{ki})^T$  - the calculated values, with the obtained after each itegration coordinates according to (28);

$\bar{u}_{ki}^0(x_{ki}^0, y_{ki}^0)$  - the measured coordinate from the of GCP 's image.

Because of some considerations shared above for the coordinates of GCP, we shall assume the equation of floating differences from (29):

$$(31) \quad \mathbf{V}_{\bar{u}_{ki}} = (\mathbf{G}_k, \mathbf{B}_k) \begin{pmatrix} ds_k \\ d\mathbf{r}_k \end{pmatrix} + \mathbf{L}_{\bar{u}_{ki}}; \quad \mathbf{P}_{\bar{u}_{ki}};$$

$$(32) \quad ds_k = (d\Omega, di, d\omega)_k^T;$$

$$d\mathbf{r}_k = (dX, dY, dZ)_k^T;$$

$$(33) \quad \mathbf{L}_{\bar{u}_{ik}} = \bar{\mathbf{u}}_{ki}^0 - \bar{\mathbf{u}}_{ki};$$

$$(34) \quad \mathbf{G}_k = \frac{\partial \bar{\mathbf{u}}_{ki}}{\partial (\Omega, i, \omega)_k} \quad ; \quad \frac{\partial \bar{\mathbf{u}}_{ki}}{\partial (X, Y, Z)_k} .$$

By equations (31) we make several consecutive iterations, until  $ds_k$  and  $dr_k$  become smaller than the initial quantity  $\varepsilon_0$ , i.e. we have:

$$(35) \quad \begin{cases} \Omega_k = \Omega_k^1 + d\Omega_k^2 + d\Omega_k^3 + \dots, & X_k = X_k^1 + dX_k^2 + dX_k^3 + \dots \\ i_k = i_k^1 + di_k^2 + di_k^3 + \dots, & Y_k = Y_k^1 + dY_k^2 + dY_k^3 + \dots \\ \omega_k = \omega_k^1 + d\omega_k^2 + d\omega_k^3 + \dots, & Z_k = Z_k^1 + dZ_k^2 + dZ_k^3 + \dots \end{cases}$$

where  $n = 2, 3, \dots$ ,

$$ds_k^n = (d\Omega_k^n, di_k^n, d\omega_k^n)^T < \varepsilon_0^1, \quad dr_k^n = (dX_k^n, dY_k^n, dZ_k^n)^T < \varepsilon_0^2 .$$

#### 4. Coordinate georeference of the control points from the space image in the Greenwich coordinate system.

Upon obtaining the specified values for the external-orientation of the space images according to (35), it is possible to define the coordinates of the already known control points from the topographic image in the Greenwich coordinate system, by which we could remove the geometric deformations. According to the studies in [1,12,13,15], it is proved that the maximum control points must be 35-40, moreover, their optimal position on the photo is shown.

In (29) we could put  $ds_k = (d\Omega, di, d\omega)_k^T = 0$ ,  $dr_k = (dX, dY, dZ)_k^T = 0$ , and we will obtain the following equations of floating differences:

$$(36) \quad \mathbf{V}_{\bar{\mathbf{u}}_{ki}} = \mathbf{A}_i d\mathbf{R}_i + \mathbf{L}_{\bar{\mathbf{u}}_{ki}} \quad ;$$

$$(37) \quad \begin{cases} \mathbf{A}_i = \frac{\partial \mathbf{u}_{ki}}{\partial (X, Y, Z)_i} = \frac{\partial (\bar{x}_{ki}, \bar{y}_{ki})}{\partial (X, Y, Z)_i} \\ d\mathbf{R}_i = (dX, dY, dZ)_i^T \quad ; \end{cases}$$

$$(38) \quad \mathbf{L}_{\bar{\mathbf{u}}_{ki}} = \bar{\mathbf{u}}_{ki}^0 - \bar{\mathbf{u}}_{ki} = \begin{vmatrix} \bar{x}_{ki}^0 - \bar{x}_{ki} \\ \bar{y}_{ki}^0 - \bar{y}_{ki} \end{vmatrix} ,$$

$\bar{x}_{ki}^0, \bar{y}_{ki}^0$  -are the measured values of the control points from the space image ;

$\bar{x}_{ki}, \bar{y}_{ki}$  -the calculated values of the control points according to (28).

It necessary, the equation of the floating differences could be solved by iteration, by introducing in (28) the coordinate of the control points obtained after the last iteration.

Soures:

## INSTRUCTIONS TO AUTHORS

The *Aerospace Research in Bulgaria* series publishes original articles in the theoretical or applied fields of space and aviation science and practice.

### Submission:

- The articles should be submitted in duplicate in English language. Bulgarian authors should also supply a Bulgarian version for verification of the translation.
- Manuscripts (including tables and references) should not exceed 15 standard pages (30 lines per page, 60 strokes per line) typed on white non-transparent paper in standard office format (210x297).
- Each article should have a summary (up to 15 lines).
- Each article should be accompanied by a diskette containing text and figures.

### Conditions:

- The articles should not be published, neither submitted for publication elsewhere.
- All manuscripts are subject to editorial review.

### Arrangement:

• **Title page.** The first page of each article should indicate the title, the authors' names and the Institute where the was conducted.

• **Tables and illustrations.** Tables and captions to illustrations should be submitted on separate sheets. The proper place of each figure in the text should be indicated in the left margin of the corresponding page. All illustrations (photos, graphs and diagrams) should be referred to as "figures" and given in abbreviation "Fig." The author's name, the number of the figure with indication of its proper orientation (top, bottom) should be slightly marked on the back on each figure. All illustrations should be submitted in duplicate too.

• **References.** They should be indicated in the text by giving the corresponding number in parentheses. The references should be typed on a separate sheet, arranged chronologically by numbers figuring in the text. The name of the first author should be given with inversion. The title of the article is followed by that of the journal (collection), volume, year of publication, issue number and the pages cited. The titles of the monographs should be followed by the city, publisher, year of publication and the cited page.

### Example:

1. B u l a r d, E., I. C o o p e r. The determination of the masses necessary to produce a given gravitational field. - Proc. Royal Soc., London, 194, 1948, 332-347.

2. Y a n o v s k a y a, T., L. P o r o k h o v a. Inverse Geophysical Problems. Leningrad, Leningr. Univ. Publ, 1983.

### Further details:

- Measurement units should be used only according to SI.
  - Authors have to accomplish one proof-reading within term specified by the publishers)
- Only type-setting errors are subject to correction.

**Address.** The authors may submit articles in person or send them to the following address:

Editorial Board of  
*Aerospace Research in Bulgaria*,  
Space Research Institute  
Bulgarian Academy of Sciences,  
6, Moskovska St., Sofia 1000, Bulgaria

## УКАЗАНИЯ ЗА АВТОРИТЕ

В тематичната поредица „Аерокосмически изследвания в България“ се отпечатват оригинални научни статии от областта на аерокосмическата наука и практика.

### Условия:

- Статиите трябва да бъдат представени в 2 екземпляра на английски език. Българските автори трябва да представят статиите си и на български език.
- Обемът на статията (включително таблиците и литературата) не трябва да превишава 15 стандартни машинописни страници (30 реда на страница, 60 знака на ред) във формат 210x297 mm.
- Всяка статия трябва да бъде придружена от резюме (до 1/2 стандартна страница) на български и на английски език.
- Материали, приети за печат или публикувани в други издания, не се приемат.
- Статията се придружава и с дискета, съдържаща текста.

### Подреждане:

- На първата страница на всяка статия трябва да бъдат написани заглавието, имената на авторите и местоработата.
- Таблиците и илюстрациите. Таблиците и текстът към илюстрациите трябва да се представят на отделни страници. Местото им в текста да се посочи в полето на съответната страница. На гърба на илюстрациите (фотоси, чертежи, графики и др.) с молив да се напишат заглавието на статията, имената на авторите, номера на фигурата и да се посочи ориентацията.
- Литература. Цитираната литература се представя на отделен лист по номерация, появяваща се хронологично в текста. Името на първия автор се дава с инверсия. Следват заглавието на статията, заглавието на списанието (сборника), том, година, книжка, страница, а при монографиите — град, издателство, година, страница.

### Пример:

1. Кръстанов, Л. К. Серафимов. — Сп. на БАН, XX, 1974, №2, с. 29.
2. Несторов, Г. Физика на ниската йоносфера. С., БАН, 1969, с. 63.

### Други изисквания:

- Мерните единици задължително да бъдат по СИ.
- Авторите преглеждат една коректура в определен срок. Допускат се само поправки на грешки, направени при набора.

**Адрес.** Авторите могат да представят лично материалите си или да ги изпратят на адрес:

София 1000  
ул. „Московска“ № 6  
Институт за космически изследвания — БАН  
Редакционна колегия на „Аерокосмически изследвания в България“